NASA CR-175091
TELEDYNE CAE

Report No. 2231

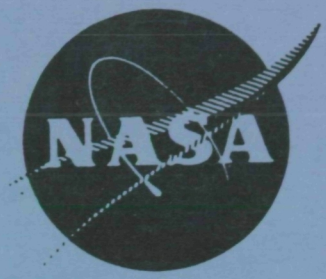

VARIABLE AREA RADIAL TURBINE FABRICATION AND TEST PROGRAM

BY

C. ROGO

TELEDYNE CAE

PREPARED FOR
NATIONAL AERONAUTICS AND SPACE ADMINISTRATION

NASA LEWIS RESEARCH CENTER
CONTRACT NAS3-23173

(NASA-CR-175091) VARIABLE AREA RADIAL TURBINE FABRICATION AND TEST PROGRAM (Teledyne CAE) 91 p CSCL 21E

N86-28947

Unclas
G3/07 43483

1. Report No.	2. Government Accession No.	3. Recipient's Catalog No.
NASA CR-175091 AVSCOM TR-86-C-13		

4. Title and Subtitle	5. Report Date
Variable Area Radial Turbine Fabrication and Test Program	AUGUST, 1986
	6. Performing Organization Code

7. Author(s)	8. Performing Organization Report No.
Casimir Rogo	TELEDYNE CAE 2231
	10. Work Unit No.

9. Performing Organization Name and Address	11. Contract or Grant No.
Teledyne CAE 1330 Laskey Road Toledo, OH 43612	NAS3-23173
	13. Type of Report and Period Covered
12. Sponsoring Agency Name and Address	Contractor Report
Army Aviation Research & Technology Activity - Propulsion Directorate, NASA Lewis Research Center, Cleveland, Ohio 44135	14. Sponsoring Agency Code RTOP 505-40-8K 1L161101AH45

15. Supplementary Notes

Richard J. Roelke, Project Manager, Propulsion Systems Division, NASA Lewis Research Center, Cleveland, Ohio 44135

16. Abstract

A variable area radial turbine with a moveable nozzle sidewall was experimentally evaluated. The turbine was designed for an advanced variable capacity gas turbine rotorcraft engine. The turbine had a mass flow rate of 2.27 kg/sec (5.0 lbs/sec), and a rotor inlet temperature of 1477K (2200°F). Testing was conducted at a reduced inlet temperature, but the aerodynamic parameters and Reynolds numbers were duplicated. Overall performance was obtained for a range of nozzle areas from 50% to 100% of the maximum area. The test program determined the effect on performance of: 1) Moving the hub or shroud sidewall; 2) Sidewall-vane clearance leakage; 3) Vaneless space geometry change; and 4) Nozzle cooling flows. Data were obtained for a range of pressure ratios and speeds and are presented in a number of performance maps.

17. Key Words (Suggested by Author(s))	18. Distribution Statement
Turbine, Radial flow, Variable geometry, Rotorcraft engine	Unclassified STAR Category 07

19. Security Classif. (of this report)	20. Security Classif. (of this page)	21. No. of pages	22. Price*
Unclassified	Unclassified	82	

FOREWORD

The Variable Stator Radial Turbine Fabrication and Test Program is co-sponsored by the U. S. Army Research Technology Laboratories and the National Aeronautics and Space Administration. The work described herein has been conducted by Teledyne CAE in accordance with the terms of Contract No. NAS3-23173 issued by NASA-Lewis Research Center. The program is in support of efforts to demonstrate a significant improvement in component performance of small gas turbine engines for future rotorcraft.

PRECEDING PAGE BLANK NOT FILMED

TABLE OF CONTENTS

PRECEDING PAGE BLANK NOT FILMED

LIST OF TABLES

LIST OF ILLUSTRATIONS

LIST OF ILLUSTRATIONS (CON'T)

LIST OF ILLUSTRATIONS (CON'T)

LIST OF ILLUSTRATIONS (CON'T)

SECTION 1.0

SUMMARY

Recent studies have shown that the variable capacity (VARICAP) turboshaft engine concept offers the potential for significant reductions in fuel consumption. This concept is based on matching the engine components at their highest efficiency rating points and modulating power by using variable geometry that changes flow while maintaining near constant temperatures and pressure ratios. One component, identified as the key to the success of the concept was the gas generator radial turbine configured with a cooled variable area nozzle. This turbine was rated at 2.27 kg/sec (5.0 lbs/sec), 1477K (2200°F) rotor inlet temperature and an equivalent work of 89.4 J/g (38.4 B/lb) at maximum conditions.

In the current program a twice size rig turbine, that permitted testing at engine Reynolds numbers, was designed with a capability to move either the hub or shroud nozzle sidewalls. The program objectives were to measure the overall performance and effects of coolant flow injection, vane leakage control and the variable geometry penalties on the radial turbine.

At the design equivalent speed and pressure ratio the test results showed that the uncooled efficiency peaked at 87.9 percent at the design flush wall cruise setting (78% maximum flow) with positive sealing on the vanes. The use of engine-typical metal seals were found to be effective in limiting efficiency loss to 1.0 points. With the addition of 5.6 percent nozzle and 1.0 percent rotor backface coolant flows the efficiency was reduced by 1.6 points to 86.3 percent.

At settings from 50 to 100 percent of maximum the same uncooled performance was obtained with both moveable hub (MH) and moveable shroud (MS) sidewall geometries. At off design conditions, however, the MH nozzle configuration showed up to 2.0 points improvement over the MS sidewall.

The cooled turbine efficiency fell within a $\pm$ 2.2 point band over a 55 to 100 percent flow range when the turbine was operated at constant speed and pressure ratio. This is within the efficiency change assumed in earlier engine studies. This band can be further narrowed by locating the sidewall splitline closer to the rotor tip where a 1.0 point improvement was measured. The cooling penalty could also be reduced or eliminated by the use of a ceramic nozzle assembly. The program demonstrated that the moveable sidewall radial turbine concept can achieve the performance required to significantly reduce the part power SFC of the VARICAP engine.

SECTION 2.0

INTRODUCTION

Aircraft Turbine Engine manufacturers have been making continuous efforts to improve component performance to lower fuel consumption. As the level of sophistication in design has increased over the years, the incremental improvements have become smaller and more difficult to achieve. Another approach to making further fuel consumption improvements is to employ more complicated cycles such as regeneration, variable capacity, compounding and combinations thereof. However, the advantages of these approaches also are predicated on the achievable performance of the components used. The Variable Capacity (VARICAP) turboshaft engine cycle is based on engine operation with each of the components matched near their highest efficiency point. Power is then modulated by changing the engine airflow with variable geometry of the components while maintaining near-constant turbine inlet temperature and engine pressure ratios. This concept has been studied in some detail, References 1 and 2, and a considerable improvement in fuel consumption was shown, provided that leakage and variable geometry losses could be held to reasonable values. Confirming experimental data on the unique variable geometry required was not available at the time of the study. This report summarizes the fabrication and testing of a radial turbine with a moveable sidewall nozzle that typifies the high pressure driver of a VARICAP engine. Aerodynamic testing was conducted to evaluate turbine overall performance effects of variable geometry, cooling injection, and leakage.

2.1 OBJECTIVES

The program objectives were to evaluate the overall performance of an engine-suitable configuration variable stator area radial turbine for an advanced variable capacity gas turbine engine for a rotorcraft application. The design specifications for the turbine were: an airflow of 2.27 kg/sec (5.0 lbs/sec) and a rotor inlet temperature of 1477K - 1589K (2200°F - 2400F). The primary mode of operation was to vary the power of the engine by changing the flow capacity while holding the pressure ratio, rotative speed and turbine inlet temperature constant. The uncooled turbine life was to be 4000 hours based on the duty cycle given in Table I.

The turbine aerodynamic performance was evaluated at flow rates that corresponded to 50-to-100 percent of maximum engine power, speeds from 50-to-100 percent of design, and pressure ratios from 50 percent below to 50 percent above the design pressure ratio.

The performance effects of nozzle cooling injection and variable geometry leakage flows were also included.

The above variables and ranges were selected to evaluate the turbine over a range of performance parameters that may be incurred in an engine mission and to provide a data base for future turbine improvements.

TABLE I

TURBINE DUTY CYCLE

PERCENT POWER	PERCENT TIME
100	20
60	50
55	20
35	5
Idle	5

SECTION 3.0

TURBINE DESCRIPTION

The variable capacity radial turbine concept was studied in considerable detail under recent NASA/ARTL contracts, references 1-5. In reference 1, several turbine configurations were conceptually evaluated and performance analyses conducted on various cycles including simple, VARICAP single-shaft and free-turbine engine configurations. The study concluded that an uncooled 1477K (2200°F) rotor with a cooled moveable sidewall nozzle was one turbine configuration with a high performance potential. The simple regenerated and VARICAP cycles were also studied in reference 2. Reference 3 examined cooled and uncooled radial turbine configurations based on a simple cycle parametric study and concluded that a 1589K (2400°F) cooled rotor with a cooled articulated trailing-edge or a locally moveable sidewall variable stator were the best candidates for further evaluation. References 4 and 5 present experimental data on a research turbine for a number of moveable sidewall configurations. The effect on performance of controlling the rotor reaction by changing the downstream flow area was also investigated.

All of these studies showed a high performance potential for the VARICAP concept and a requirement for additional turbine experimental test data - particularly on an engine orientated configuration.

3.1 AEROMECHANICAL DESIGN

The VARICAP evaluation of reference 1 was a comprehensive study conducted as it was carried through cycle analysis, engine preliminary design, and detailed turbine design phases. Figure 1 shows the VARICAP engine cross-section and component configuration for a 683 kw (916 hp) engine for a rotorcraft application of the 1990's. This four component engine consists of a two stage 16:1 pressure ratio centrifugal compressor driven by a single stage radial turbine exhausting to a single stage axial free power turbine. The compressor has variable inlet guide vanes and moveable sidewall diffusers. The gas generator turbine flow capacity is varied by a moveable sidewall nozzle and the power turbine flow is varied by pivoted trailing edge vanes. The variable geometry for the four components is controlled by a single gear screw master positioner. The table in Figure 1 shows the VARICAP near-constant fuel consumption over a range from 60 percent to maximum power conditions.

The gas generator turbine for this engine was designed for a 1477K (2200°F) inlet temperature and a 4000 hour life when operated on the duty cycle of Table I. The life of the rotor was predicted in excess of 10,000 start-stop cycles as defined in Table II.

TABLE II

LCF CYCLE

1. Start, accelerate to idle and hold for five minutes.
2. Accelerate to Intermediate Rated Power and hold for five minutes.
3. Decelerate to idle and hold for five minutes.
4. Shut down
5. Cool 60 minutes
(All accelerations and decelerations to take place within three seconds.)

Full Page - Sideways
Art 70539/L4-097

Figure 1. Engine Configuration Study Results

The 4000 hour stress rupture life on the turbine assumes the use of a commercial rapid solidification (CRS) powder metal rotor with directionally recrystallized blade tips. Cooling was not required on the rotor but one percent of mainstream flow was assigned to purge the backface cavity area. The nozzle vanes were designed to be impingement cooled with a trailing edge discharge for minimum aerodynamic penalty. The cooling air flow requirement for the nozzle vanes is 3.0 percent. The nozzle sidewalls are cooled by 1.5 and 1.1 percent hub and shroud flows, respectively. The rotor shroud is also impingement cooled by 0.4 percent of the compressor discharge flow. The sidewall impingement cooling flows are ejected downstream of the vane trailing edges in a direction closely approaching the mainstream flow direction so that mixing losses are minimized. The cooling flow requirements and turbine geometry are given in Figure 2.

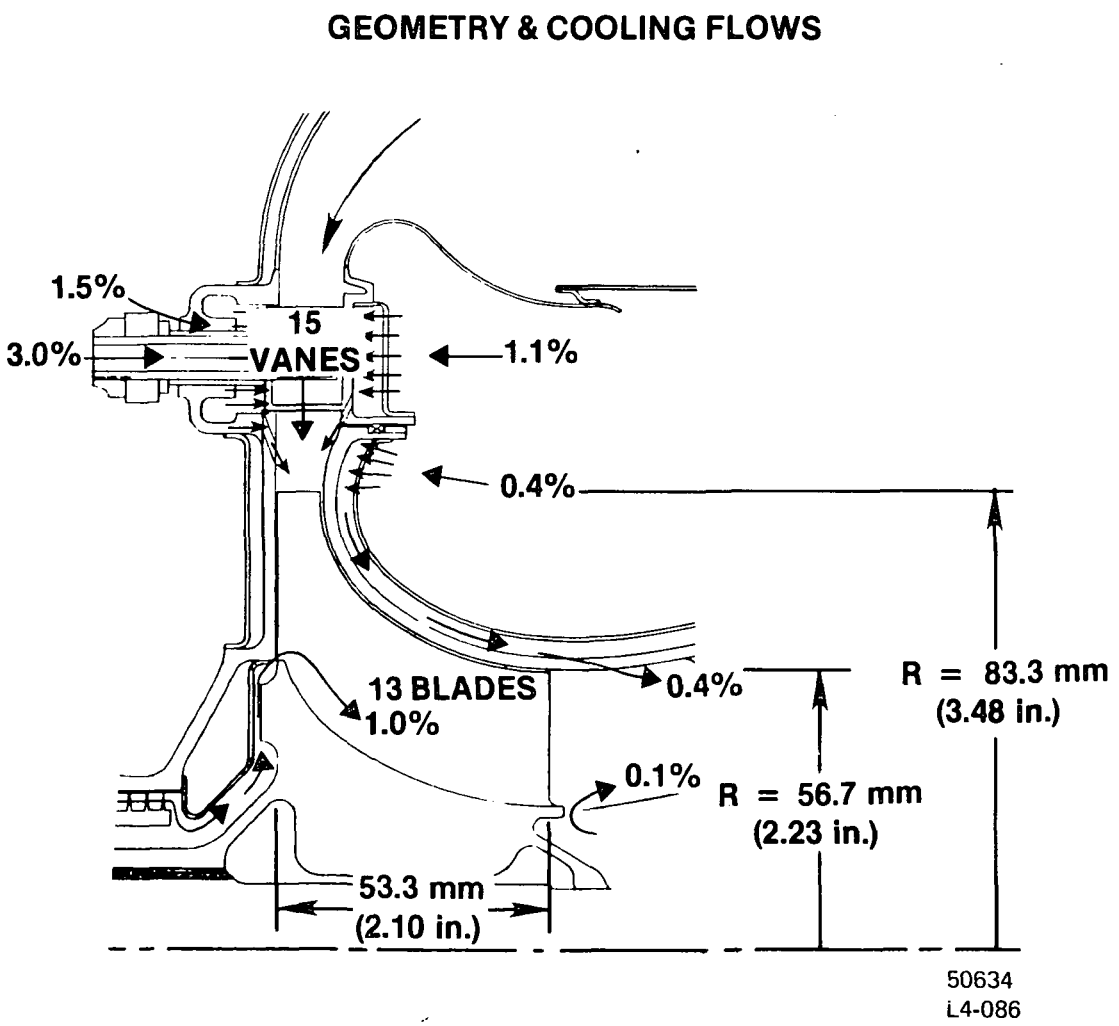

Figure 2. Turbine Geometry And Cooling Flow Requirements

The aerothermodynamic design point requirements of the turbine are given in Table III. The design point velocity diagrams are given in Figure 3. The turbine was designed with a low exit swirl of 10 degrees against rotation and an exit Mach number of 0.30 at the mean radius. The low values were selected to minimize leaving and interturbine transition duct losses. To meet life requirements, the blade tip speed was limited to 657 m/s (2155 fps) with radial blading and this restriction resulted in a small compromise in desired tip incidence. Further details on the turbine are given in reference 1.

TABLE III

TURBINE AEROTHERMODYNAMIC DESIGN REQUIREMENTS

INLET TOTAL TEMPERATURE	T, K; °F	1477	2200
INLET TOTAL PRESSURE	P, kPa; psia	1602	232.4
EQUIVALENT FLOW $W\sqrt{\theta}_{cr}\epsilon/\delta$	kg/s; lbs/s	0.261	0.574
EQUIVALENT WORK $\Delta H/\theta_{cr}$,	J/g; B/lb	89.51	38.35
MECHANICAL SPEED N, rpm		71,000	
EQUIVALENT SPEED $N/\sqrt{\theta}_{cr}$, rpm		31,877	
EQUIVALENT PRESSURE RATIO P/P		4.54	
BLADE TOTAL TO TOTAL EFFICIENCY, η_t		88.0	
TIP BLADE SPEED U_T, m/s; ft/s		657	2155
WORK FACTOR gJ $\Delta H/U_T^2$		1.024	

72118
L4-139

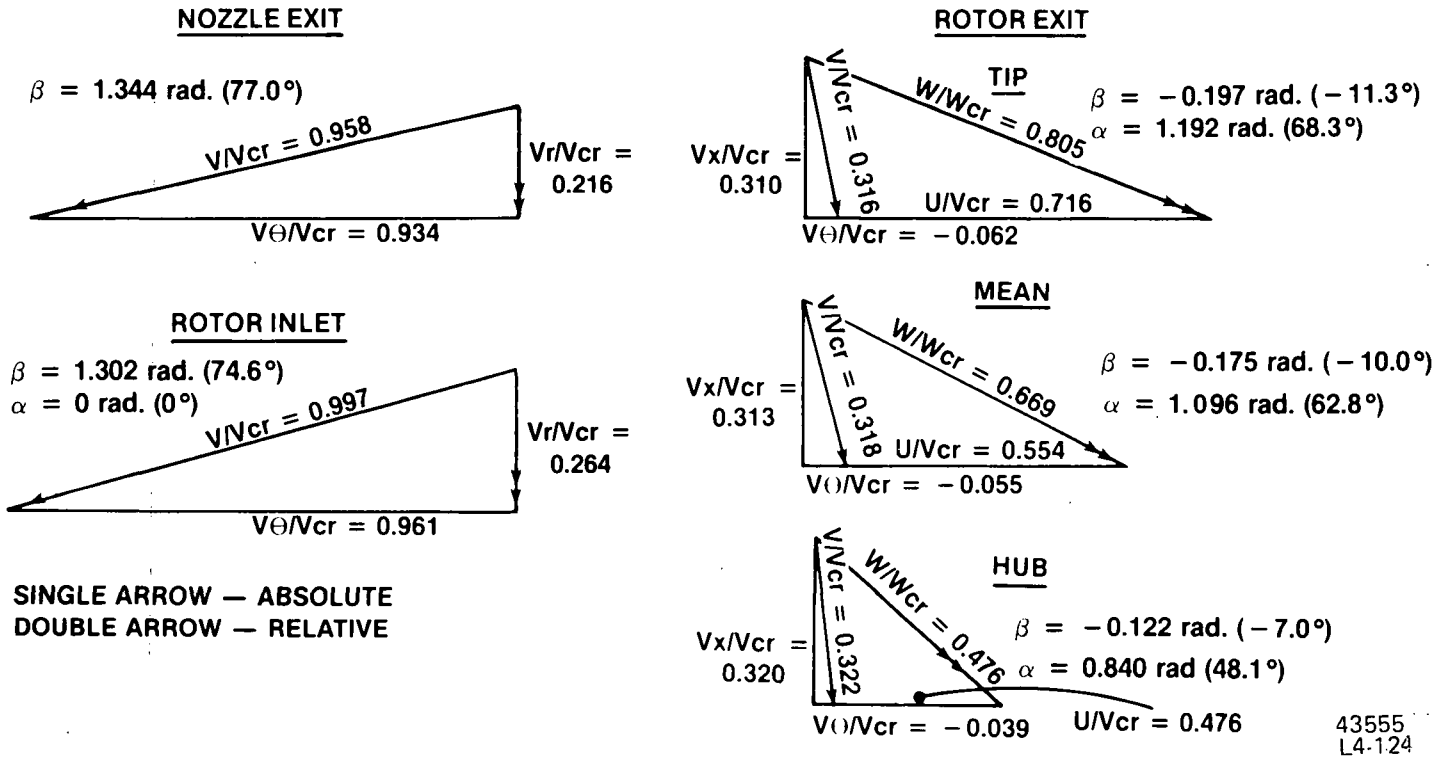

Figure 3. Turbine Design Point Velocity Diagrams

3.2 SCALING CONSIDERATIONS

The most desireable turbine test environment for experimental evaluation is to duplicate the engine aerothermodynamic conditions. This is not always practical and testing is usually conducted at equivalent conditions in a cold or warm air flow test rig where temperature and pressure ratios, Mach numbers, and corrected flows can be simulated. If the inlet conditions can be varied, then testing can be conducted at several Reynolds numbers and performance can then be corrected for Reynolds number effects. The approach taken in this program was to test the turbine at identical engine Reynolds number conditions. This was accomplished by chosing a combination of fixed inlet temperature and pressure, and scaling the turbine up to match to the desired Reynolds number. The rig inlet temperature was selected as 394K (250°F) or a value high enough to prevent freezing conditions at the turbine exit. The turbine inlet pressure was set as 164 kPa (23.8 psia) approaching the upper limit of the turbine facility. The required scale factor for engine Reynolds number duplication was 2.0. The selected 2X size rig turbine has the additional advantage of minimizing aerodynamic size effects of instrumentation blockage that must be located in the flowpath. Lower rotational speeds and higher torque values also can be more accurately measured. Table IV shows how all the engine turbine aerodynamic parameters are duplicated in the rig. Figures 4 and 5 are photographs of the fabricated 2X turbine rotor, nozzle sidewall and turbine nozzle vanes.

TABLE IV

RIG TURBINE SCALED TO DUPLICATE ENGINE AERODYNAMICS

	ENGINE	RIG
INLET PRESSURE, kPa, (psia)	1602 (232.4)	164 (23.8)
INLET TEMPERATURE, K (°F)	1477 (2660)	394 (250)
MACH NUMBERS, M	DESIGN	SAME
EQUIVALENT PRESSURE AND TEMPERATURE RATIOS	DESIGN	SAME
SCALE FACTOR	1X	2X
ROTOR DIA., mm (in.)	176.7 (6.96)	353.4 (13.92)
EQUIVALENT FLOW $\frac{W\sqrt{\theta}_{CR}\epsilon}{\delta}$, kg/s (lbs/s)	0.261 (0.574)	1.044 (2.296)
EQUIVALENT SPEED $\frac{N}{\sqrt{\theta}\,CR}$, rpm	31877	15939
NOZZLE REYNOLDS NO. $\frac{V\, d_H \rho}{\mu}$	4.37×10^5	4.37×10^5
ROTOR REYNOLDS NO. $\frac{W\, d_H \rho}{\mu}$	1.42×10^5	1.42×10^5

72094
L4-140

ORIGINAL PAGE IS
OF POOR QUALITY

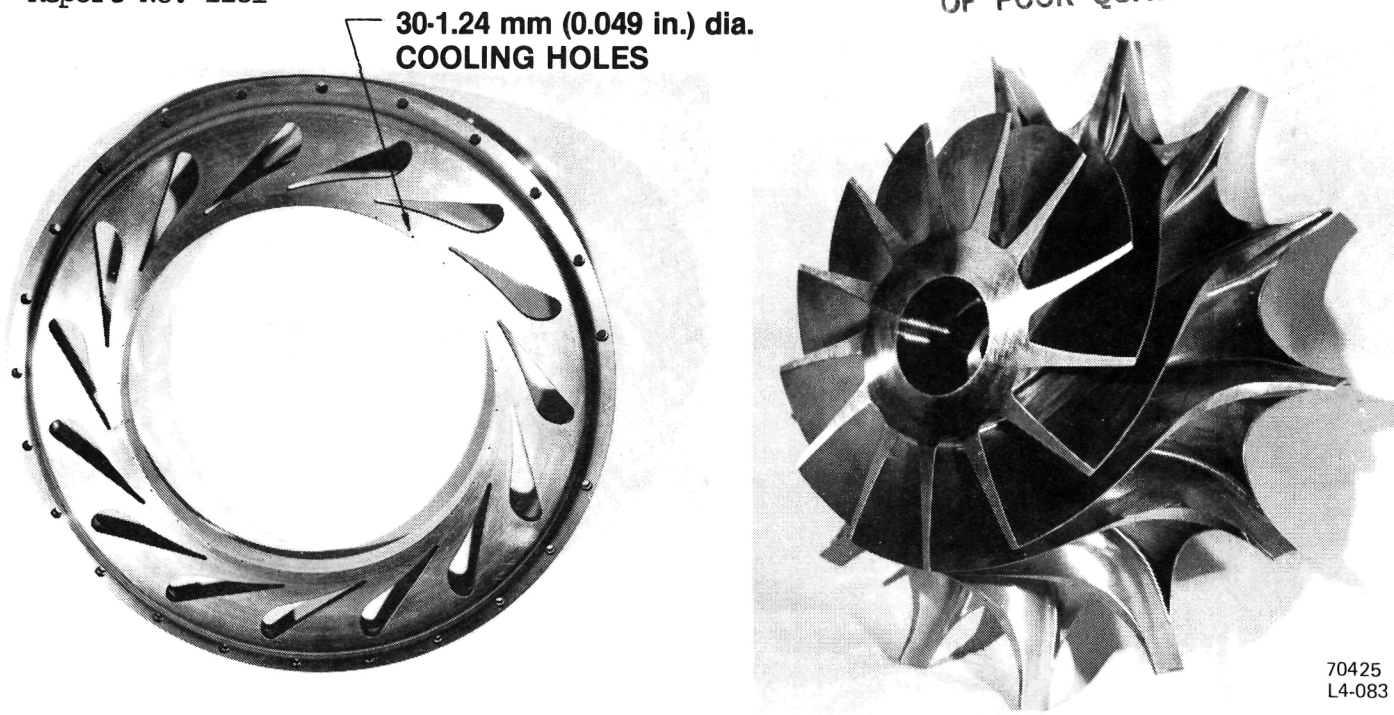

Figure 4. 2X Nozzle Ring And Rotor Rig Hardware

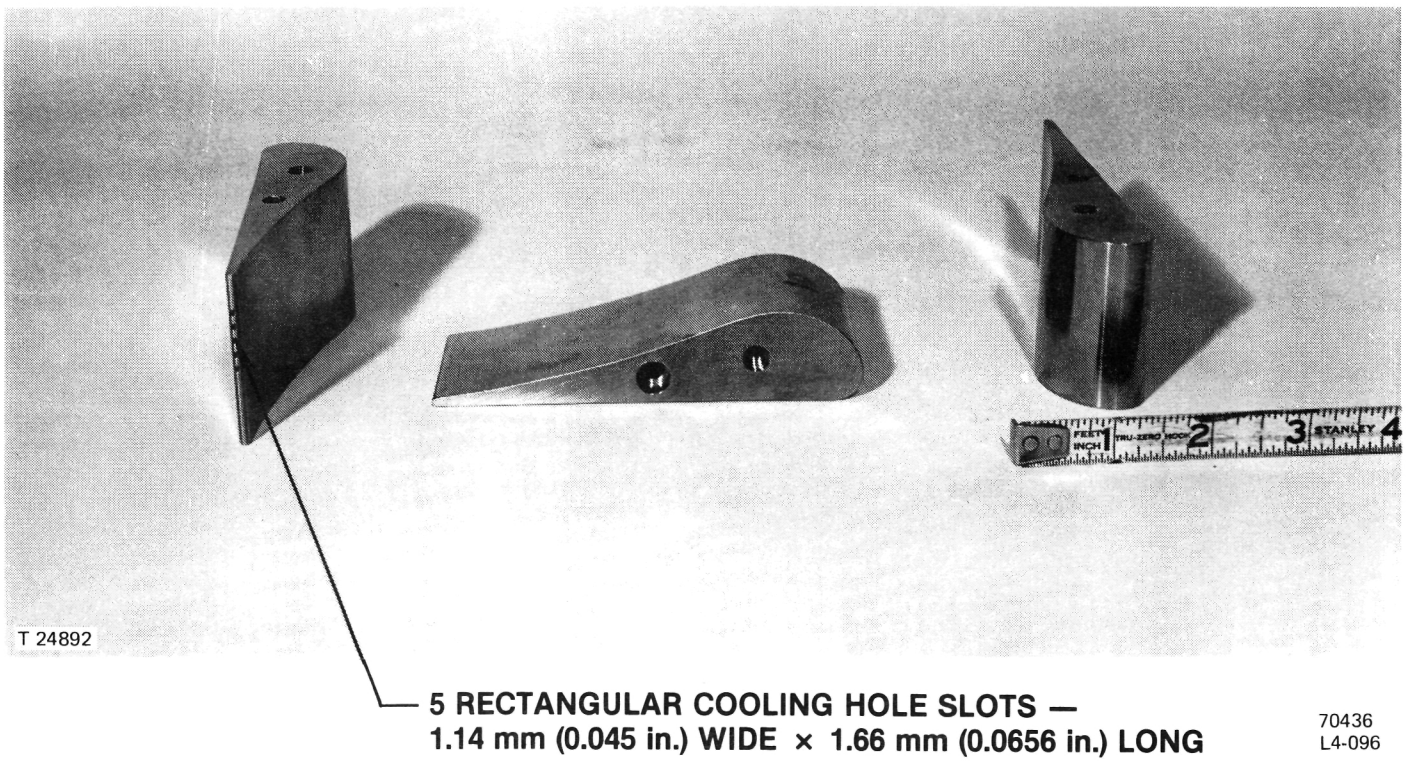

Figure 5. 2X Nozzle Vane Rig Hardware

SECTION 4.0

TURBINE TEST RIG

4.1 TEST CONFIGURATION

The baseline turbine test geometry was designed to simulate, as closely as possible, engine configuration effects. The engine flowpath, moveable sidewall geometry, cooling flow ejection geometry, sidewall nozzle vane clearances and rotor running clearances were all incorporated into the design. Figure 6 shows a cross-section of the baseline geometry with the moveable sidewall of the nozzle on the shroud side. The nozzle vanes are cantilevered from the annular moveable shroud sidewall piston. The vanes, which slide through slots in the stationary hub sidewall, are attached to another annular piston on the hub that accurately positions the vanes with respect to the sidewall slots. Leakage flows between the nozzle vanes and the sidewall gaps are minimized by the use of metal "L" seals as shown. These flexible "L" seals are typical of those that might be used in an actual engine configuration. Provision is made so that testing can be conducted with or without the seals in place. The entire nozzle assembly can be locked in place by four positioning studs located on the shroud side of the turbine.

Each of the nozzle vanes was fabricated with five rectangular cooling hole ejection slots in the trailing edge. These slots are located so that all five holes are ejecting cooling flow to the mainstream flowpath when the sidewall is in the wide open or 100 percent position. In this position the maximum surface area of the vane would be exposed to hot gases. When the sidewall is moved to the 50 percent wall position only one half of the surface area of the vanes would be in the hot gas stream and only half as much vane cooling is required. Then, one half of the cooling slots would be buried in the sidewall and deactivated from the cooling circuit. Rotor backface cooling or purge flow was supplied from a separate circuit in back of the rotor.

Testing on a similar research wheel, Reference 4, showed that the performance with variable geometry was significantly influenced by the location of the split-line radius of the moveable sidewall. Provision was also made in this test program to evaluate the effect of this split-line location. Figure 7 shows the moveable shroud sidewall geometry with a high radius split-line. This required a new sidewall ring and split-line ring to be added to the assembly. Hardware was also designed and fabricated to test the turbine with the nozzle moveable sidewall on the opposite side, also shown in Figure 7.

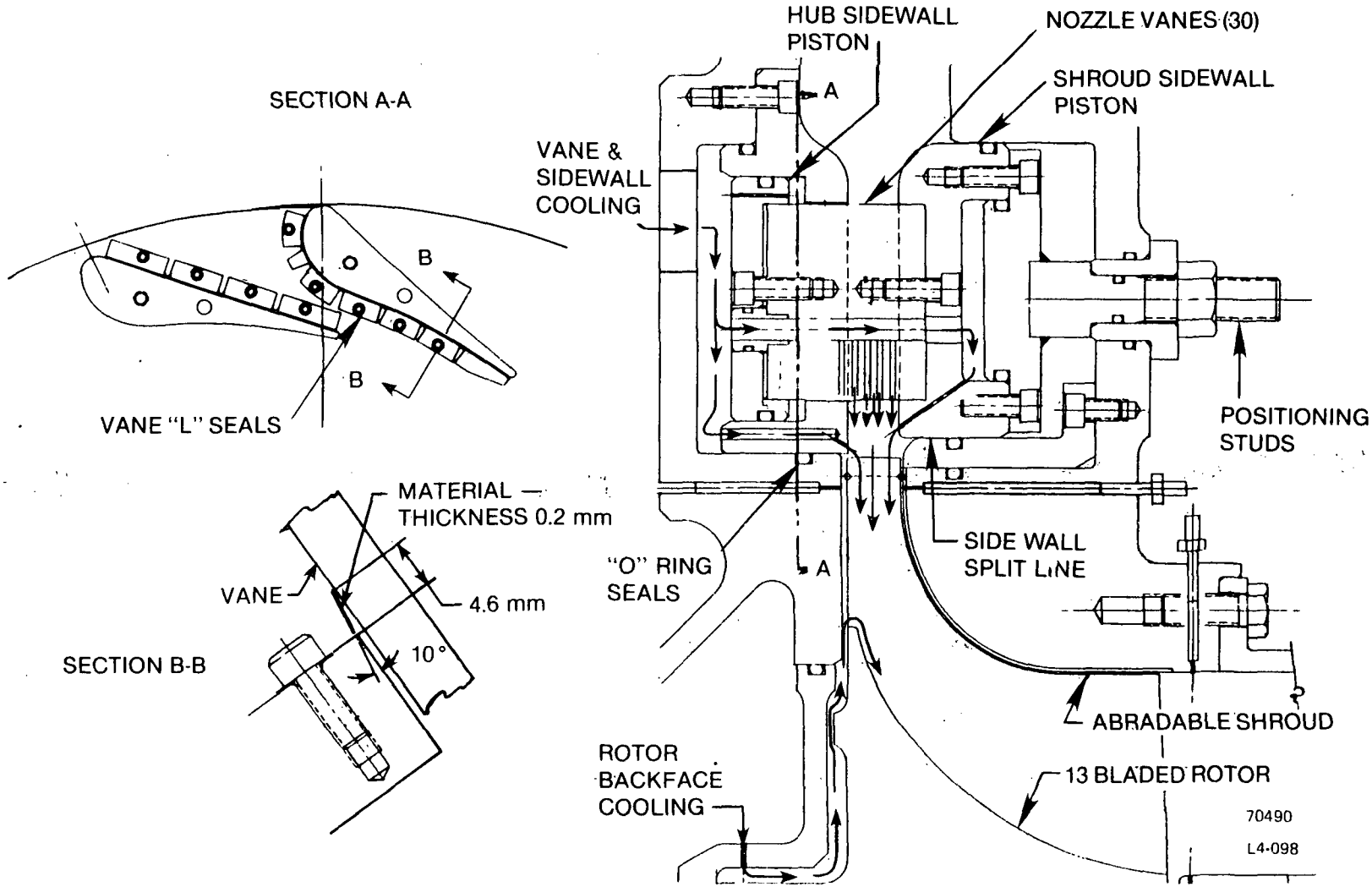

Figure 6. Baseline Configuration - Turbine Nozzle With Moveable Sidewall On Shroud Side

ORIGINAL PAGE IS
OF POOR QUALITY

Figure 7. Moveable Sidewall Geometries Tested

4.2 RIG LAYOUT

Figure 8 shows a cross-section of the cold flow turbine rig. Ram air is supplied to the turbine at an inlet total temperature of 394K (250°F) and an inlet pressure of 164k Pa (24 psia). Flow distortion to the turbine is removed by two inlet screens in series. One is located at the exit from the plenum and a second one is located in the elbow just preceeding the inlet to the turbine nozzle assembly. The exhaust from the turbine rotor is directed to a series of vacuum pumps which can be adjusted to produce desired pressure ratio across the turbine stage. Power from the turbine is absorbed by a "Kahn" water brake. A "Lebow" torque measuring device is splined between the "Kahn" water brake and the turbine rotor. This torquemeter allows dynamic torque to be measured directly from the turbine.

Desired rotor clearances were established by shimming the rotor with respect to the housing. The nozzle assembly could also be shimmed with respect to the rotor to hold the same inlet geometry. The rotor housing was provided with an abradable shroud so that the rotor would not be damaged in the case of a rub.

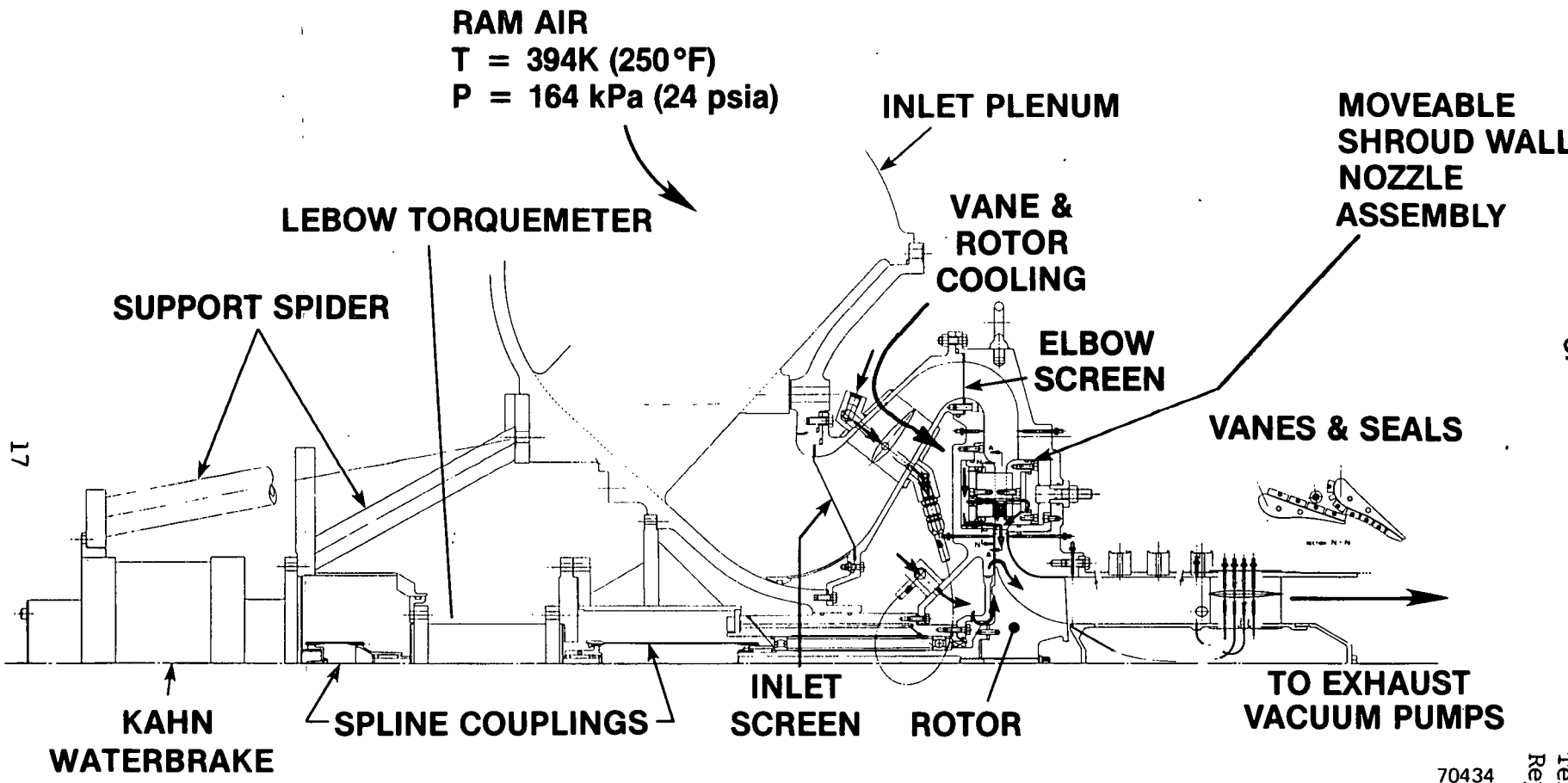

Figure 8. Layout And Cross Section Of Turbine Rig

ORIGINAL PAGE IS
OF POOR QUALITY

4.3 INSTRUMENTATION

Instrumentation was provided to determine the overall performance of the turbine in terms of total and static efficiencies, and mass flow rate over a range of stator areas for each of the selected stator area variation concepts. Overall performance was measured with and without stator cooling flow. All clearances were set to correspond to those designed for actual engine operation. The turbine specific work was determined from both torque and temperature measurements. Instrumentation was provided to measure flow rates, stator inlet and exit total and static pressures, rotor exit total and static pressures and temperatures, rotor exit flow angle, turbine mechanical speed, and rotor torque. The instrumentation is shown in Figure 9. This instrumentation can be grouped by station locations as shown in the Figure and detailed as follows:

Station 1 - Turbine Stator Inlet

3 total temperature rakes (4 elements each)

3 total pressure rakes (4 elements each)

2 total pressure, total temperature and flow angle survey probes

4 static pressure taps - inner wall

4 static pressure taps - outer wall

The turbine stator inlet instrumentation station is located approximately one half vane chord upstream of the vane leading edges. The rake sensing elements are located at centers of equal chord span areas. The equal circumferential spacing of the rakes is defined in Figure 10.

Station 2 - Vaneless Space and Rotor Shroud

4 static pressure taps - inner wall

4 static pressure taps - outer wall

8 static pressure taps - rotor shroud

The eight static pressure taps in the rotor shroud are positioned at equal meridional increments, as indicated in Figure 9 and the vaneless space pressure tap locations are shown in Figure 11.

Station 3 - Turbine Rotor Exit

4 Static pressure taps - inner wall

4 static pressure taps - outer wall

The static pressure taps are located 6.35 mm (0.25 in.) and 9.53 mm (0.375) in. downstream of the rotor exit at the inner and the outer walls respectively, and circumferentially located as shown in Figure 12.

Station 4 - Exhaust Duct

3 total temperature rakes (4 elements each)

3 total pressure rakes (4 elements each)

3 total pressure, total temperature and flow angle survey probes

The exhaust duct instrumentation plane is located 173 mm (6.8 in.) downstream of the rotor trailing edge. In this plane all the rotor blade wakes are mixed out and performance includes losses typical of an interturbine transition duct. The circumferential location of the stationary rakes with sensor elements at centers of equal areas is defined in Figure 13.

Miscellaneous Instrumentation

total pressure - main flow orifice

total temperature - main flow orifice

static pressure differential - main flow orifice

total pressure - coolant flow orifice

total temperature - coolant flow orifice

static pressure differential - coolant flow orifice

static pressure - front coolant plenum

static pressure - rear cooling plenum

total temperature - front cooling plenum

total temperature - rear cooling plenum

turbine shaft torque via a "Lebow" inline torquemeter

turbine shaft mechanical speed

ORIGINAL PAGE IS
OF POOR QUALITY

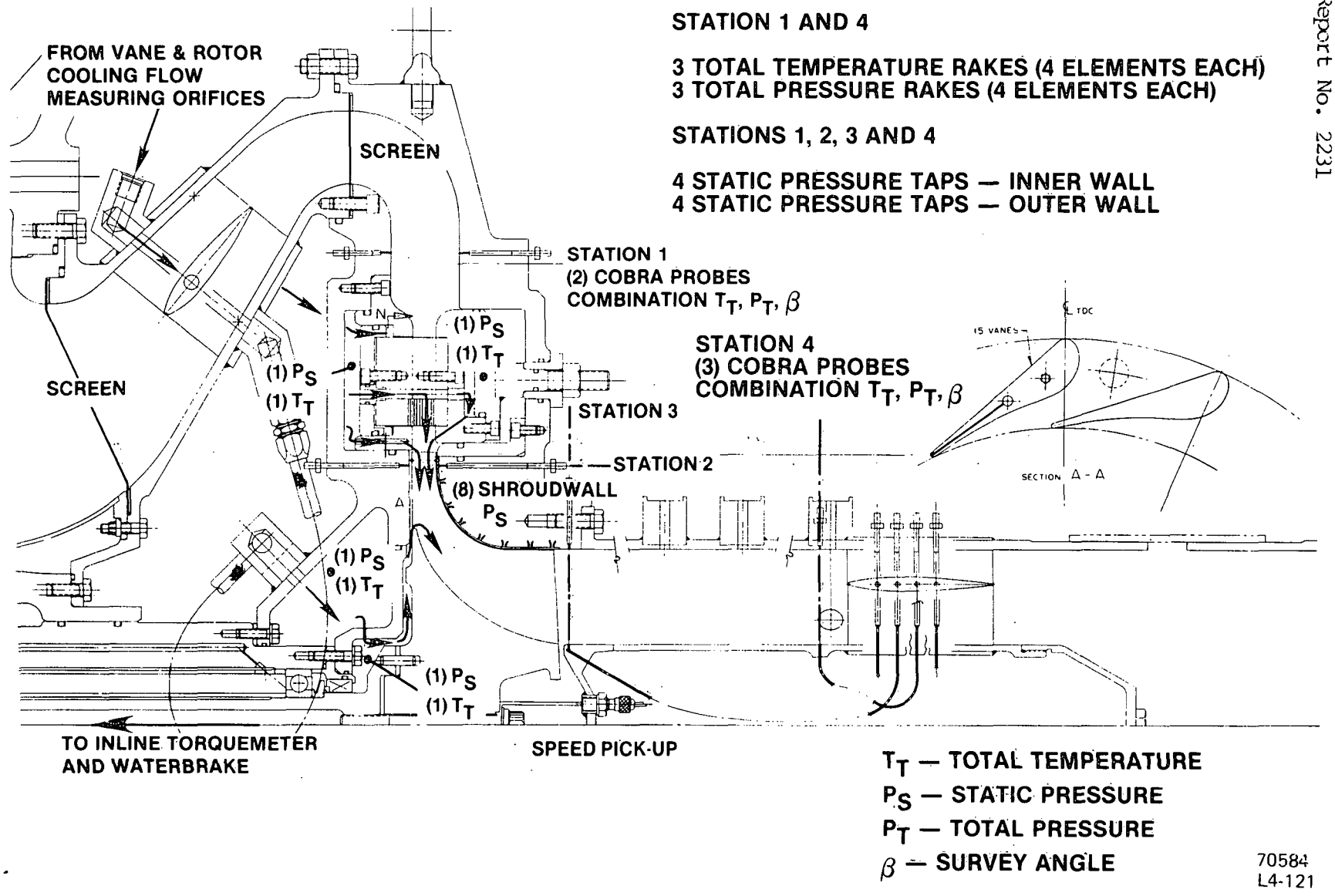

Figure 9. Turbine Rig Instrumentation

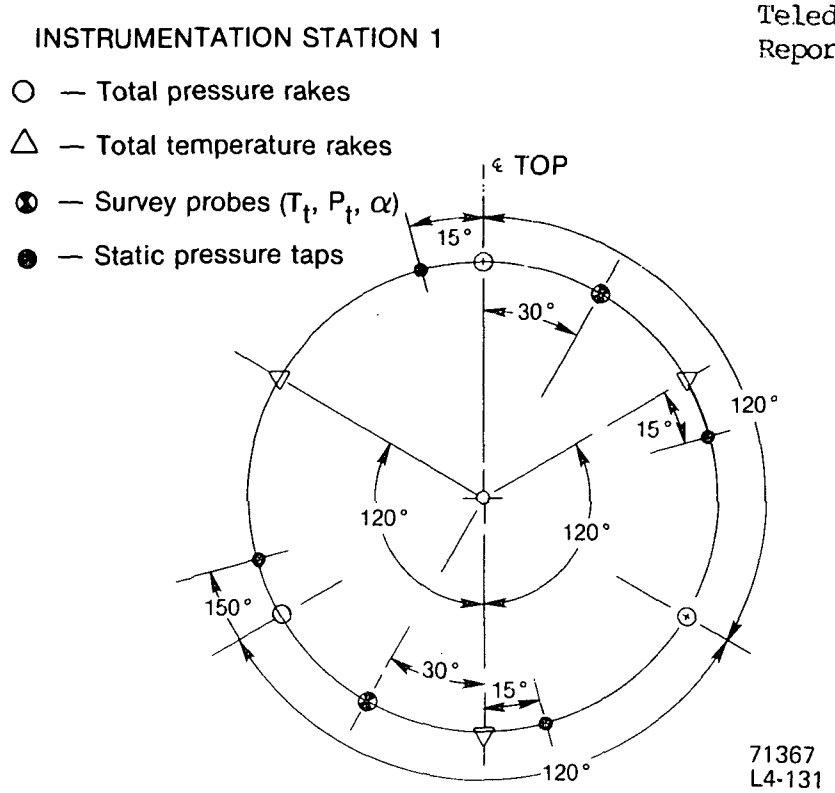

Figure 10. Stator Inlet Instrumentation (Station 1) Circumferential Locations

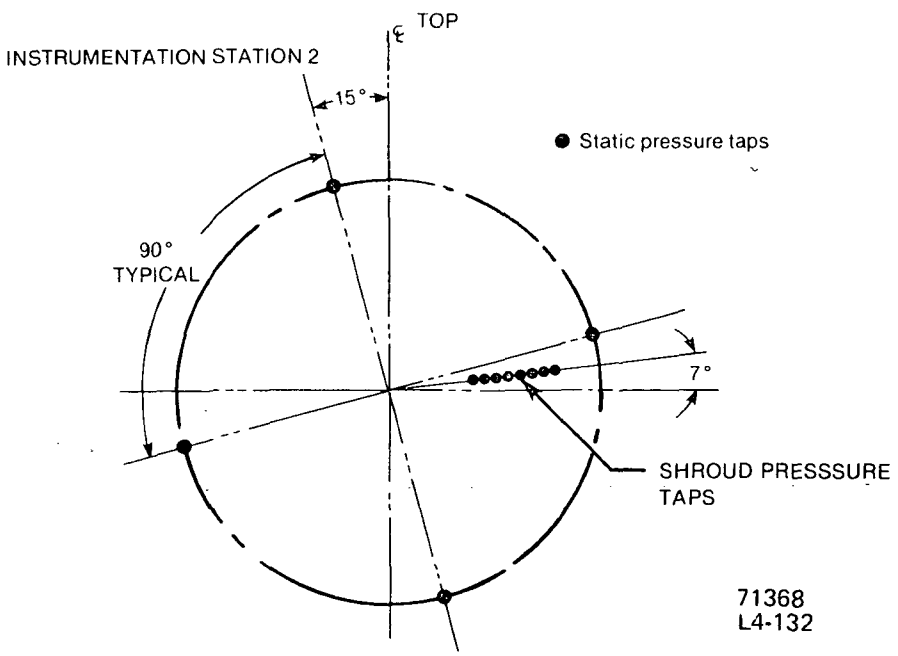

Figure 11. Vaneless Space (Station 2) and Rotor Shroud Static Pressure Circumferential Locations

ORIGINAL PAGE IS
OF POOR QUALITY

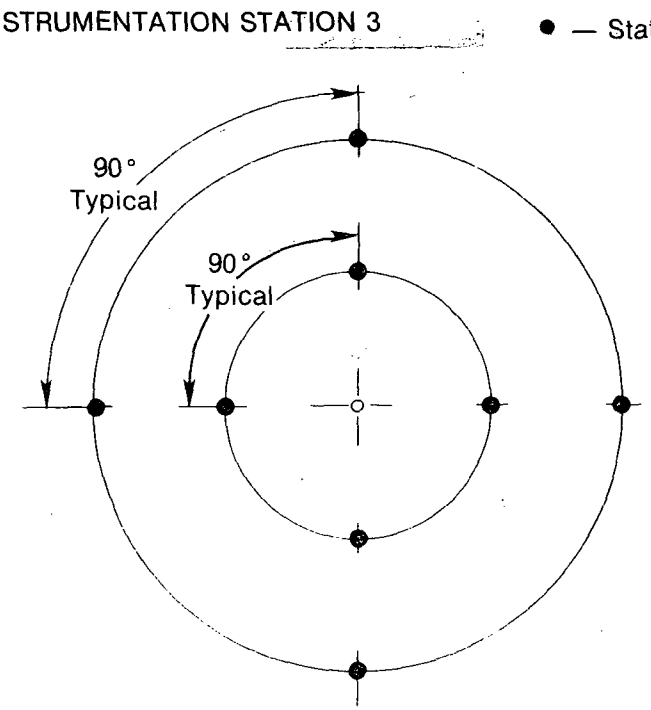

Figure 12. Rotor Exit (Station 3) Static Pressure Circumferential Location

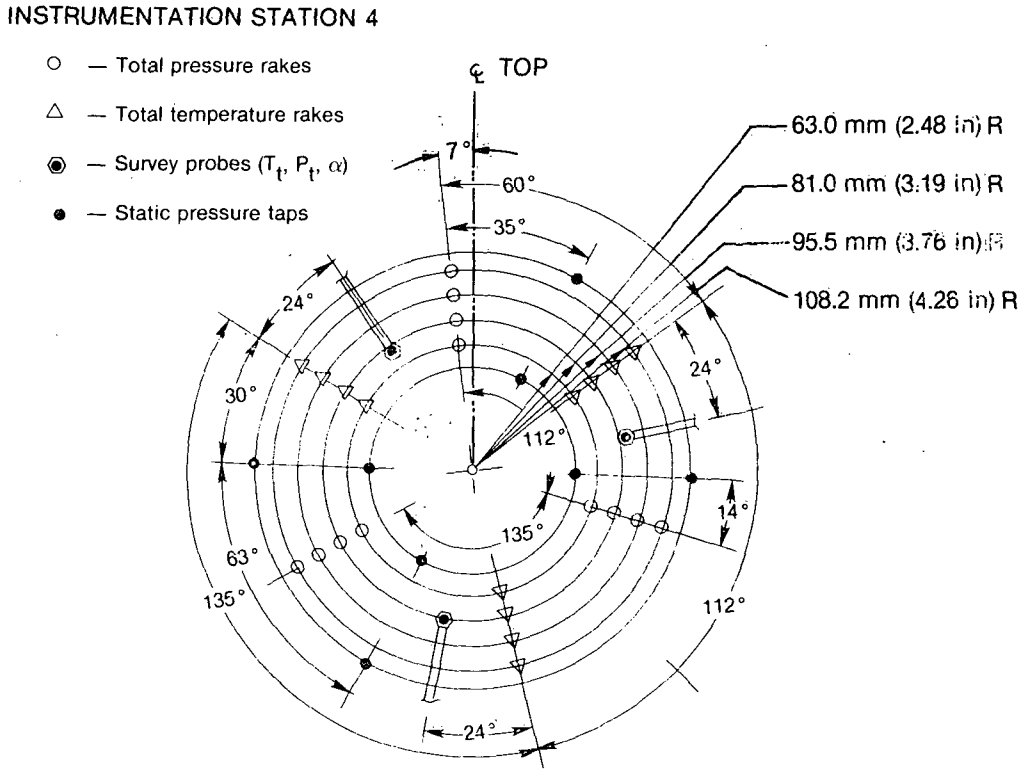

Figure 13. Exhaust Duct Mixed Out Plane (Station 4)- Circumferential Instrumentation Location

4.3.1 Instrumentation Type

The total pressure and the total temperature rakes as well as cobra survey probes used in this program are of conventional design. Figure 14 shows a 4-element total pressure rake designed to minimize the sensitivity to flow angle changes. An example of a 4-element, shielded total temperature rake is depicted in Figure 15. The shielded thermocouple was used because it requires much smaller Mach number correction in comparison to an exposed thermocouple and also possesses insensitivity to angle changes. Conventional self-nulling cobra probes (typical, shown in Figure 16) were used to conduct the total temperature, total pressure and the flow angle surveys. The probe was designed for simultaneous measurements of temperature, pressure and angle for any given insertion depth.

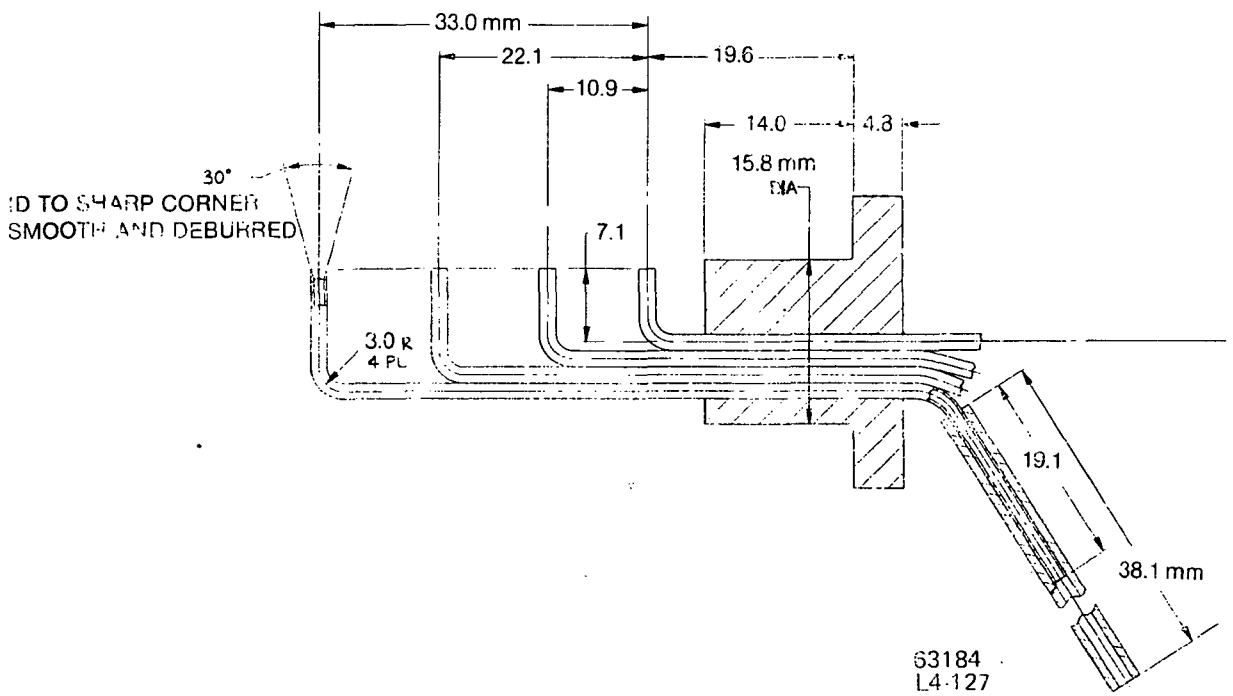

ure 14. Total Pressure Multi-Element Rake

ORIGINAL PAGE IS
OF POOR QUALITY

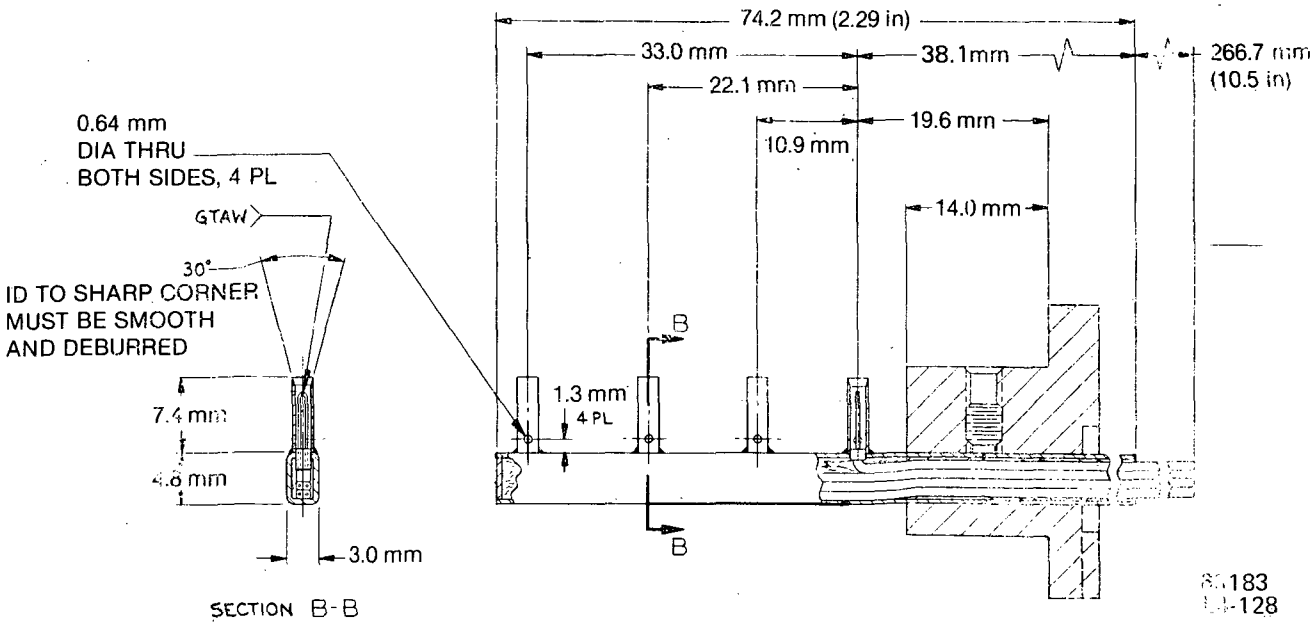

Figure 15. Total Temperature Multi Element Rake

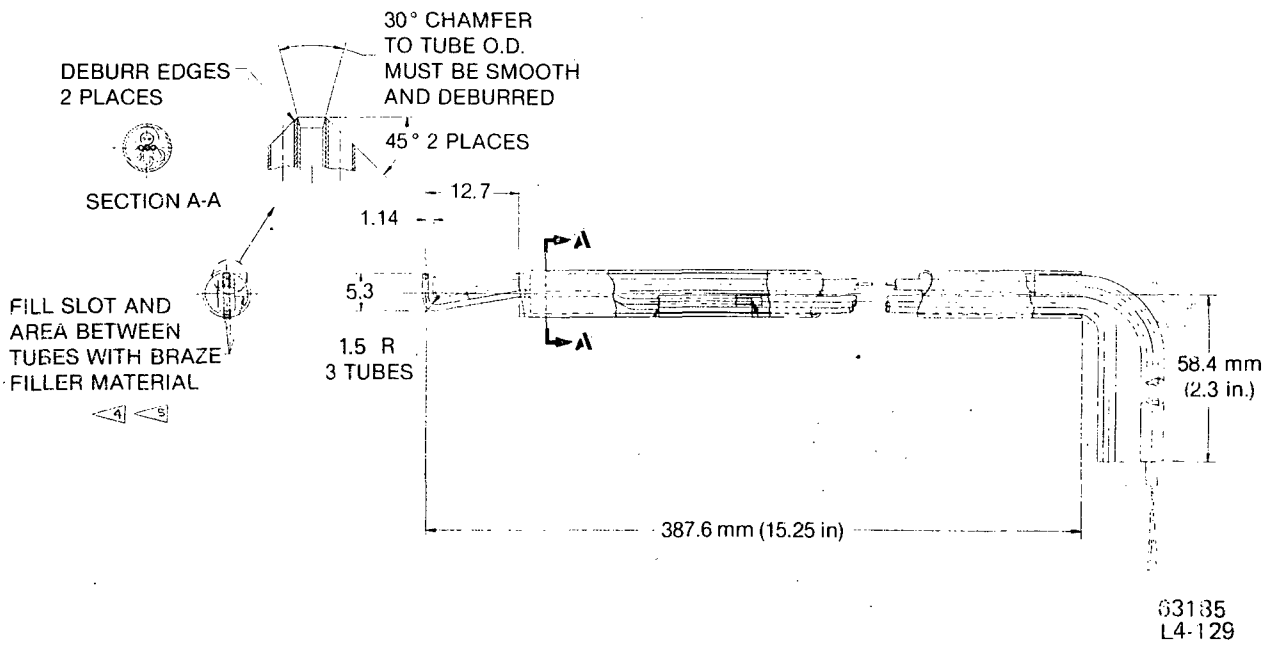

Figure 16. Multi Element Total Pressure, Total Temperature And Flow Angle Survey Probe

4.3.2 Instrumentation And Data Accuracy

All the static and the total pressures were measured with the use of the "AMETEK" Model 52 low range pressure transducers. The same type of transducer (but different range) was also used for the differential pressure measurements at the main flow orifice.

The temperature measurements are taken using a type "K" (Chromel/Alumel) thermocouple wire in conjunction with "ACROMAG" Model 344 thermocouple references.

The turbine shaft torque was measured with the use of a "Lebow" in-line torquemeter.

An estimation of the uncertainty associated with measurements of basic aerodynamic parameters as well as the error propagation for the data reduction calculations was carried out according to the statistical model of R. B. Abernethy et. al, Reference 6. Tables V, VI and VII show the precision and the bias error summaries for the pressure transducer, temperature sensor and the torque meter calibrations respectively. The estimated uncertainty of the measured and the calculated parameters is given in Table VIII.

TABLE V

BIAS AND PRECISION - PRESSURE TRANSDUCERS

PRESSURE CALIBRATION

COMPARISON	BIAS	PRECISION ERROR
NBS - Interlab Standard CEC 6-201 Primary Pressure Standard (to 600 psia)	±0.021% of Reading	±0.002 of Reading
Interlab Standard - Transfer Standard MENSOR UH-3 Quartz Manometer (to 200 psia)	±0.01% of Reading	±0.002% of Full Scale = 0.004 psi @ 25 psia = 0.016% of Rdg. @ 20 psia = 0.020% @ 13 psia = 0.031% @ 5 psia = 0.080% @ 3 psia = 0.133%
Transfer Standard - Working Standard (1)	-----	
Working Standard - Measuring Instrument (2) AMETEK Model 52 Pressure Transducer	±0.25% of Full Scale @ 15 psia = 0.0375 psi @ 50 psia = 0.125 psi @ 25 psia = 0.5% of Rdg @ 20 psia = 0.625% @ 13 psia = 0.288% @ 5 psia = 0.75% @ 3 psia = 1.25% @ 2 psia = 0.005 psi @ 50" H_2O = 0.275% of Rdg.	±0.25% of Full Scale @ 15 psia = 0.0375 psi @ 50 psia = 0.125 psi 0.5% of Rdg. 0.625% 0.288% 0.75% 1.25% 0.005 psi 0.275% of Rdg.

Nominal Pressure	3	5	13	20	25	50" H_2O Differential
BIAS % of Rdg.	1.250	0.751	0.289	0.625	0.500	0.276
Precision % of Rdg.	1.257	0.754	0.290	0.625	0.500	0.275
Uncertainty % of Rdg.	3.764	2.259	0.869	1.875	1.500	0.826

(1) MENSORS used as Working Standards
(2) Includes Data Acquisition System and Transducer Calibration

72095
L4-133

ORIGINAL PAGE IS
OF POOR QUALITY

TABLE VI

BIAS AND PRECISION - TEMPERATURE SENSORS

TEMPERATURE CALIBRATION TYPE "K"

COMPARISON	BIAS	PRECISION ERROR
NBS - Interlab Standard		
Interlab Standard Fluke 8575A	±0.00% of mv Reading 0.0075°F @ 250°F	-----
Interlab Standard - Working Standard LDC M V100/B	±0.005% of mv Reading 0.0125°F @ 250°F	-----
Working Standard - Measuring Instrument Elmer Perkins 7/32 Data Acquisition System	±1.44°F	0.61°F
Calibration and Recovery Factor Correction	±1.0 from 32°F to 530°F	-----

$$B = \pm \sqrt{(0.0075)^2 + (0.0125)^2 + (1.44)^2 + (1.0)^2}$$

$$= \pm 1.75°F$$

$$S = \pm \sqrt{(0.61)^2} = \pm 0.61°F$$

$$U = \pm (B + t_{95}S) = \pm [1.75 + 2(0.61)]$$

$$= \pm 2.97°F$$

72091
L4-134

TABLE VII
BIAS AND PRECISION SUMMARY-TORQUE MEASUREMENT SYSTEM

TORQUE MEASUREMENT

COMPARISON	BIAS	PRECISION
NBS - Interlab Standard	----	----
Interlab Standard - Transfer Standard	±0.05% of Reading	±0.02% of Reading
Transfer Standard - Measurement Instrument Strain Gage Torque Sensor 0-1000 in-lbs	±0.10% of Full Scale ±1 lb @ 500 = 0.2% of Rdg. @ 800 = 0.125%	±0.05% of Reading
Readout Model 770 Strain Gage Indicator 0-1500 in-lbs	±0.033% of Full Scale ±0.5 in lb @ 500 = 0.1% of Rdg. @ 800 = 0.0625%	±0.033% of Full Scale ±0.5 in lb @ 500 = 0.1 @ 800 = 0.0625

NOMINAL VALUE, in-lbs	500	800
Bias % of Rdg.	0.229	0.148
Precision % of Rdg.	0.114	0.0825
Uncertainty % of Rdg.	0.457	0.313

72092
L4-135

ORIGINAL PAGE IS
OF POOR QUALITY

TABLE VIII

SUMMARY - UNCERTAINTY-MEASURED AND

CALCULATED - AERODYNAMIC PARAMETERS

PARAMETER	UNITS	NOMINAL	BIAS	PRECISION INDEX	UNCERTAINTY	UNCERTAINTY IN PERCENT OF NOMINAL VALUE
Shaft Speed	rpm	19300	-	± 10	± 20	0.104
Shaft Torque	in-lbs	500	±1.145	±0.57	±2.285	±0.457
		800	±1.184	±0.66	±2.504	±0.313
Pressure	psia	25	±0.125	±0.125	±0.375	±1.500
		20	±0.125	±0.125	±0.375	±1.875
		13	±0.03757	±0.0377	±0.113	±0.869
		5	±0.03755	±0.0377	±0.113	±2.259
		3	±0.0375	±0.0377	±0.113	±3.764
	in_{H2O} Differential	50	±0.138	±0.1375	±0.413	±0.826
Temperature	°F	250	±1.75	±0.61	±2.97	±1.188
		40	±1.75	±0.61	±2.97	±7.425
Airflow	lb/sec	3.719	±0.42*	±0.328*	±1.076*	±1.076
Total-to-total Efficiency	percent	89	±0.478*	±0.171*	±0.82*	±0.82*

*Percentages of nominal value

72096
L4-136

4.4 DATA ACQUISITION

Several representative total temperature rakes and one survey probe were calibrated for recovery of the thermocouples. The recovery factor versus Mach no. data generated by this calibration was used in the data acquisition program to correct all temperature readings from the rigs and survey probes. This procedure was periodically repeated throughout all the test phases.

The nozzle inlet and rotor exit stations were each surveyed in the spanwise direction by three combination probes equally spaced around the circumference. Total pressure, temperature, and flow angle data was mass averaged to obtain a representative circumferential-radial average. Each of the survey probes were then stationed at fixed center of equal area locations. The average obtained from the three radially fixed probes was printed out for on-line review. A complete mass averaged survey was periodically conducted to determine correction as necessary.

The metering orifices for the nozzle and rotor coolant flow were calibrated over a range of total to static pressure ratios. The nozzle assembly was also calibrated separately.

The overall efficiency of the radial turbine was calculated using both the work based on temperature measurements as well as work based on the measured torque. In order to obtain the true torque deliverd by the turbine rotor, the measured torque was corrected for the effects of bearing and disk windage power dissipation. This was achieved by driving a bladeless rotor spindle with an air turbine drive and measuring the shaft torque. The bearing and windage losses measured in this manner was then used to correct the torque produced by the turbine.

An Interdata 732 computer was linked for data acquisiton and test support. All the probe readings and processed performance data were stored in the computer disk and also printed out by a deck writer for on-line review. Data stored in the computer disk were then transferred to magnetic tapes for additional data reduction and storage. A data point was reduced approximately every two and one half seconds and the average of ten values was then printed out for any given test point configuration. The data included corrected flow, flow speed parameter, equivalent speed, equivalent work, total-to-total pressure ratio, and total-to-total efficiency. A typical data output sheet is shown in Figure 17.

4.4.1 Test Matrix

The overall performance of the radial turbine was evaluated for various values of mass flows, shaft speeds, and pressure ratios. In addition, conditions with and without cooling and with and without vane sidewall leakage were investigated. A summary of all the test conditions evaluated can be found in Tables IX and X. The pressure ratio groups I and II referred to in this table consisted of 5 and 10 pressure ratios, respectively, each group covering a range from 50 percent below to 50 percent above and including the design pressure ratio. At selected test points, surveys of total pressure, total temperature, and flow angle at the turbine exit were conducted. Testing was conducted with a moveable shroud wall and a moveable hub wall geometry. A ring insert in the sidewall permitted evaluations with a high radius and low radius split line.

COMPONENT TEST CT1656 — N.A.S.A. TURBINE DATA REDUCTION POINT # 75

TIME / PT1 / TT1	SPEED / PT3 / TT3	PNHCOR / PT4 / TT4	WORK / PR1 / PR2	TORQH / PR3 / PRBD	TORQ / WA/C / WABD	FSP / WAM / WLAB	TUMX / WAN / WAR	PRAT / WPU / WPL	UVOI / WAFT / RAD	E-TEMP / ETS / YAW	E-TORQ / ETS / LOC	TREF1 / E-AERO / %BLDN	TREF2 / PS2AV / %BLDR
20:26:17	15859	99.50	38.49	38.48	41.41	607.11	50.80	0.00	0.93	87.92	87.92	459.7	459.7
23.11	0.00	5.09	4.542	5.210	2.297	3.024	0.000	0.000	0.000	82.09	82.08	87.92	11.05
737.7	0.0	510.5	5.239	2.091	4.805	0.000	0.000	0.000	0.00	0	0	0.00	0.00
20:26:20	15857	99.49	38.47	38.37	41.35	607.79	51.02	0.00	0.94	87.88	87.65	459.7	459.7
23.11	0.00	5.09	4.542	5.211	2.300	3.028	0.000	0.000	0.000	82.04	81.83	87.88	11.04
737.9	0.0	510.7	5.240	2.093	4.814	0.000	0.000	0.000	0.00	0	0	0.00	0.00
20:26:21	15822	99.27	38.49	38.40	41.47	606.45	50.87	0.00	0.93	87.94	87.73	459.7	459.7
23.11	0.00	5.09	4.541	5.211	2.300	3.028	0.000	0.000	0.000	82.09	81.89	87.94	11.04
737.9	0.0	510.6	5.240	2.093	4.815	0.000	0.000	0.000	0.00	0	0	0.00	0.00
20:26:22	15855	99.48	38.48	38.33	41.33	607.97	50.73	0.00	0.94	87.92	87.57	459.7	459.7
23.11	0.00	5.09	4.542	5.211	2.301	3.030	0.000	0.000	0.000	82.07	81.74	87.92	11.04
737.6	0.0	510.4	5.240	2.094	4.819	0.000	0.000	0.000	0.00	0	0	0.00	0.00
20:26:23	15845	99.41	38.48	38.36	41.37	607.27	50.80	0.00	0.94	87.92	87.66	459.7	459.7
23.11	0.00	5.09	4.541	5.211	2.300	3.028	0.000	0.000	0.000	82.06	81.82	87.92	11.03
737.7	0.0	510.5	5.240	2.095	4.819	0.000	0.000	0.000	0.00	0	0	0.00	0.00
20:26:25	15854	99.47	38.45	38.39	41.35	607.22	51.02	0.00	0.94	87.86	87.72	459.7	459.7
23.11	0.00	5.09	4.540	5.211	2.298	3.026	0.000	0.000	0.000	82.00	81.87	87.86	11.03
737.7	0.0	510.7	5.240	2.095	4.817	0.000	0.000	0.000	0.00	0	0	0.00	0.00
20:26:27	15842	99.39	38.48	38.52	41.41	605.13	50.66	0.00	0.93	87.92	88.02	459.7	459.7
23.11	0.00	5.09	4.540	5.211	2.292	3.019	0.000	0.000	0.000	82.05	82.15	87.92	11.03
737.4	0.0	510.4	5.240	2.096	4.804	0.000	0.000	0.000	0.00	0	0	0.00	0.00
20:26:28	15825	99.29	38.47	38.53	41.42	603.85	50.80	0.00	0.93	87.89	88.03	459.7	459.7
23.12	0.00	5.09	4.541	5.213	2.289	3.016	0.000	0.000	0.000	82.03	82.16	87.89	11.03
737.6	0.0	510.5	5.242	2.097	4.801	0.000	0.000	0.000	0.00	0	0	0.00	0.00
20:26:29	15809	99.19	38.43	38.33	41.44	606.13	51.45	0.00	0.93	87.81	87.58	459.7	459.7
23.12	0.00	5.09	4.541	5.212	2.300	3.029	0.000	0.000	0.000	81.95	81.73	87.81	11.02
738.2	0.0	511.1	5.242	2.098	4.827	0.000	0.000	0.000	0.00	0	0	0.00	0.00
20:26:31	15848	99.43	38.45	38.36	41.34	607.16	51.09	0.00	0.94	87.85	87.65	459.7	459.7
23.12	0.00	5.09	4.540	5.212	2.299	3.027	0.000	0.000	0.000	81.99	81.80	87.85	11.02
737.8	0.0	510.8	5.242	2.098	4.824	0.000	0.000	0.000	0.00	0	0	0.00	0.00
AVERAGED DATA REDUCTION VALUES													
20:26:32	15842	99.39	38.47	38.41	41.39	606.61	50.93	0.00	0.93	87.89	87.75	459.7	459.7
23.11	0.00	5.09	4.541	5.211	2.297	3.026	0.000	0.000	0.000	82.04	81.91	87.89	11.02
737.7	0.0	510.6	5.241	2.095	4.814	0.000	0.000	0.000	0.00	0	0	0.00	0.00
AVERAGED DATA REDUCTION VALUES IN * S.I. UNITS													
20:26:32	15842	99.39	89.42	89.27	96.20	275.15	118.37	0.00	0.93	87.89	87.75	255.4	255.4
159.36	0.00	35.09	4.541	5.211	1.042	1.372	0.000	0.000	0.000	82.04	81.91	87.89	75.96
409.9	0.0	283.7	5.241	2.095	2.184	0.000	0.000	0.000	0.00	0	0	0.00	0.00

* SI UNITS: Temperature (k), Pressures (kPa), Mass Flow (kg/s), Work (kJ/kg), FSP (rev.kg/s^2)

Figure 17. Typical Data Reduction Output Sheet.

TABLE IX

MOVEABLE SHROUD WALL TEST MATRIX

TEST SERIES	TEST NO.	STATOR AREA SETTING % OF MAX	STATOR CONFIGURATION	COOLING		LEAKAGE		SPEED% OF DESIGN	PRESSURE RATIO GROUP
				WITH	WITHOUT	WITH	WITHOUT		
A	1-5	100	MOVEABLE SHROUD LOW RADIUS DUMP		0	0		100	I
B	6-10	78	MOVEABLE SHROUD HIGH RADIUS DUMP		0		0	100	I
C	11-15	100	↓	0		0		100	II
D	16-45	100	↓		0	0		100, 80, 64	I
E	46-50	78	↓	0		0		100	I
F	51-80	78	↓		0	0		100, 80, 60	II
G	81-85	50	↓	0		0		100	I
H	86-115	50	↓		0	0		100, 80, 60	II
I	116-120	100	MOVEABLE SHROUD LOW RADIUS DUMP		0		0	100	I
I	121-125	78	↓		0		0	100	I
I	126-130	50	↓		0		0	100	I

70427
L4-084

TABLE X

MOVEABLE HUB WALL TEST MATRIX

TEST SERIES	TEST NO.	STATOR AREA SETTING % OF MAX	STATOR CONFIGURATION	COOLING		LEAKAGE		SPEED % OF DESIGN	PRESSURE RATIO GROUP
				WITH	WITHOUT	WITH	WITHOUT		
J	131-135	100	MOVEABLE HUB HIGH RADIUS DUMP	0		0		100	I
J	136-140	100			0	0		80	I
J	141-145	100			0	0		60	I
K	146-150	78		0		0		100	I
K	151-155	78		0		0		80	I
K	156-160	78		0		0		60	I
L	161-165	50		0		0		100	I
L	166-170	50			0	0		80	I
L	171-175	50			0	0		60	I

70428
L4-088

SECTION 5.0
OVERALL PERFORMANCE

5.1 MOVEABLE SHROUD WALL CONFIGURATION

5.1.1 Baseline Tests

The first turbine configuration was built with the moveable nozzle sidewall in the design or flush wall position with the vane sidewall gaps sealed, Figure 18.. Due to deviant tolerances and stack-up the initial rotor clearances were higher than desired. The measured and design clearances are given in the table of Figure 18. The larger than design rotor/shroud clearances allowed shake down testing to be conducted and reduced the probabilities of a rub occurance. The clearance between the nozzle vane profile and the sidewall was 0.406 mm (0.016 in). This value was considered as representative of a minimum practical value required in an engine application. To establish a baseline, the first test, Series I, Table IX, was conducted with this sidewall gap sealed with a room temperature vulcanized silicone "Silastic" adhesive. Figure 19 shows the overall efficiency measured on this configuration at 100 percent equivalent speed. The overall efficiency is based on the turbine total-to-total pressure ratio and temperature drop. Data is also shown based on measured torque values. Excellent agreement is shown between the two methods of calculating the turbine efficiency. At the design pressure ratio of 4.54 the efficiency was 86.8 percent. The design point efficiency of 88.0 percent, as given in Reference 1, is based on the total-to-total pressure ratio from inlet to the turbine to the exducer trailing edge and did not include rotor wake mixing and duct pressure losses. In reference 5 a research turbine with very similar geometry and characteristics was surveyed immediately downstream of the exducer and also in a mixed out plane nearly identical to the current tests. The wake mixing and duct losses were measured as 0.7 points of turbine total-to-total efficiency. Applying this value gives a design point efficiency of 87.3 percent at the mixed out measuring plane station 4, Figure 9. The 0.5 lower than design efficiency is mostly attributable to high running clearances.

Figure 19 also shows the turbine equivalent work as a function of total-to-total pressure ratio. The measured work at design pressure ratio was 88.7 kJ/kg (38.02 Btu/lb). This is slightly lower than design (0.7 points) and again due to high first build running clearances. The equivalent work continues to increase at all pressure ratios tested up to a pressure ratio of 6.0. Testing was limited to this pressure ratio due to freezing of the thermocouples at the turbine exit and the limits of the turbine facility. The equivalent work curve shows that limit loading on the turbine was not approached since the characteristic shows increasing work with increasing pressure ratio.

Figure 20 shows the equivalent flow and exit swirl characteristics measured on the turbine. At the design pressure ratio of 4.54 the design flow of 1.044 kg/s was achieved. The measured average exit swirl was 25 degrees against rotation as compared to the design value of 10 degrees against rotation at the mean section. This higher than design exit swirl is indicative of the higher operating clearances and perhaps a nozzle to rotor area mismatch.

ORIGINAL PAGE IS
OF POOR QUALITY

BUILD GEOMETRY
NOZZLE AREA = 78% MAXIMUM

	BACK FACE		FRONT FACE		EXDUCER	
	mm	% TIP WIDTH	mm	% TIP WIDTH	mm	% EXDC. HEIGHT
1ST BUILD	1.42	9.2	0.68	4.4	0.79	1.3
DESIGN	0.86	5.5	0.41	2.6	0.43	0.7

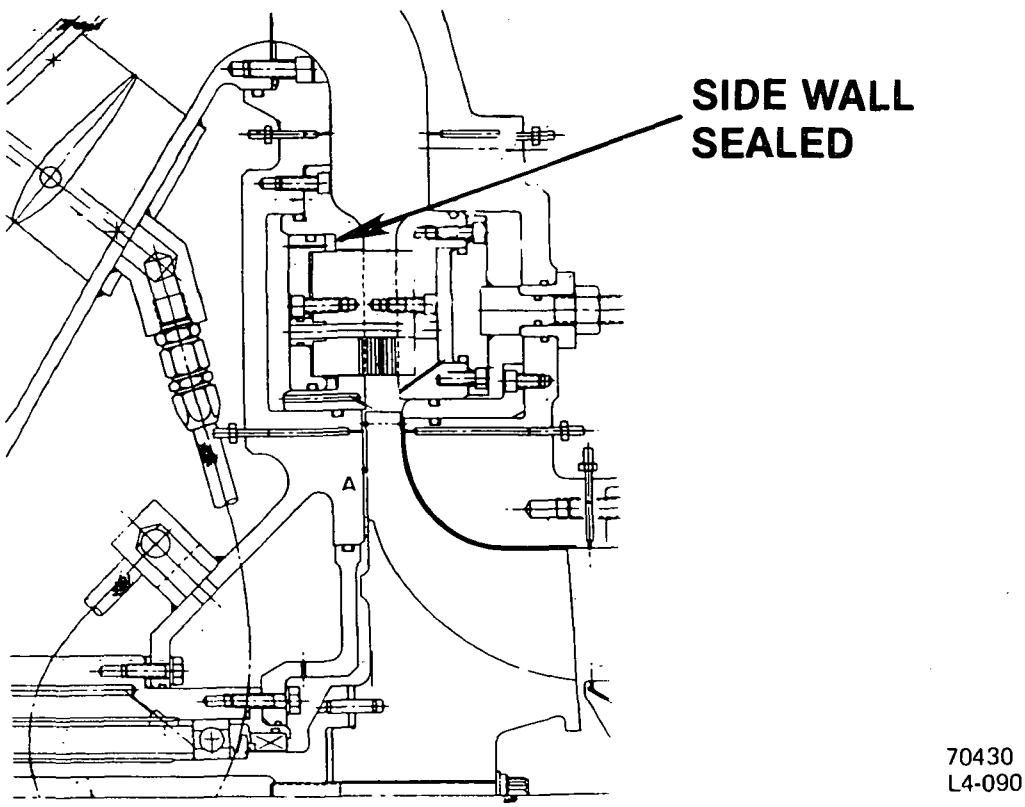

Figure 18. First Build Test Configuration.

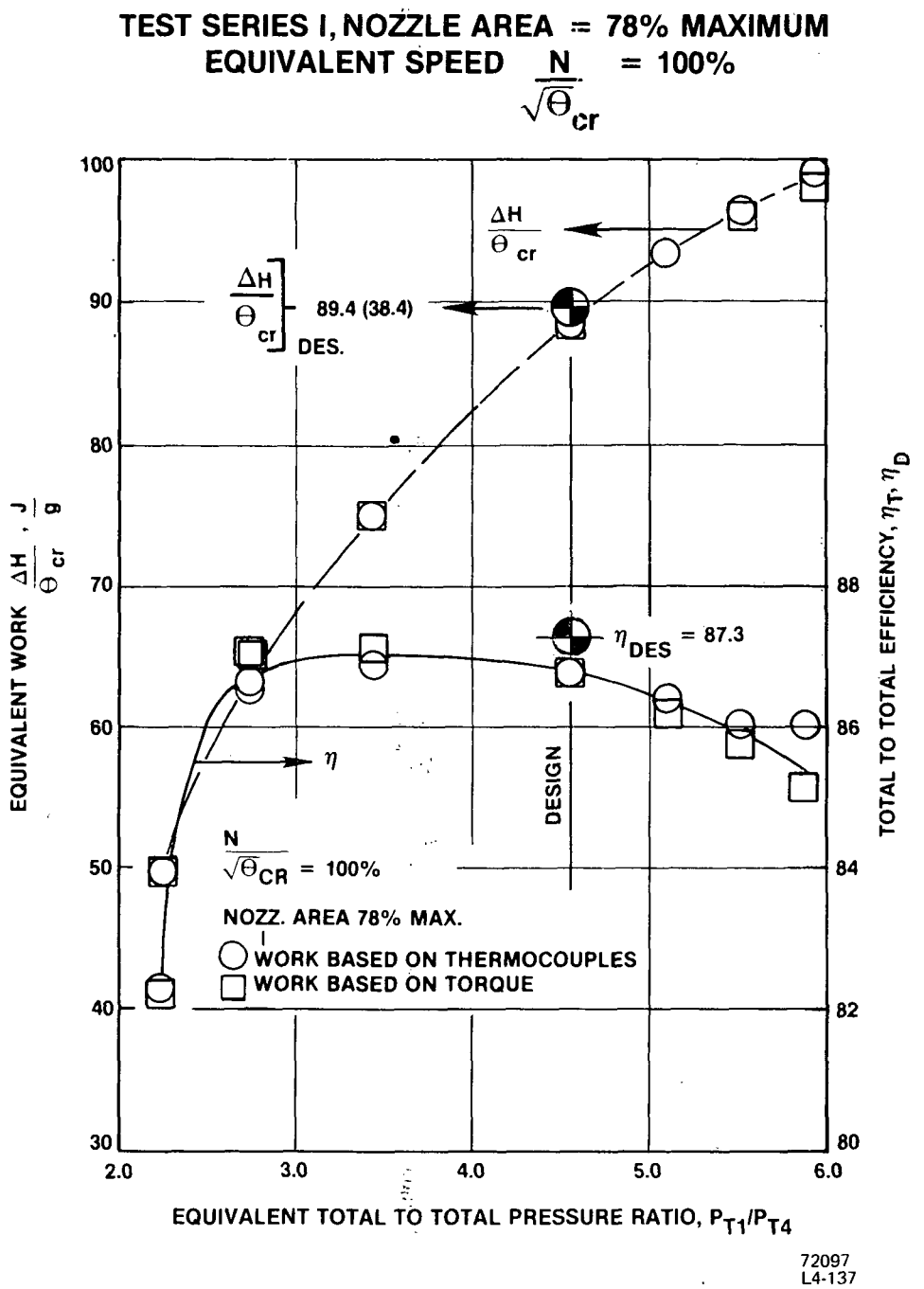

Figure 19. First Build - Overall Turbine Performance.

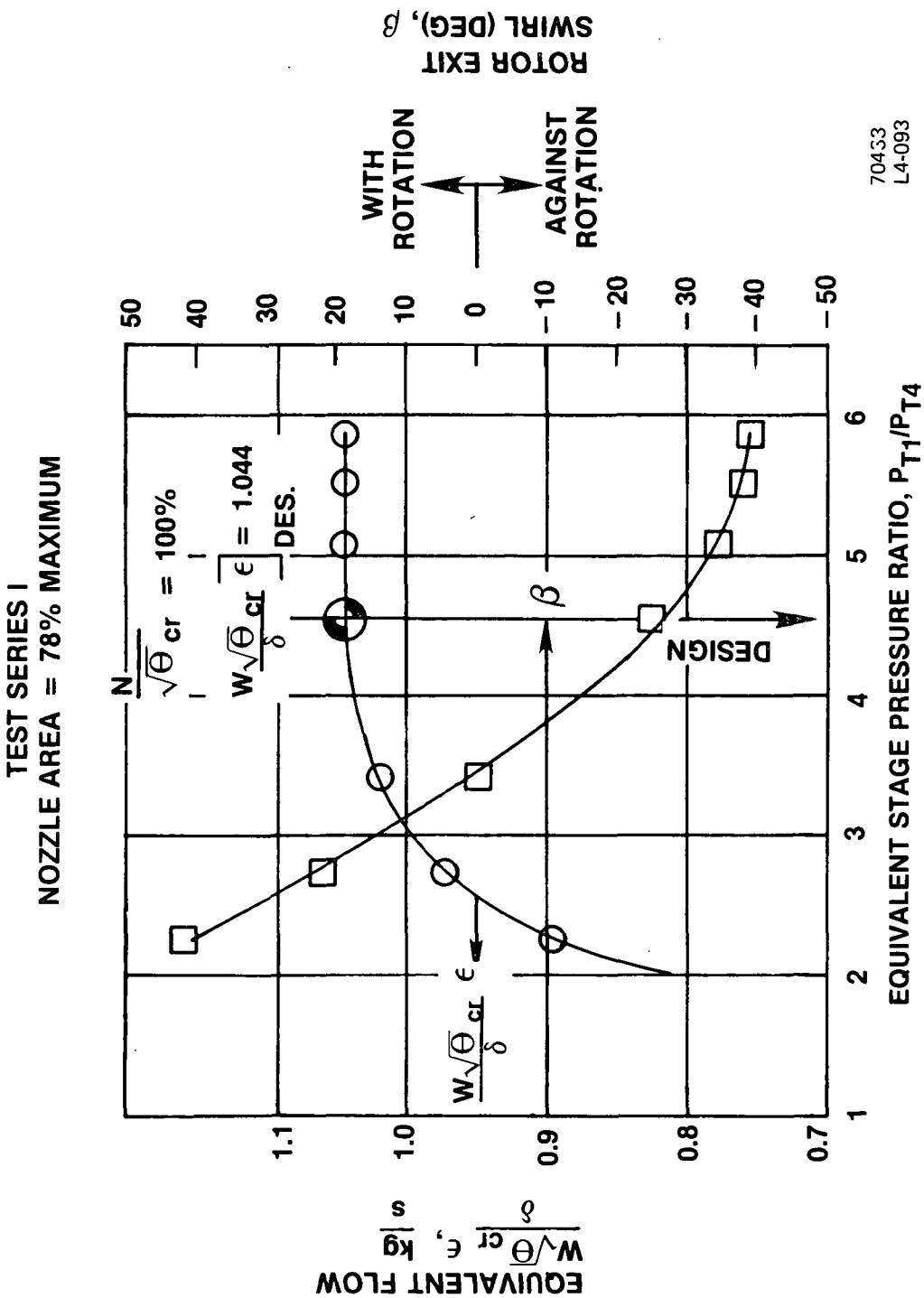

Figure 20. First Build - Flow and Exit Swirl Characteristics at 100 Percent Equivalent Speed.

The overall efficiency of this turbine build at design clearances was estimated from the test data of References 7 through 9. The efficiency loss data from these references were normalized and plotted as a function of percent passage clearance height for the exducer, inducer backface, and inducer front face clearances, Figure 21. Figure 22 shows the efficiency of the turbine normalized to the design clearance values shown in Figure 19. At the design total-to-total pressure ratio a total-to-total efficiency of 88.1 is shown which exceeds the design value of 87.3. However, additional losses were incurred later when cooling flows were injected, Section 5.1.4. All subsequent testing on the turbine was conducted with the rotor clearances close to the values as shown in Figure 18 and did not require clearance correction.

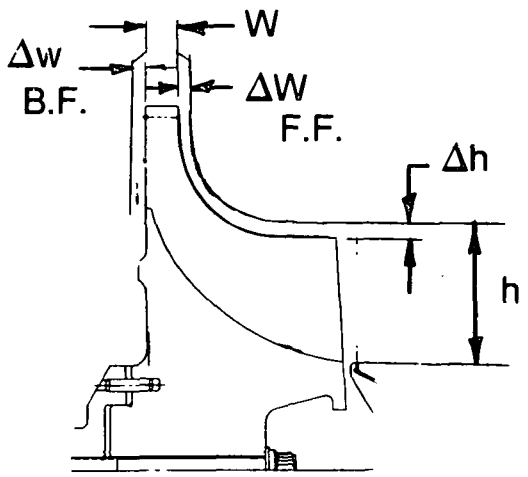

CLEARANCE CORRECTION

$$\Delta\eta/\eta]_{TOT} = 0.17\,(\Delta w/w - \Delta w_D/w_D)_{B.F.}$$

$$+ 0.14\,(\Delta w/w - \Delta w_D/w_D)_{F.F.}$$

$$+ 1.10\,(\Delta h/h - \Delta h_D/h_D)$$

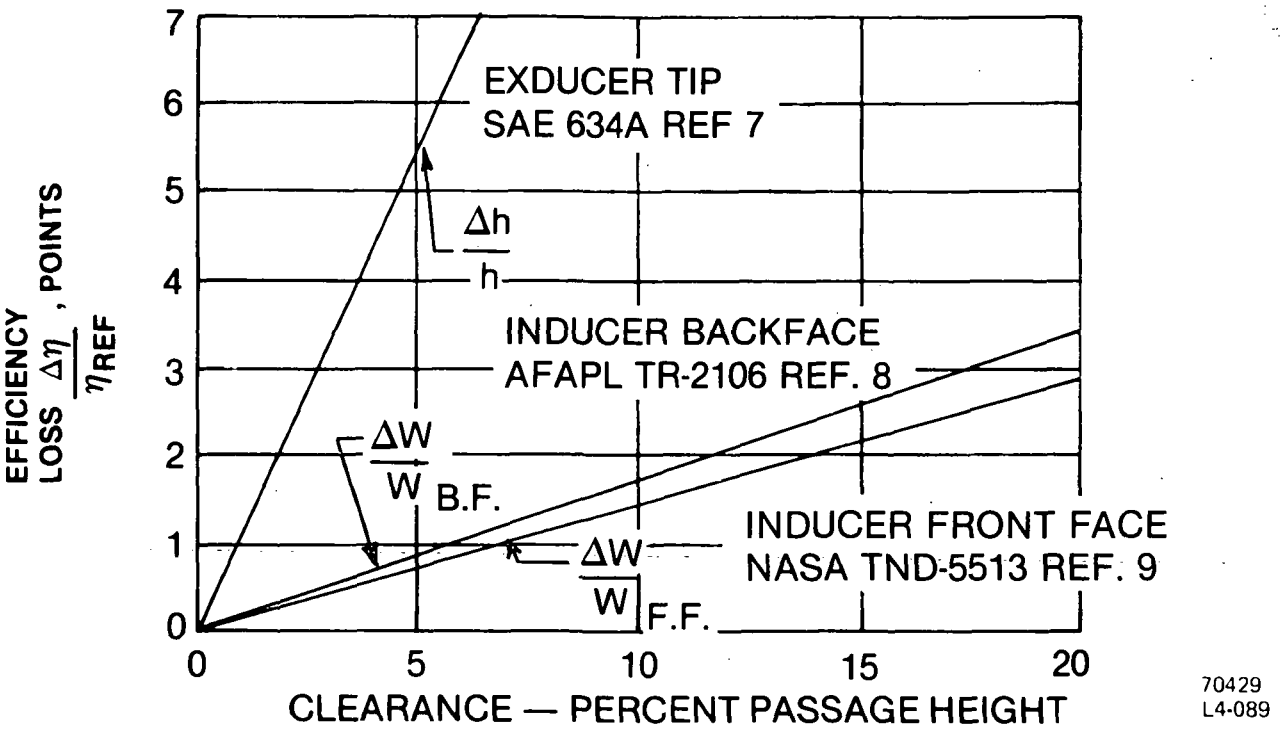

Figure 21. Rotor Clearance Effects on Stage Efficency.

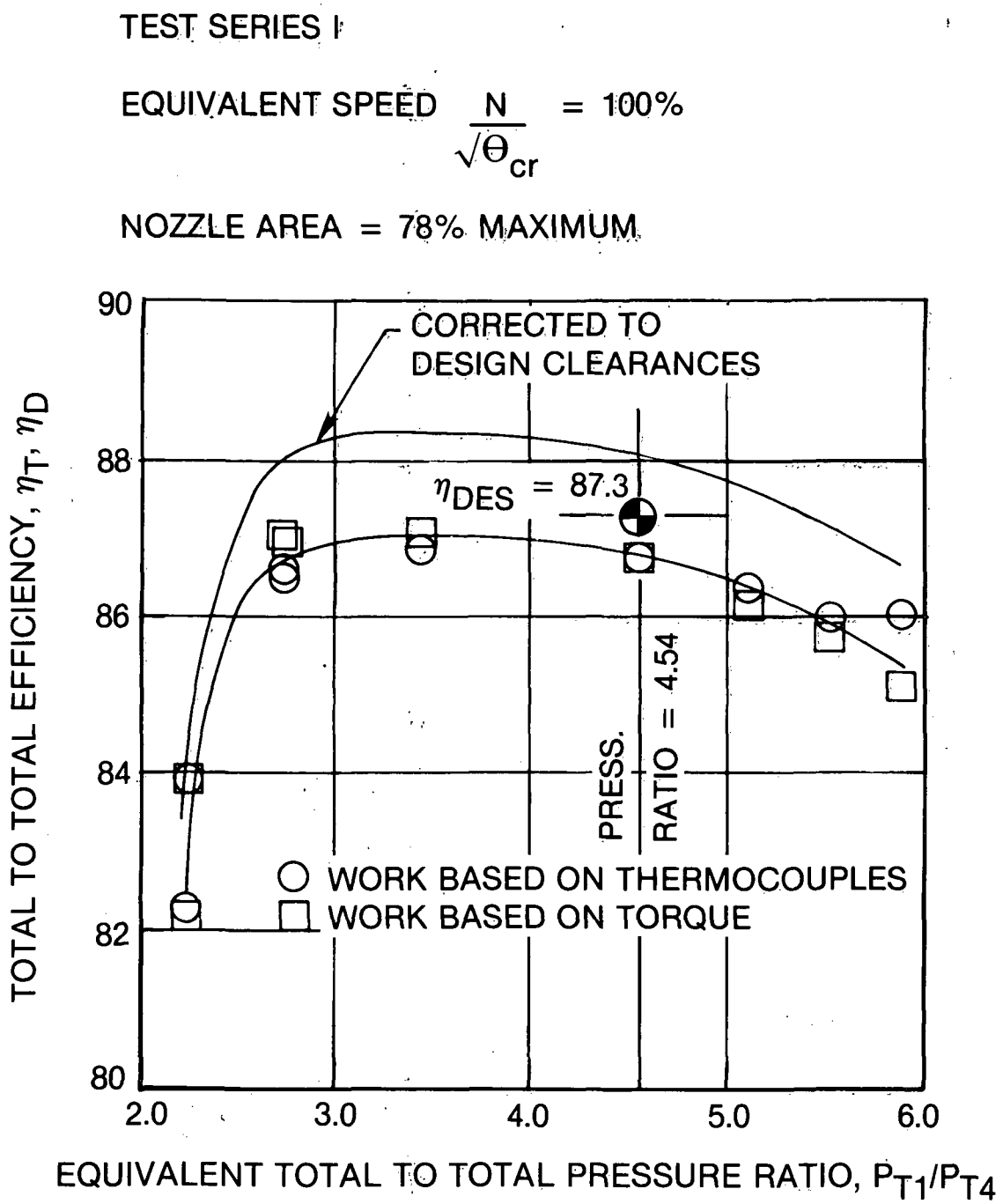

Figure 22. First Build - Overall Stage Performance Corrected to Design Clearances.

5.1.2 Effect Of Sidewall Leakage And Splitline Radius

Figure 23 shows a cross-section of the turbine and the nozzle assembly. A principle source of leakage and efficiency loss in the nozzle is shown in this figure. A clearance gap of 0.406 mn (0.016 in) between the cantilvered vanes and the nozzle sidewall is required to allow free movement of the nozzle assembly. The leakage flow moves from the high pressure source along the vane to sidewall clearance gap and re-enters the mainstream downstream of the nozzle throat. Reference 4 showed that an efficiency loss as high as 2.5 points can be incurred along with a flow increase of nearly 8 percent with this leakage source. Section A-A of Figure 23 shows a sealing arrangement that was devised to reduce this leakage flow. Flexible metal "L" seals were attached around the pressure and suction surfaces of the nozzle and were fixed to the inner nozzle sidewall by a number of attaching screws. A variation of this seal arrangement with welded attachments could be typically used in an actual high temperature environment.

A test was conducted at 100 percent equivalent speed with the "L" seals in place and with the nozzle sidewalls in the flush position, i.e. 78 percent maximum area. Figure 24 shows a comparison between this current Test Series and a similar test with the sidewall completely sealed with a vulcanized silicone material, Test Series F, Table IX. Over most of the pressure ratio range of interest the efficiency loss with the "L" seals in place was less than 1/2 point.

A similar test was conducted with the sidewall moved to the 100 percent maximum area position. Figure 25 shows the comparative data and the loss due to leakage past the "L" seals. The indicated efficiency loss is shown as approximately 1.0 points over most of the pressure ratio range tested.

This leakage loss could be further reduced by relocating the seal as shown in Figure 26. Locating the seal near the main flowpath wall would narrow the leakage path to a fraction of its present value.

The next test was conducted to evaluate the effect of splitline radius on the moveable shroud wall geometry. The sidewall nozzle was disassembled and reassembled with a high radius ring, as shown in Figure 27. The nozzle sidewall was positioned at 100 percent maximum area and the test was conducted at 100 percent speed. Figure 27 shows the performance comparison between a low radius splitline and a high radius splitline configuration. The low radius splitline configuration showed an approximate 1.0 point better efficiency over a pressure ratio range from 3.0 to 5.0.

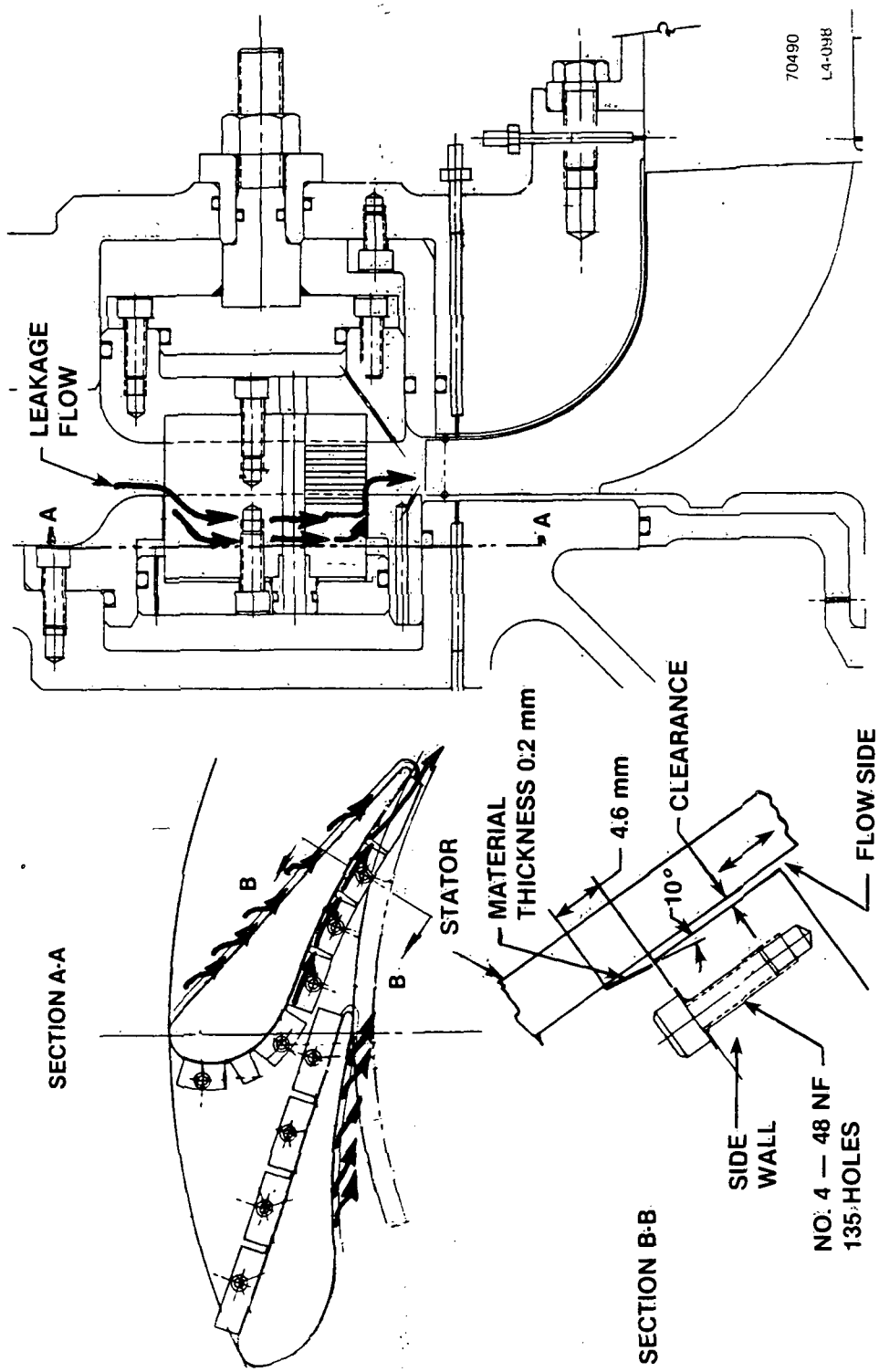

Figure 23. Nozzle Sidewall Leakage Paths.

ORIGINAL PAGE IS
OF POOR QUALITY

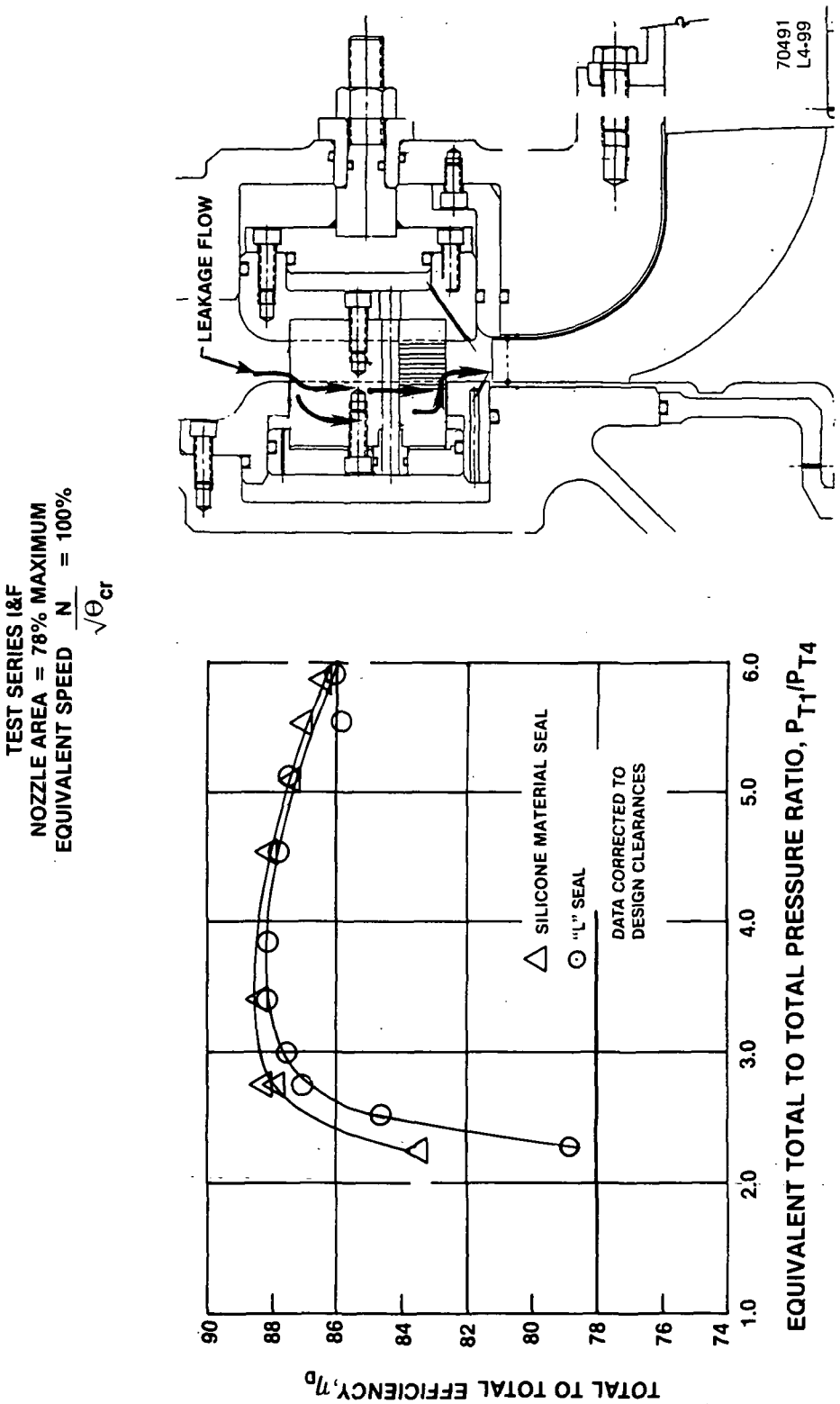

Figure 24. Overall Performance - Effect of Vane Sidewall Leakage with Nozzle in Flush Position.

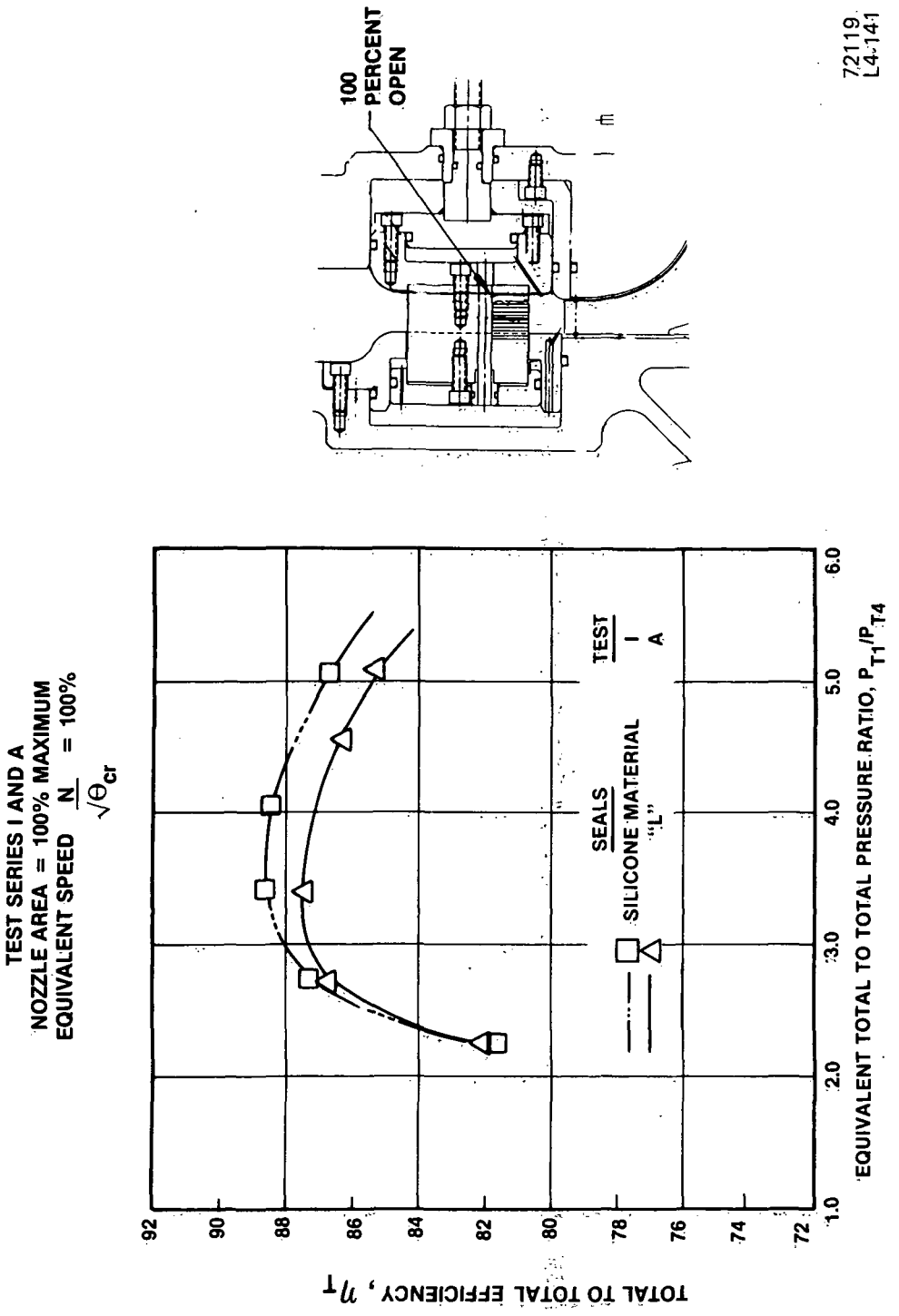

Figure 25. Overall Performance - Effect of Vane Sidewall Leakage with Nozzle in 100 Percent Open Position.

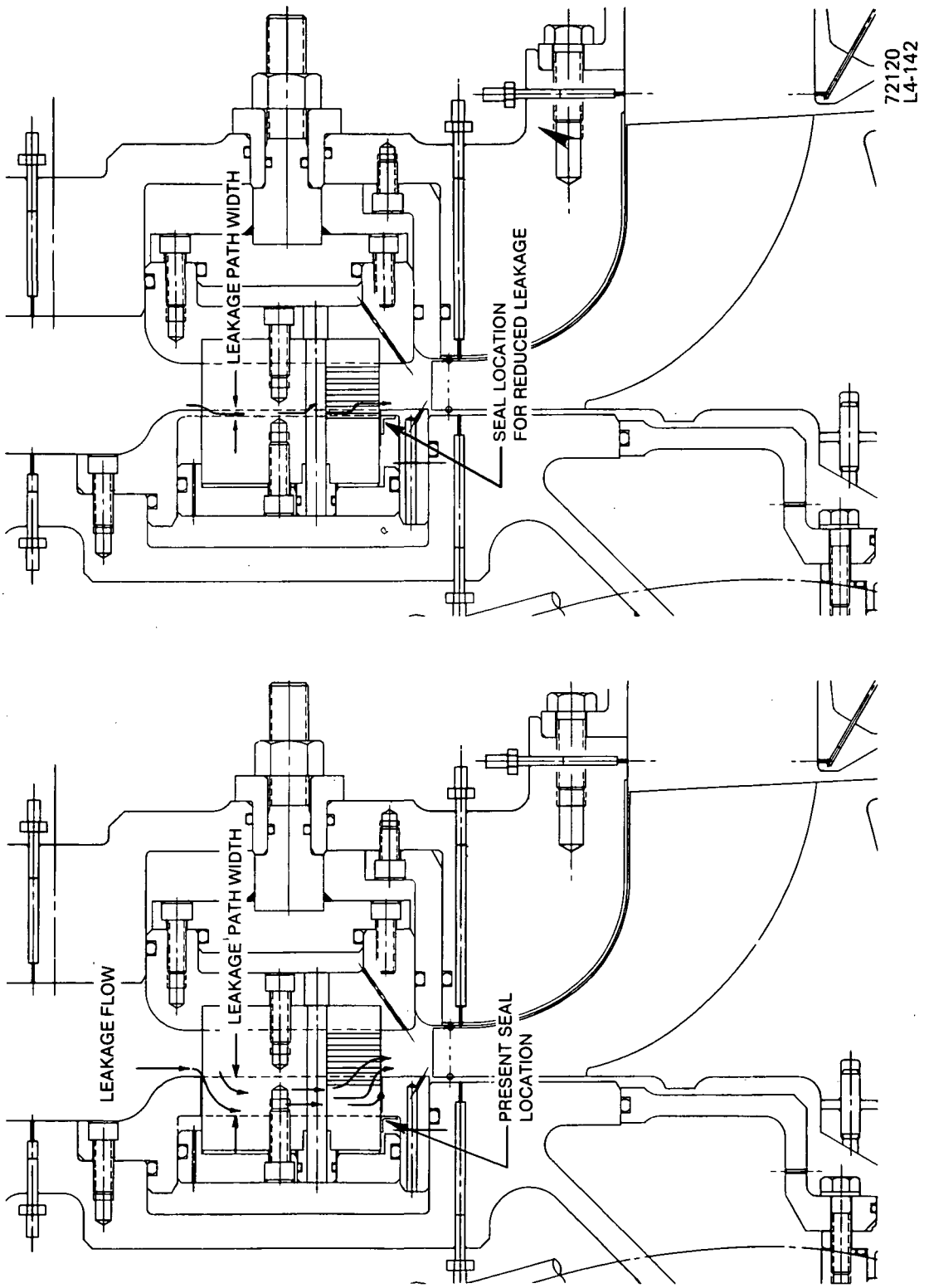

Figure 26. Relocation of Nozzle Seals to Reduce Sidewall Leakages.

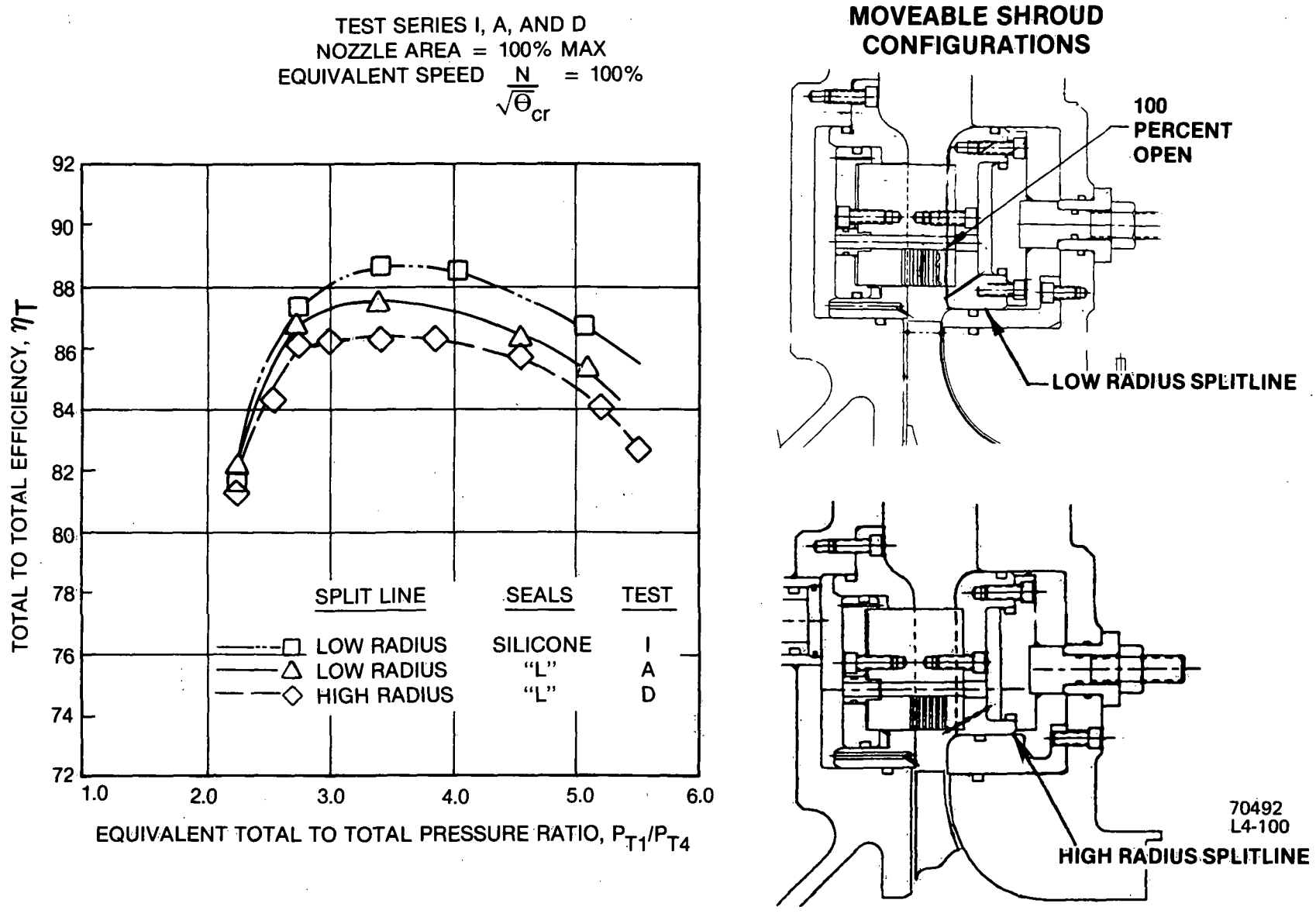

Figure 27. Overall Performance - Effect of Nozzle Splitline Location.

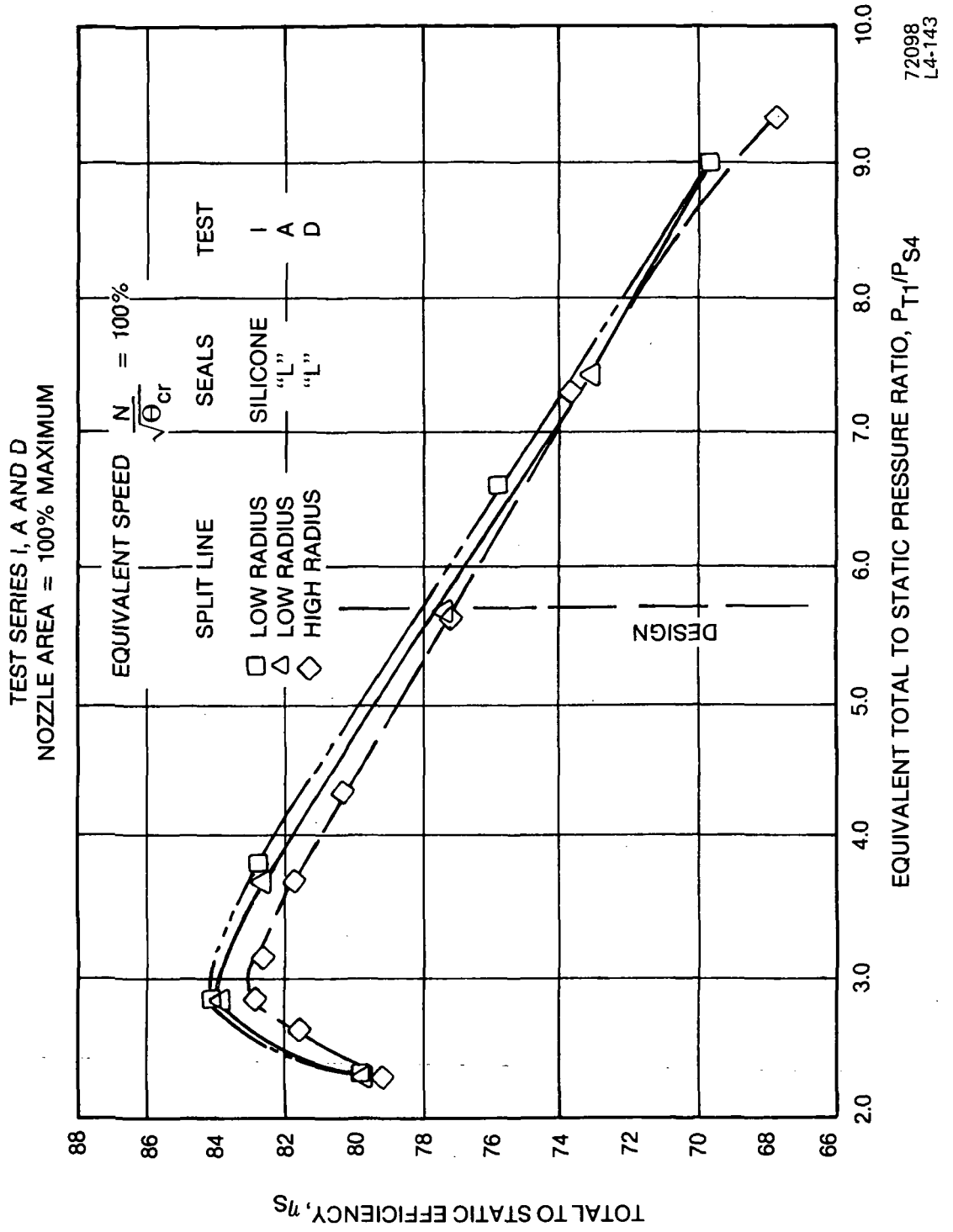

Figure 28. Effect of Leakage and Splitline Location on Performance - Total to Static Efficiencies.

The low radius splitline configuration may have a higher performance potential due to the location of the sudden contraction loss. With a low radius splitline most of the flow disturbance would be expected to occur within the rotor where the relative Mach numbers are considerably lower than the absolute plane. Also the high radius splitline would have disturbances occuring at higher absolute Mach number levels, therefore contributing to higher losses.

The performance data of Figures 25 and 27 is also given in the form of total to static efficiencies vs. total to static pressure ratio in Figure 28. In the wide open nozzle position the duct Mach numbers and swirl values are very high and the exit total pressure measurements could be less accurate than static pressures. The performance trends are confirmed. Leakage loss is negligible and the low radius split line shows about 1.0 points improvement over the high radius configuration over most of the pressure ratio range tested.

5.1.3 Overall Performance - Nozzle In Flush Wall Position

Additional data were acquired with the sidewall in the flush position with rotative speeds of 100 percent, 80 percent and 64 percent. The metal "L" seals were used on this test and throughout all the remaining test configurations. Figure 29 shows the overall efficiency as a function of total-to-total pressure ratio and equivalent speed. The turbine work is measured directly by thermocouple rakes and alternatively from flow, speed, and inline shaft torque. Data agreement between the two methods was usually very good as shown on the 100 percent design equivalent speed line. In some of the tests, however, the data were acquired with the power absorption water brake operating in an unstable region causing high torque fluctuations. In this case a low pass filter attenuates the torque signal and biases readings to lower than true values. Because of their low response rate, the thermocouples used to measure work provided a more reliable measure of efficiency and were used for all subsequent comparisons.

Figure 30 shows the equivalent flow and work as a function of total-to-total pressure ratio and referred speed. The choking characteristics, at lower speeds and above a pressure ratio of 3, show that the nozzle is controlling the flow. At design speed the choke flow decreased 1.2 precent indicating rotor flow control. The work characteristics shown in this same figure show that at all pressure ratios tested, up to the facility limit, the turbine did not approach a limit loading condition. Figure 31 shows an overall performance map for the Test Series F with the moveable shroud wall in the flush position and with metal wiper seals on the vanes.

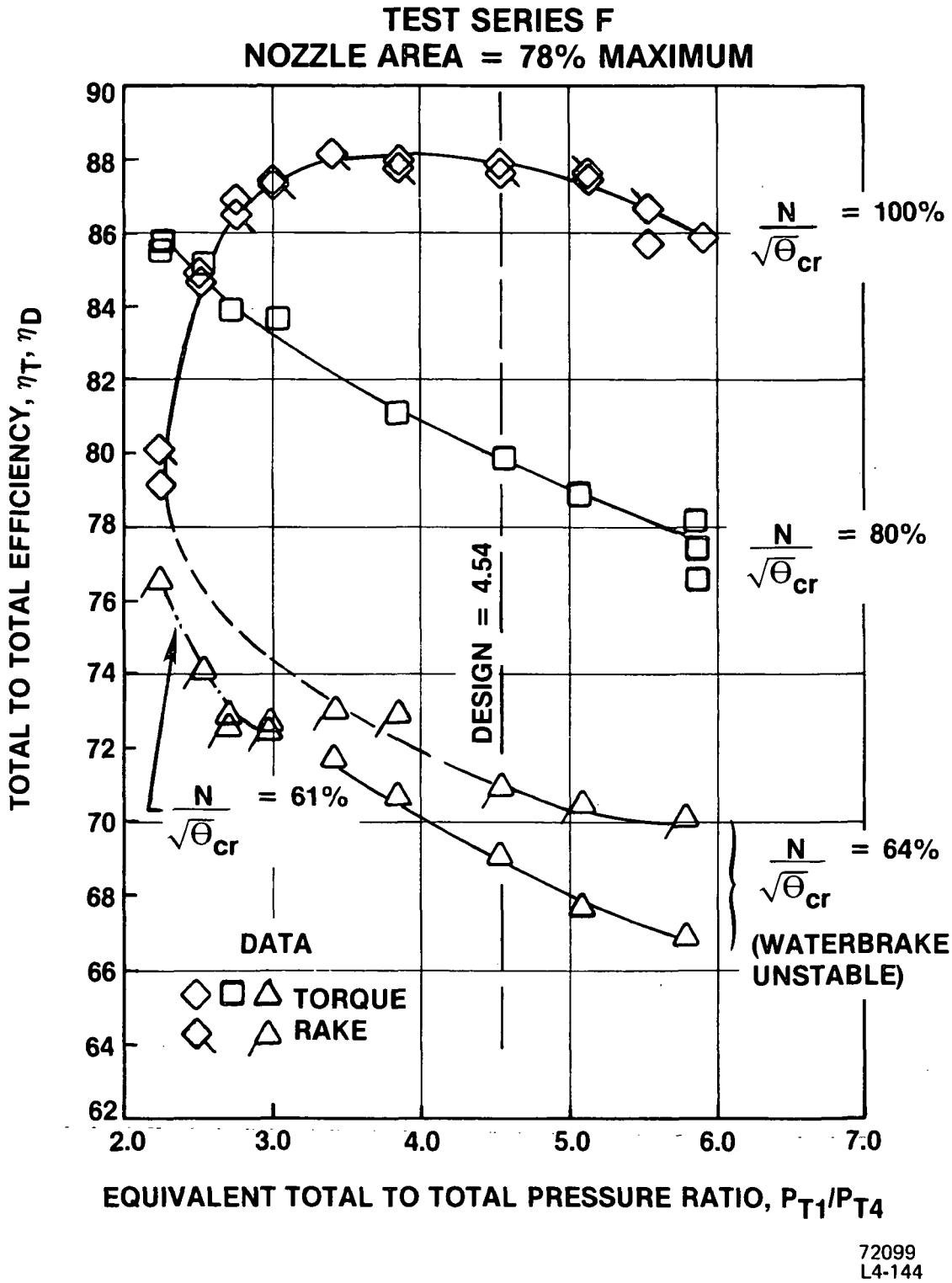

Figure 29. Overall Performance - Efficiency vs. Equivalent Speed and Pressure Ratio.

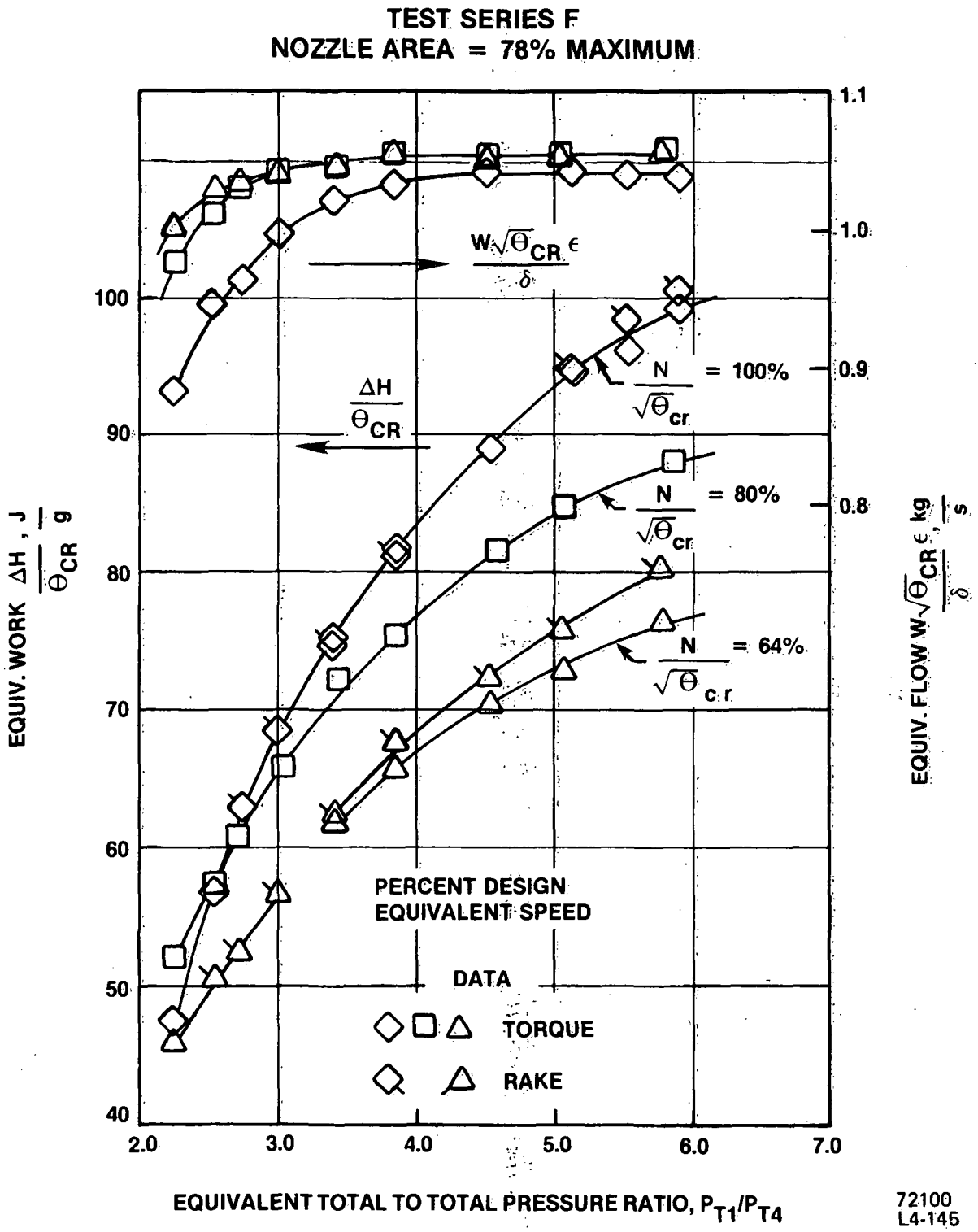

Figure 30. Flow - Work Characteristics - Nozzle in Nominal Position.

ORIGINAL PAGE IS
OF POOR QUALITY

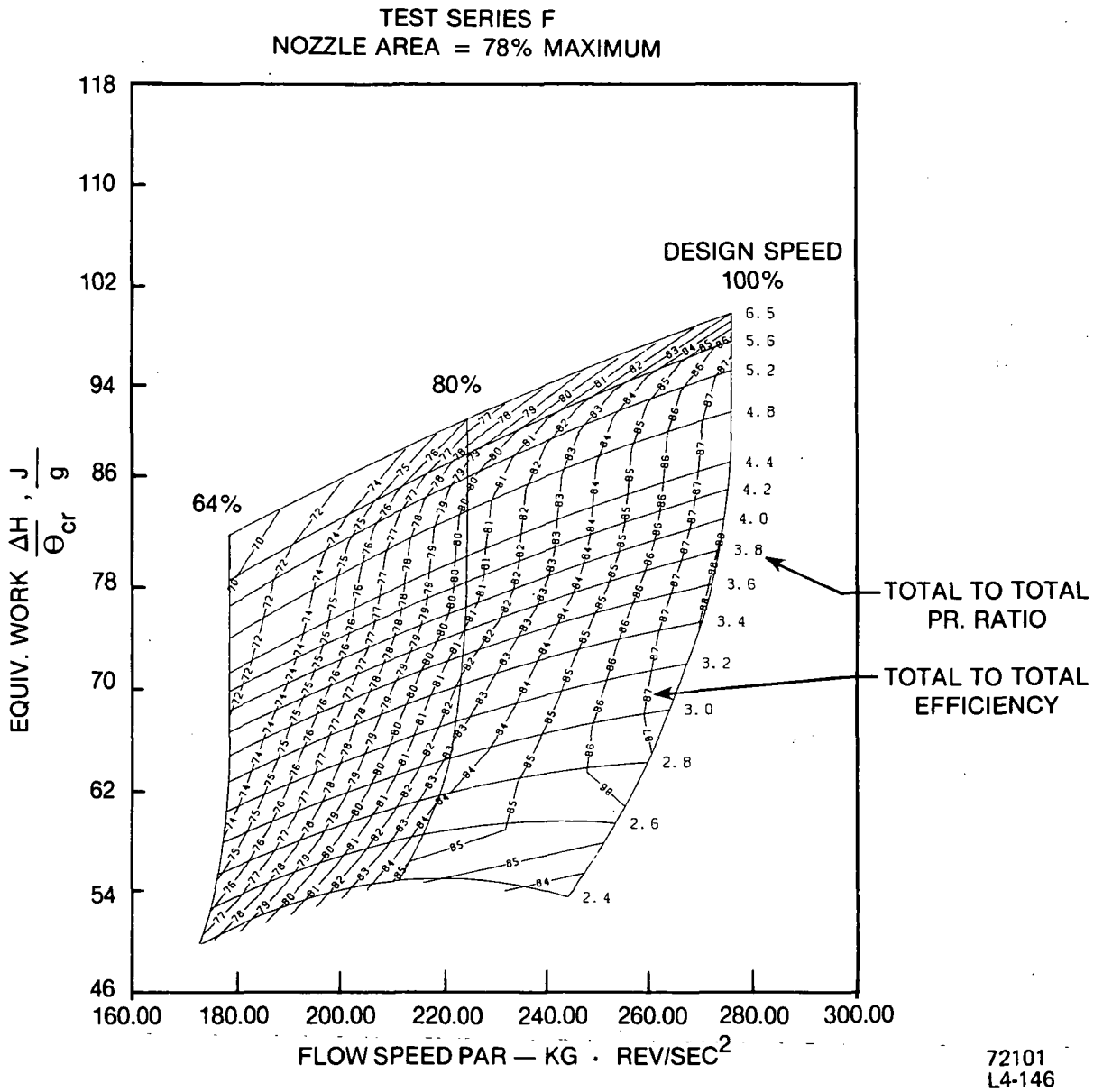

Figure 31. Stage Overall Performance Map with "L" Seals - Nozzle in Nominal Position.

5.1.4 Effects Of Shroud Wall Movement

With the "L" wiper seals in place, the moveable shroud wall was next moved to the 50 percent nozzle area position, Test Series H, Table IX. The total-to-total efficiency as a function of turbine stage pressure ratio is shown in Figure 32 at 100, 80 and 60 percent equivalent speed. At design pressure ratio and speed the efficiency was 82.6 compared to 87.9 for the flush nozzle wall test, Figure 29, a decrease of 5.3 points. Typical flow, rotor exit swirl, and work characteristics as a function of turbine pressure ratio are shown in Figure 33 and 34. Choking flow progressively decreases with speed and shows the rotor to be controlling the flow. At design speed and pressure ratio the choking flow decreased from 1.042 kg/s (2.293 lbs/s) to 0.683 kg/s (1.503 lbs/s) when the wall was moved from the 78 to 50 percent position. This corresponds to a near linear flow change of 34.5 percent for an area change of 35.9 percent and indicates that the nozzle is choked at the 50 percent position. Rising work characteristics with pressure ratio, Figure 34, shows no indication of approach of turbine limit load, also a characteristic of a choked nozzle.

The nozzle was then moved to the wide open or 100 percent area position and a similar set of tests conducted. Figure 35 gives the efficiency characteristics for Test Series D, Table IX, with the nozzle in the wide open position and with "L" seals on the vanes. At the design pressure ratio, the efficiency fell from 87.9 to 85.8 (2.1 points) when the wall was moved from the flush wall position to maximum open position. The average exit swirl correspondingly increased from 25 to 36 degrees against rotation. The swirl at 50 percent area was 13 degrees with rotation, Figure 33. The exhaust transition duct on an engine, then should be capable of accepting average swirl angles of $\pm$ 25 degrees with low losses. The inlet Mach number to this duct would vary from 0.28 to 0.71. This excursion suggests the desireability of a stage test with an engine suitable down stream transition duct attached to the turbine for overall performance evaluation.

The equivalent flow characteristics and specific work versus speed and pressure ratio for 100 percent area are given in Figures 36 and 37, respectively. The change in equivalent choking flow with speed indicates that the rotor is controlling the flow. The negligible work increase at higher pressure ratios, Figure 37, also points to a choked rotor and the onset of limit load.

A composite map was generated with the equivalent speed held at a constant 100 percent, with the position of the moveable shroud wall as the main variable. The overall turbine performance is shown in Figure 38. The peak efficiency occurs with the nozzle sidewall in the flush position at a value of 88.0 percent for pressure ratios between 3.4 and 4.2. If the pressure ratio is held at 4.54 and the wall moved to the open position the efficiency falls 2.1 points from 87.9 percent to a value of 85.8 percent. With the nozzle closed to 50 percent position the efficiency falls 5.3 points to a value of 82.6 percent. This would be the typical operating mode of the VARICAP engine, that is constant pressure ratio, variable capacity operation. If a lower design pressure ratio were to be selected, or if the turbine were to be modified to peak at a higher pressure ratio, then the efficiency falloff would be lower.

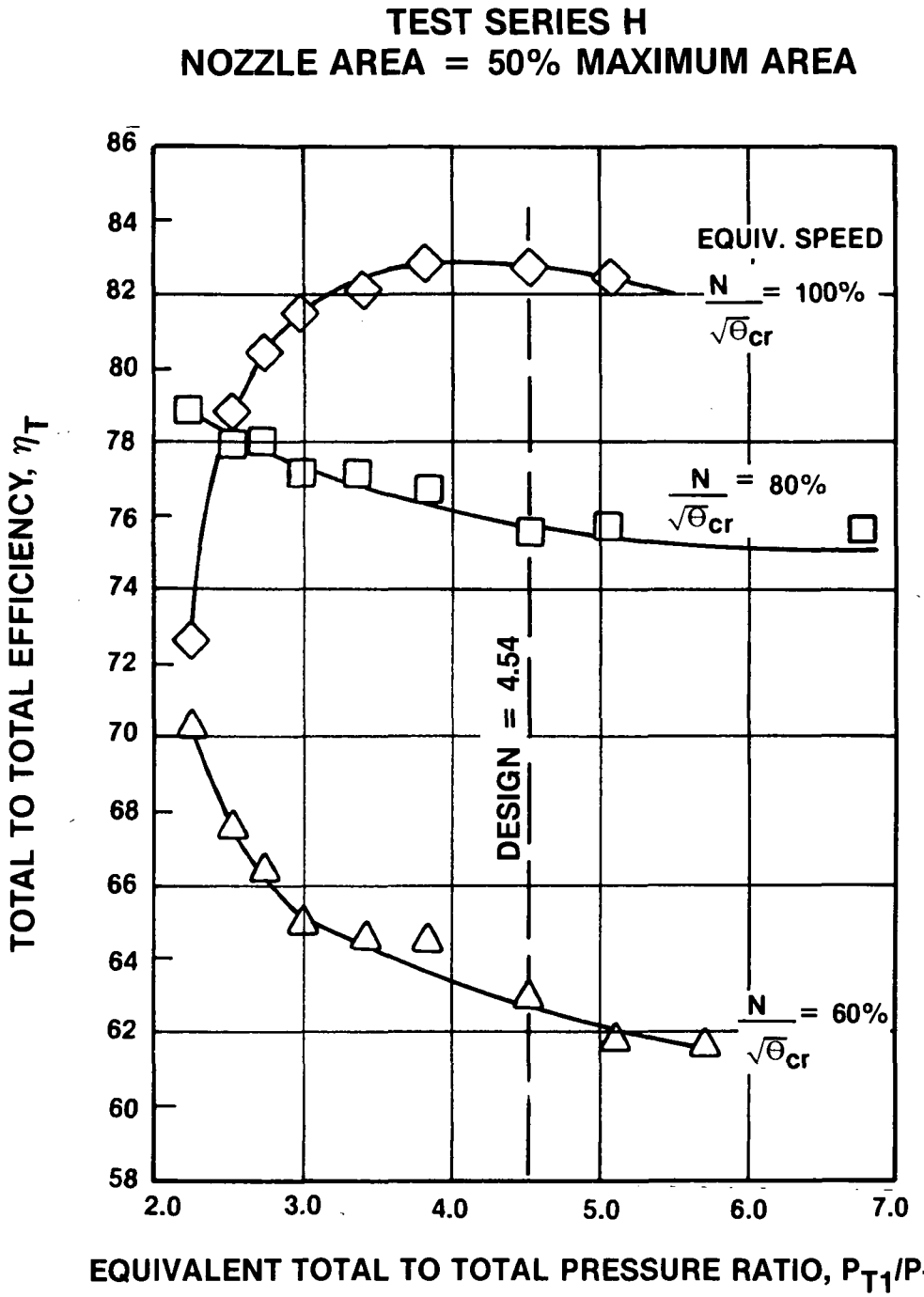

Figure 32. Moveable Shroud in Closed Position - Efficiency Characteristics.

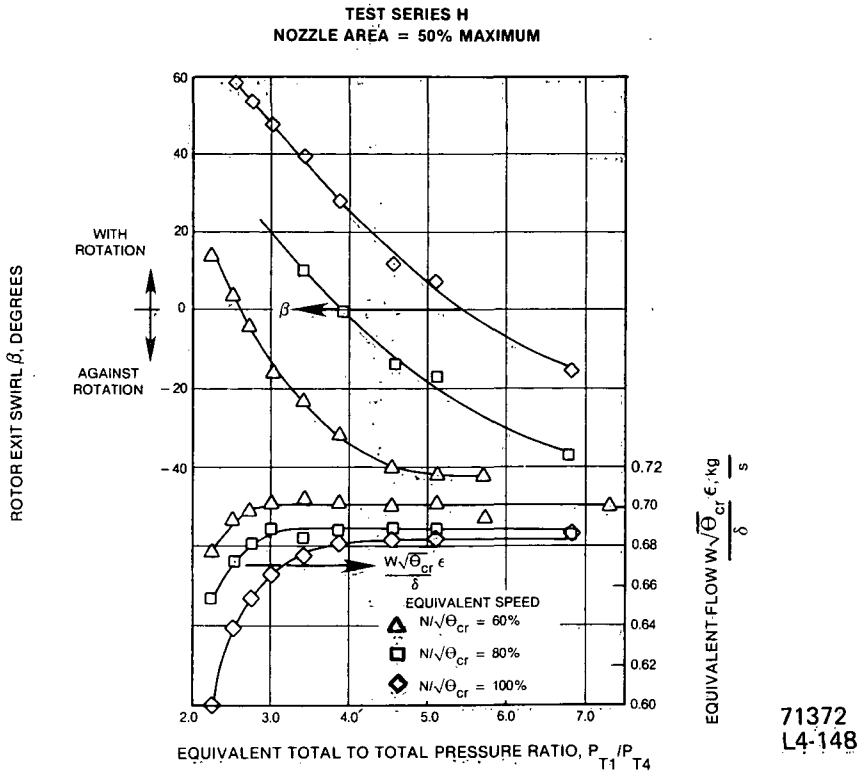

Figure 33. Moveable Shroud in Closed Position - Equivalent Flow and Exit Swirl Characteristics.

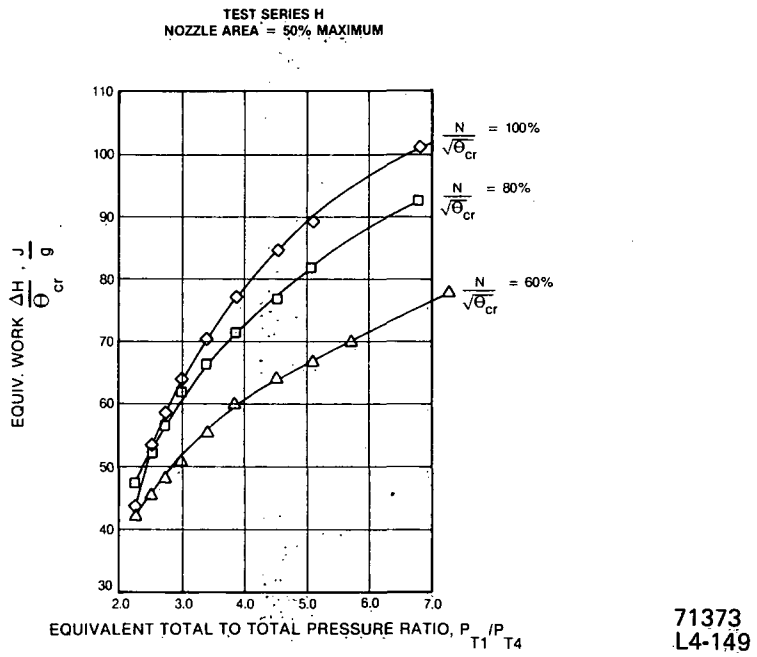

Figure 34. Moveable Shroud in Closed Position - Equivalent Work vs. Equivalent Speed and Pressure Ratio.

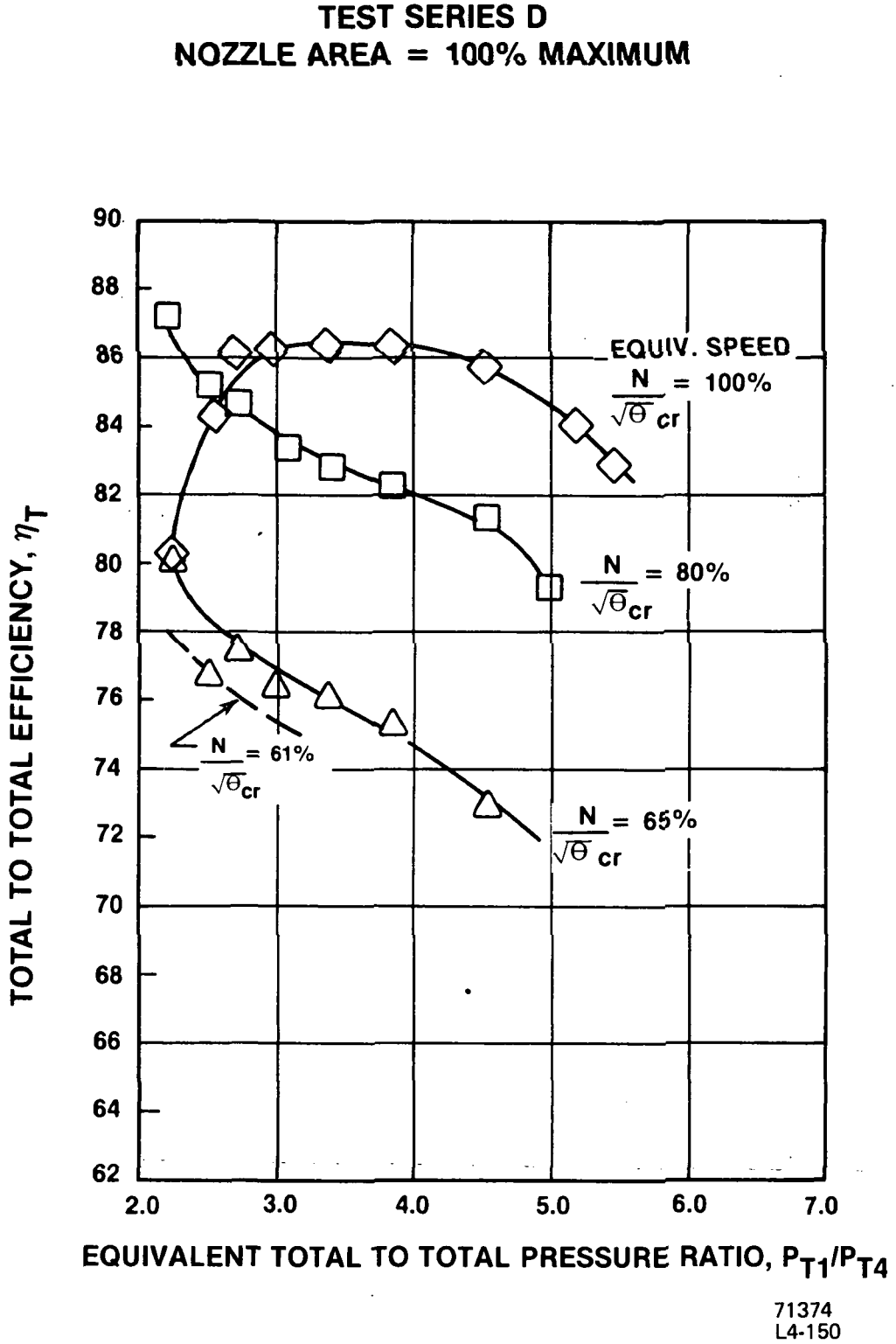

Figure 35. Moveable Shroud in Open Position - Efficiency Characteristics.

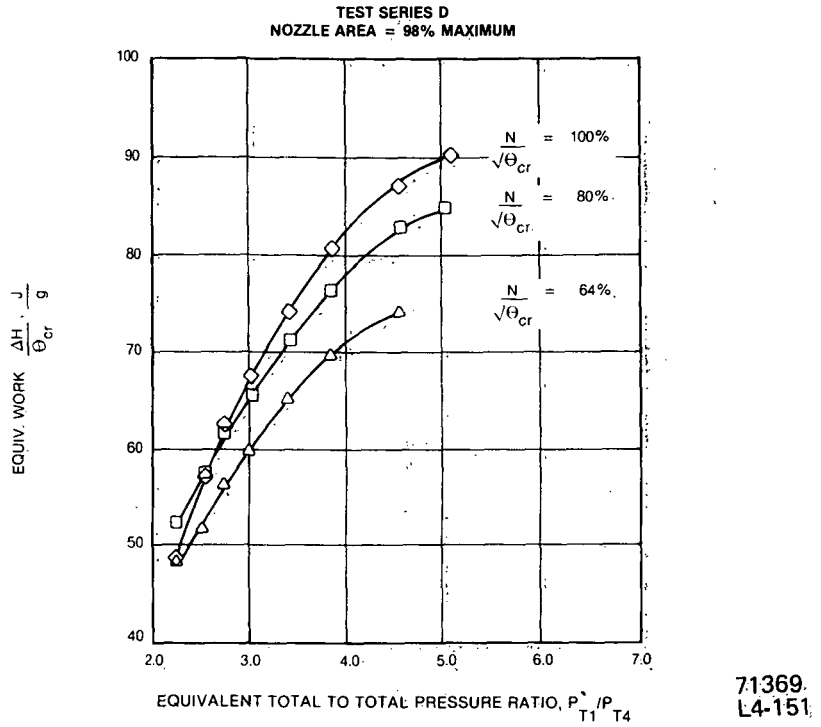

Figure 36. Moveable Shroud in Open Position - Equivalent Flow Characteristics.

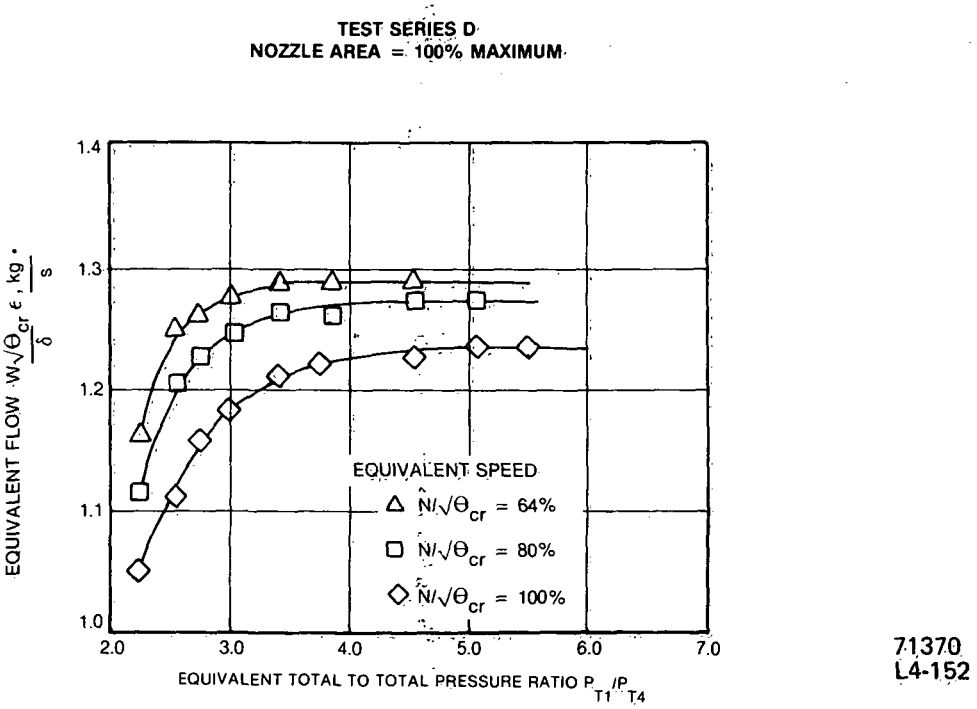

Figure 37. Moveable Shroud in Open Position - Equivalent Work vs. Equivalent Speed and Pressure Ratio.

70544
L4-107

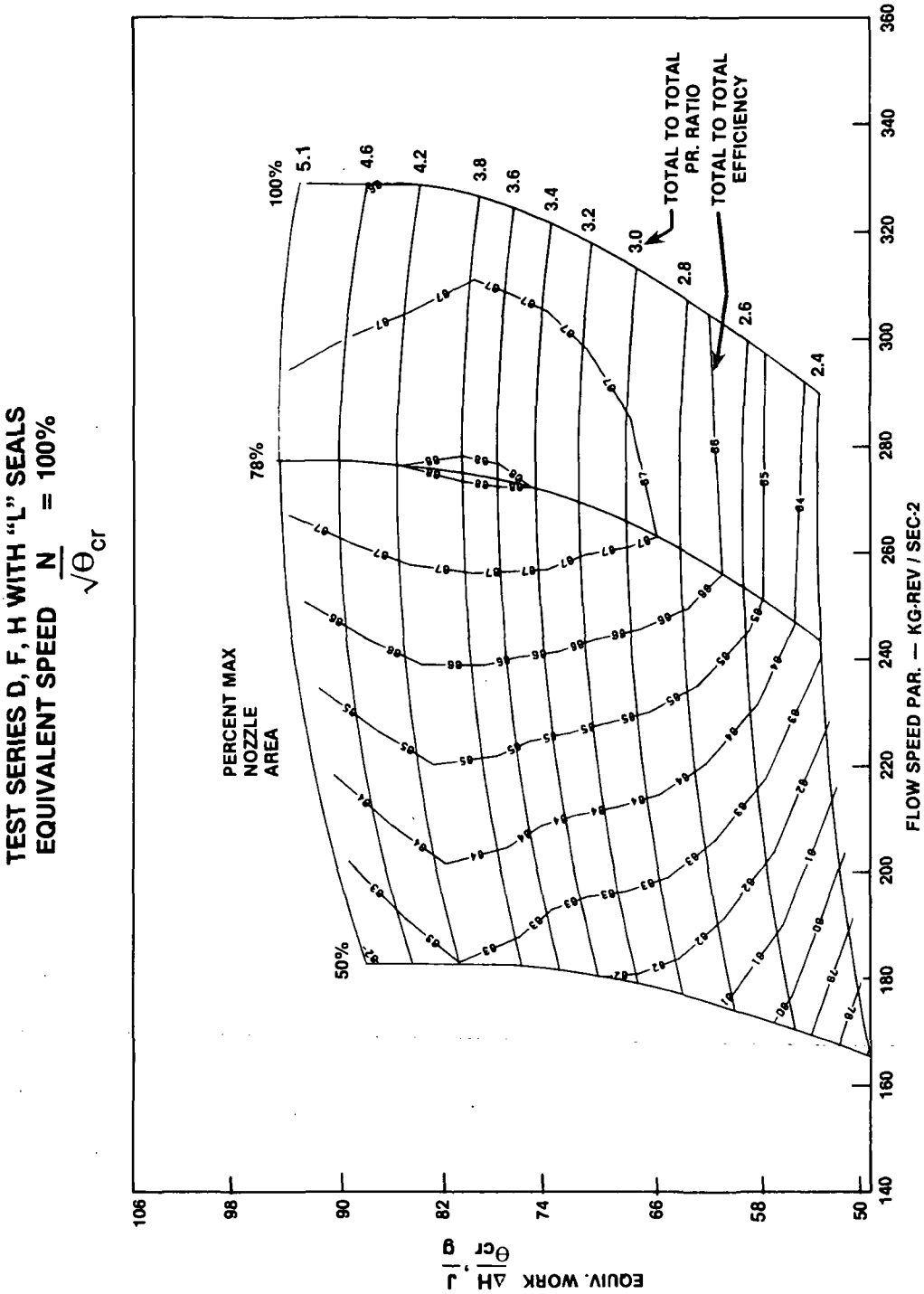

Figure 38. Overall Performance Variable Capacity Turbine Map - Moveable Shroud Nozzle.

5.1.5 Cooling Injection Effects

Test Series E, Table IX, was conducted with the moveable shroud wall in the flush wall position with "L" seals and with cooling injection flows on the nozzle and the rotor backface. The nozzle and disk backface cooling injection flows were fixed at values of 4.5 and 1.0 percent, respectively, of mainstream flow. Figure 39 shows a comparison of cooled and uncooled measured stage efficiency at 100 percent equivalent speed over a range of pressure ratios. Both total-to-total and total-to-static efficiencies are given. At the design total-to-total pressure ratio of 4.54 the efficiency penalty due to the cooling injection is 1.4 points. Based on the measured total-to-static pressure ratio at this point, the loss is 0.8 points.

Figure 40 shows the effect of cooling on exit swirl and the primary flow characteristics of the turbine. The rotor exit swirl did not change with the addition of 4.5 percent nozzle cooling and 1.0 percent rotor backface flow. The primary flow entering the rotor decreased 3.5 percent at the design pressure ratio. Since all of the cooling flow of 5.5 percent bypasses the nozzle throat, the total flow increase of only 2.0 percent indicates that the rotor exducer is limiting the stage capacity.

An additional series of tests was conducted with the nozzle sidewall in the flush wall position and with the nozzle cooling flow incrementally increased from 1.0 to 6.0 percent while holding the turbine stage pressure ratio at its design value of 4.54. The rotor backface cooling flow was held constant at 1.0 percent. The total-to-total and total-to-static stage efficiency trends are shown in Figure 41. A test point "A" with zero cooling and a reference point "B" degraded by 1.0 points for the 1.0 percent rotor cooling is also shown for comparison. The total-to-total efficiency penalty due to nozzle cooling injection alone was found to be less than 0.7 point up to a flow of 6.0 percent. Total-to-static efficiencies confirming this trend are also shown in Figure 41. At intermediate nozzle cooling flows the efficiency actually improved, probably due to a nozzle trailing edge wake filling effect.

The wall position was then moved to the 50 percent closed position, Test Series G, Table IX, and the turbine was tested at 100 percent design equivalent speed with nozzle and rotor cooling flows of 5.6 and 1.0 percent, respectively. Figure 42 shows a comparison of efficiency and flow with and without cooling injection. The flow data shown is the primary equivalent mass flow and does not include cooling flows. There is an apparent reduction of 5.9 percent in the primary equivalent mass flow with the addition of cooling flows. In the 50 percent wall position, the nozzle throat should control the flow. Since the cooling flows bypass the flow controlling nozzle throat, the data indicates higher losses and a lower flow capacity with respect to the build with no cooling. The measured efficiency penalty due to the 5.6 percent nozzle cooling and 1.0 percent rotor cooling is 3.2 points at the design pressure ratio of 4.54.

This increase in cooling loss over the flush wall tests can be attributed to the slightly increased rotor backface flow and primarily to the changed nozzle cooling circuit. Figure 43 shows the nozzle cooling flow path when the shroud wall is moved to the 50 percent position. In this position, one half of the vane cooling slots are buried in the hub wall and presumedly deactivated from the circuit. In an engine, when the sidewall is in the 50 percent position, only one half of the surface ara of the vanes would be in the hot gas environment and only one half as much vane cooling is required.

In the rig test the buried slots were not deactivated as desired. Figure 44 shows a flow calibration bench rig used to calibrate the cooling circuits. This rig was designed to adapt to the entire moveable sidewall assembly. There are four groups of cooling holes, designated A, B, C and D as shown. The cooling circuit "A" consists of 15, equally spaced, 2.18 mm (0.086 in) diameter holes to meter a simulated 0.75 percent vane sidewall coolng and leakage flow. Cooling holes "B" consisting of 30, 2.00 mm (0.079 in) diameter, holes simulate an additional vane sidewall cooling dump of 0.75 percent of mainstream flow. The moveable sidewall, circuit "C" has 30, 1.57 mm (0.062 in) diameter holes to simulate a sidewall cooling dump of 1.1 percent. the nozzle vanes, (circuit "D") have 5 rectangular cooling slots - (0.045 in) wide by 1.67mm (0.0656 in) long and a total cooling flow of 3.0 percent.

The cooling circuits in the bench rig were selectively closed off and flow calibrated against pressure ratio and sidewall position. Figure 45 summarizes the calibrations. The discharge coefficients for the unblocked nozzle trailing edge holes progressively increased from 0.82, 0.94 to 1.38 for the respective sidewall positions of 96, 78 and 50 percent of maximum. The latter two discharge coefficients indicate considerable leakage of cooling air passing through the gap between the buried vane trailing edge holes and the nozzle sidewall, Figure 43. Since this leakage flow enters at 90 degrees to the mainstream it is source for flow disturbance and high losses.

Cooling injection effects with the nozzle sidwall in the wide open position are shown in Figure 46. A nozzle cooling flow of 5.6 percent and a rotor cooling flow of 0.8 percent of mainstream were injected for this test series. In the stage pressure ratio range of 3.5 to 5.0, the loss in efficiency is approximately 1.1 points. This loss due to cooling is substantially lower than incurred when the wall was in the 50 percent closed position. In the open position the losses are lower because none of the vane cooling slots are covered and ejection is in the direction of mainstream flow.

The turbine primary flow characteristics are also shown in Figure 46. The primary flow at the design pressure ratio of 4.54 decreased from 1.228 kg/s to 1.204 kg/s or 2.0 percent with cooling injection. Since these cooling flows bypass the nozzle throat, the primary flow decrease must be a consequence of the rotor controlling the flow.

The cooling injection effects on the total-to-total efficiency and primary flow rate at design equivalent speed and pressure ratio are summarized in Table XI.

TABLE XI

COOLING INJECTION EFFECTS
MOVEABLE SHROUD CONFIGURATION

WALL POSITION, PERCENT MAX.	50	78	98
COOLING FLOW, NOZZLE/ROTOR, PERCENT	5.6/1.0	5.6/1.0	5.6/0.8
EFFICIENCY NO COOLING, PERCENT	82.6	87.9	85.8
EFFICIENCY WITH COOLING, PERCENT	79.4	86.3	84.7
EFFICIENCY LOSS, POINTS	3.2	1.6	1.1
EQUIV. PRIMARY FLOW, NO COOLING, kg/s	0.683	1.042	1.228
EQUIV. PRIMARY FLOW WITH COOLING, kg/s	0.643	1.006	1.204
PRIMARY FLOW REDUCTION, PERCENT	5.9	3.5	2.0

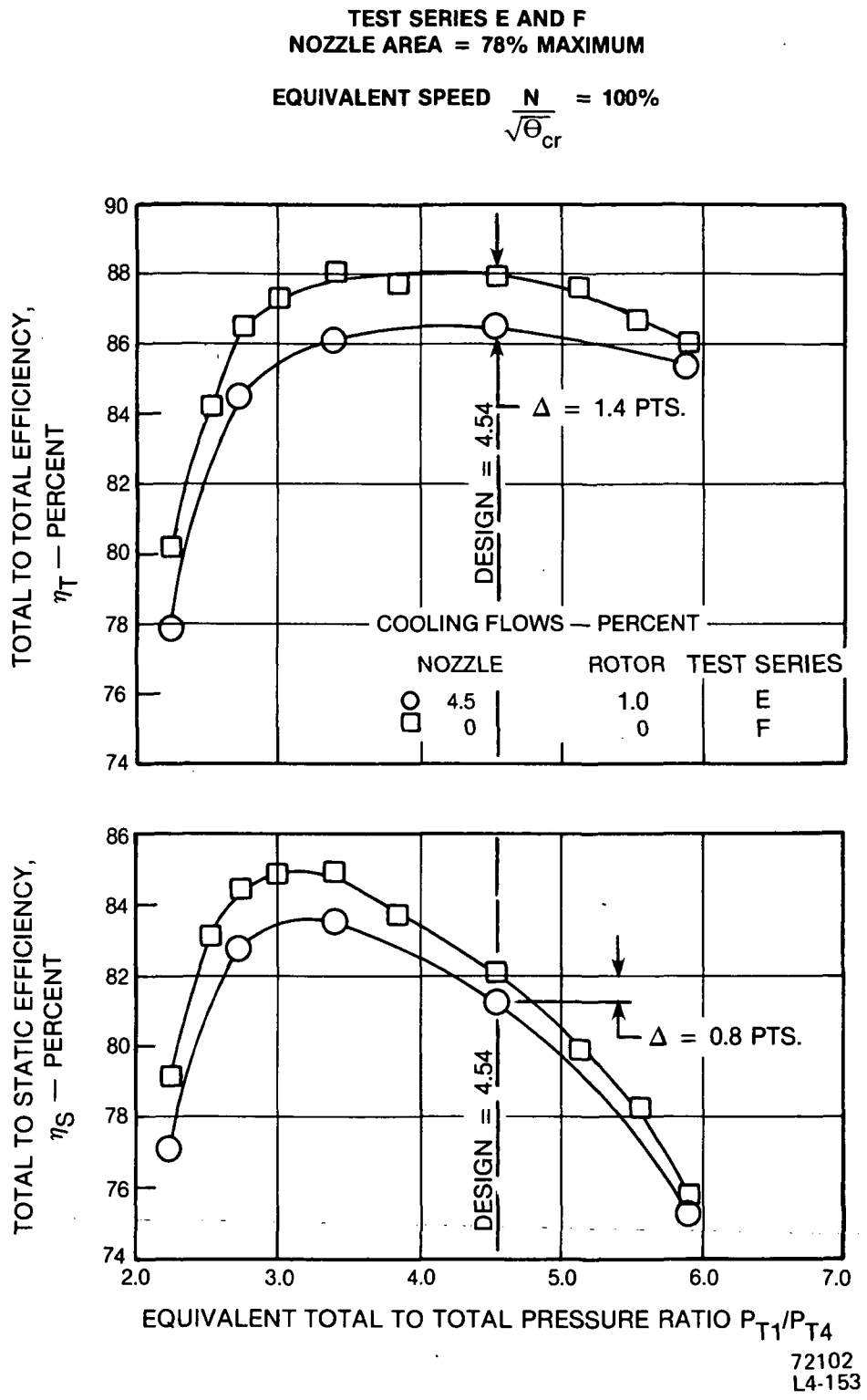

Figure 39. Cooling Injection Effects - Total to Total and Total to Static Efficiency with Nozzle Sidewalls in Flush Position.

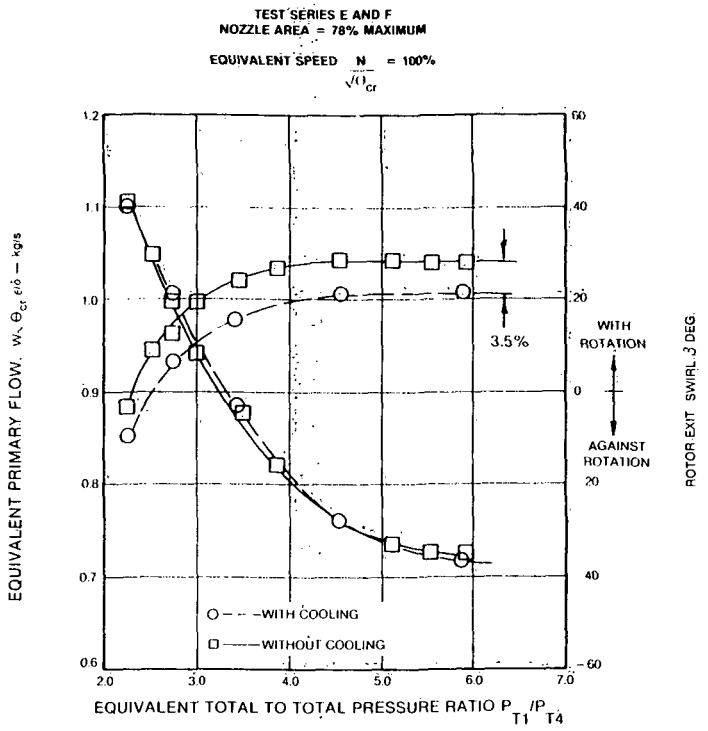

Figure 40. Cooling Injection Effects - Equivalent Flow and Rotor Exit Swirl - Nozzle Sidewalls in Flush Position.

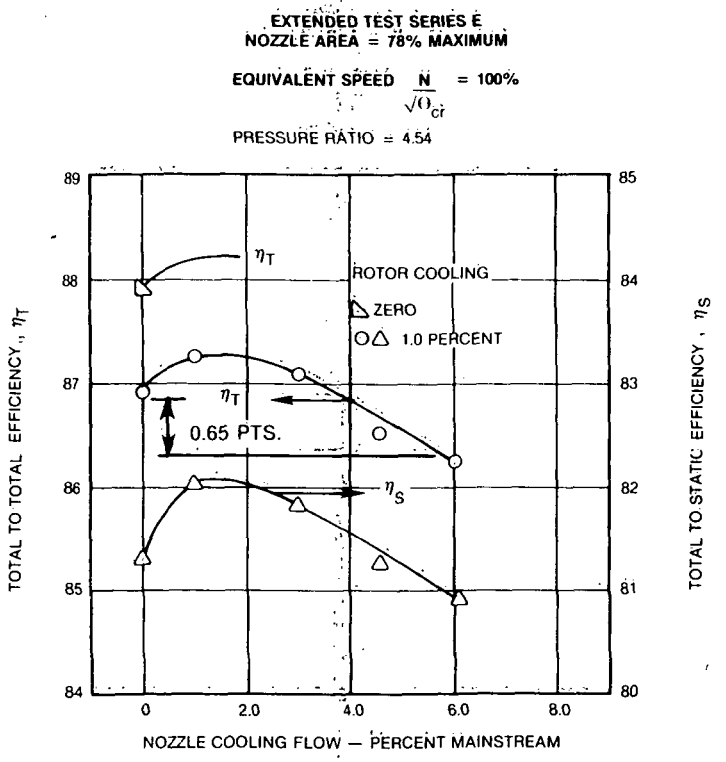

Figure 41. Total to Total and Total to Static Efficiency vs. Nozzle Cooling Flow.

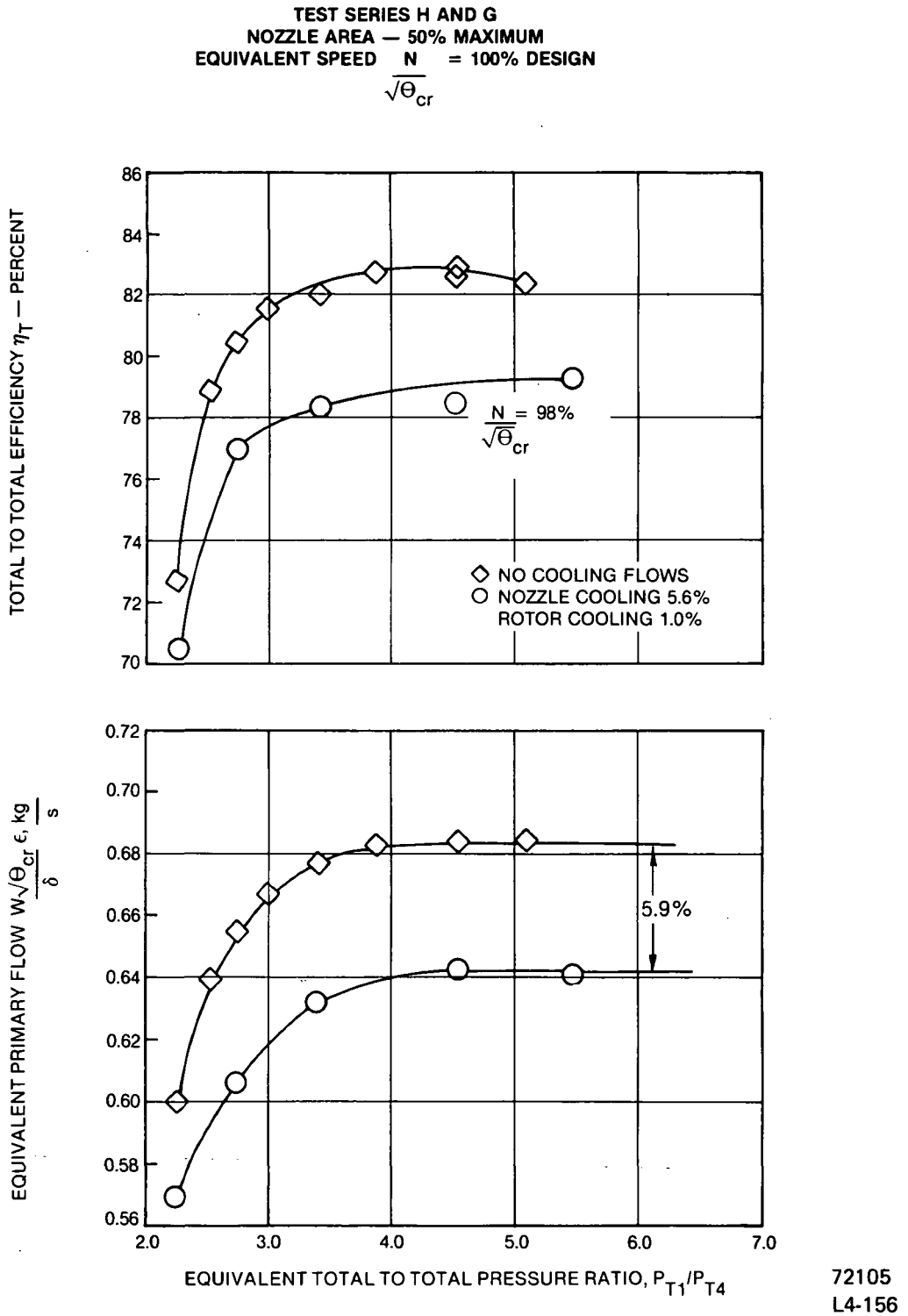

Figure 42. Cooling Injection Effects - Efficiency and Equivalent Flow with Nozzle Sidewalls in Closed Position.

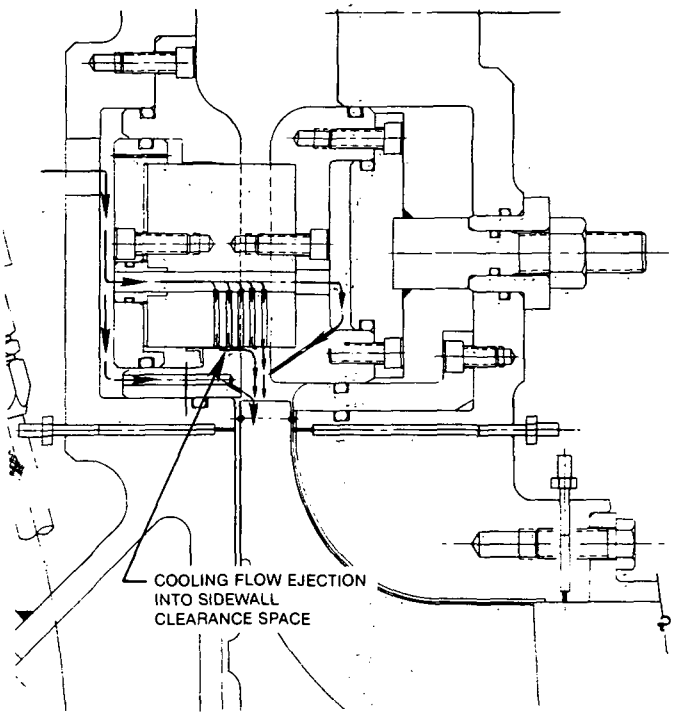

Figure 43. Nozzle Cooling and Leakage Flowpath.

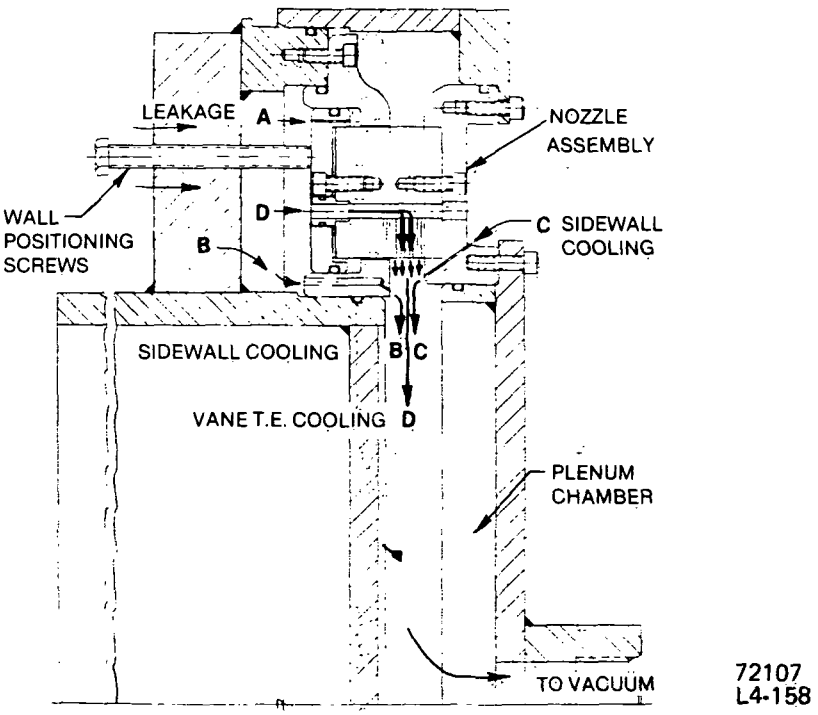

Figure 44. Cooling Circuit Flow Calibration Bench Rig.

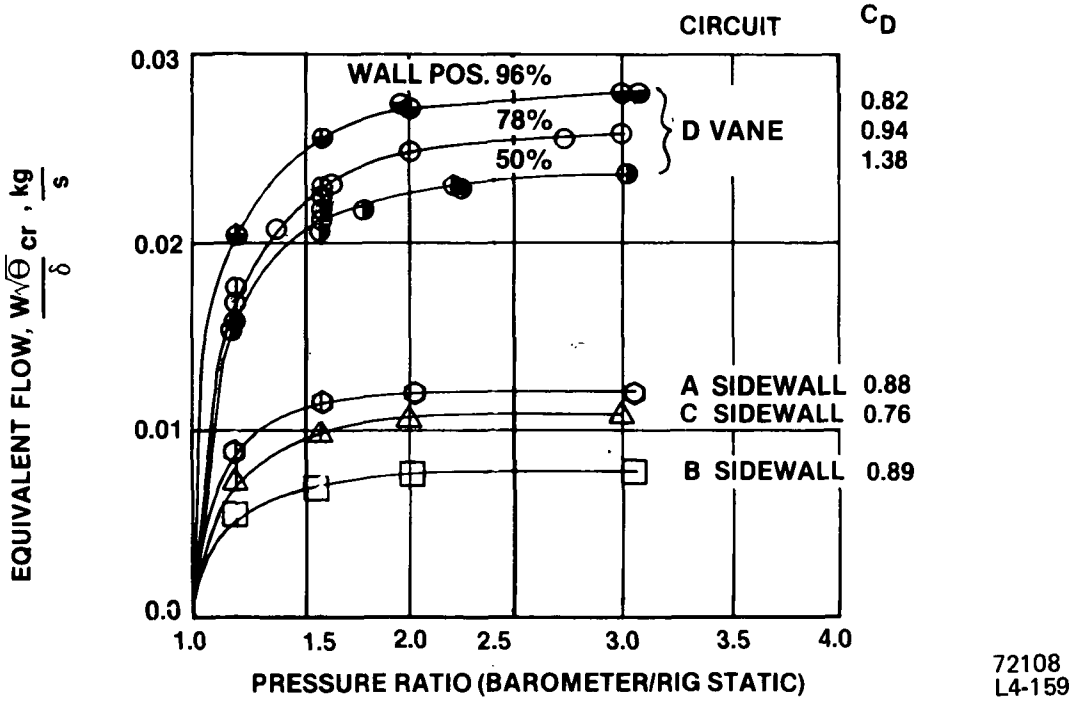

Figure 45. Cooling Circuit Flow Calibration Data.

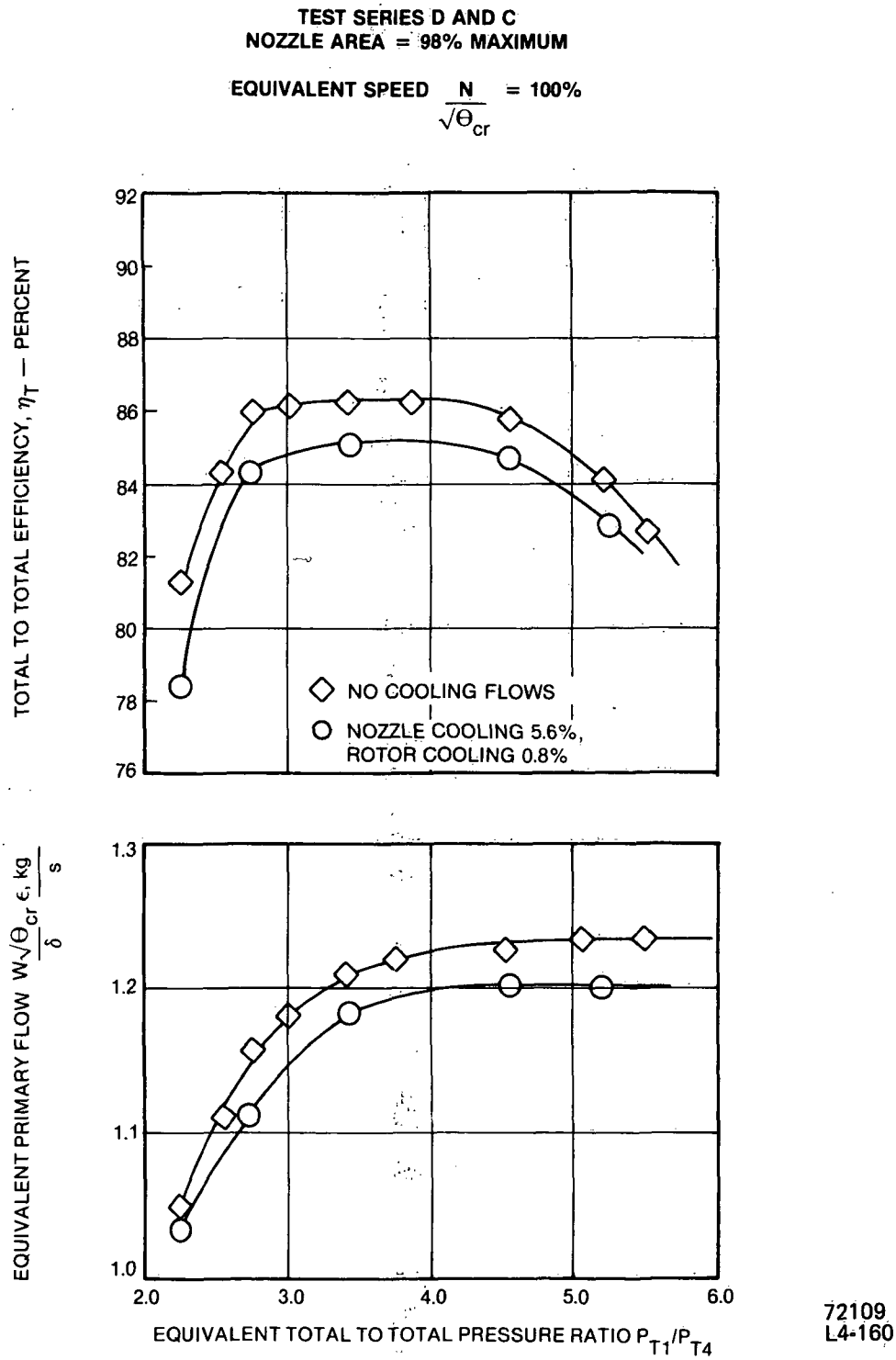

Figure 46. Cooling Injection Effects - Efficiency and Flow - Nozzle Sidewalls in Open Position.

5.2.1 Effects Of Hub Wall Movement

The remainder of testing was conducted with the turbine reconfigured to the moveable hub (MH) wall nozzle geometry with a high radius splitline, Figure 7. The turbine was evaluated over a range of pressure ratios of equivalent speeds from 100% to 60% in both 50 percent and maximum open positions. The performance was then compared to the moveable shroud (MS) nozzle configuration with the sidewall splitline at the same high radius location. Figure 47 shows the total-to-total efficiency comparison of the two configurations. In the maximum open nozzle position the MH configuration shows a performance gain over the MS configuration at all conditions tested. At design speed and a total-to-total pressure ratio of 3.0 the efficiency gain is 2 points. At the design pressure ratio the efficiency gain, however, is only 0.5 points. In the 50 percent flow capacity position, gains are only shown at an equivalent speed of 60 percent. Total-to-static efficiency data for the same tests are shown in Figure 48 and confirm the total-to-total efficiency trends.

Overall performance maps for the MH test at 50 and 100 percent wall positions are given in Figures 49 and 50. A composite VARICAP map wherein the equivalent speed is fixed at 100 percent and sidewall movement is the main variable is shown in Figure 51. For this performance map the MS data from Test Series F were used for the flush wall position (i.e. 78% nozzle area). Data from MH Test Series K were not used because only four data points were obtained vs ten in the F Series. Since the sidewall in both cases is flush to the flowpath, the performance would be expected to be the same. The limited MH data, however, showed 0.8 - 1.0 points lower efficiency than the MS. Some of this variance might be attributable to a poorer rotor tip clearance build on the MH Series (3.9 vs 2.6 percent tip front face tip clearances). Comparing the maps of Figures 51 and 38, the MH sidewall performance shows broader efficiency islands and higher performance over most of the range of test variables. If however, the mode of operation is at a constant design pressure ratio of 4.54 the gain of the MH configuration over the MH configuration is small. A composite VARICAP performance map at a reduced speed of 80 percent is shown in Figure 52. Here all the efficiency contours are substantially lower and show that it would not be desirable to operate a VARICAP engine at design pressure ratio with this turbine at the reduced speed.

5.2.2 Cooling Injection Effects

The MH sidewall nozzle configuration was also evaluated for the effects of cooling injection. Testing was conducted with a combined nozzle cooling flow injection of 1.1, 1.5, and 3.0 percent of mainstream at the nozzle sidewall hub, shroud and vane trailing edge respectively, (total 5.6 percent). Approximately 1.0 percent flow was dumped at the rotor backface scallop region. The flow conditions were stabilized before acquiring data. The cooling flows were then turned off and data was acquired at the same mainstream conditions without cooling. Figure 53 presents overall stage efficiency characteristics as a function of total-to-total pressure ratio and equivalent speed for Test Series K, Table X, with the nozzle hub sidewall in the flush or 78 percent maximum flow position. A cooling injection penalty of 1 to 2 points in efficiency is shown over most of the test operating range. At the design pressure ratio of 4.54 and 100 percent equivalent speed, the loss is 1.2 points.

Performance data for Test Series L and J, Table X, with the nozzle sidewall in the closed and maximum positions, respectively, is given in Figure 54. For this series, it was assumed that in an engine application the backface cooling would have to be increased or decreased in proportion to the flow entering the rotor. The rotor backface cooling injection was, therefore, adjusted to 0.64 and 1.3 percent for the respective 50 and 100 percent nozzle sidewall positions. The cooling loss at design pressure ratio for these two wall positions are 1.2 and 2.6 percent respectively. Figure 55 shows the MH and MS configurations in their extreme positions and gives the cooling flows and associated penalties. The highest losses are incurred when the cooling flows are injected into the hub region. The rotor reaction is the lowest in the hub and can be expected to be sensitive to these cooling flow disturbances. The nozzle cooling flow disturbance caused by those slots buried in the sidewall can be eliminated by relocation. Rotor hub cooling should be held to a minimum.

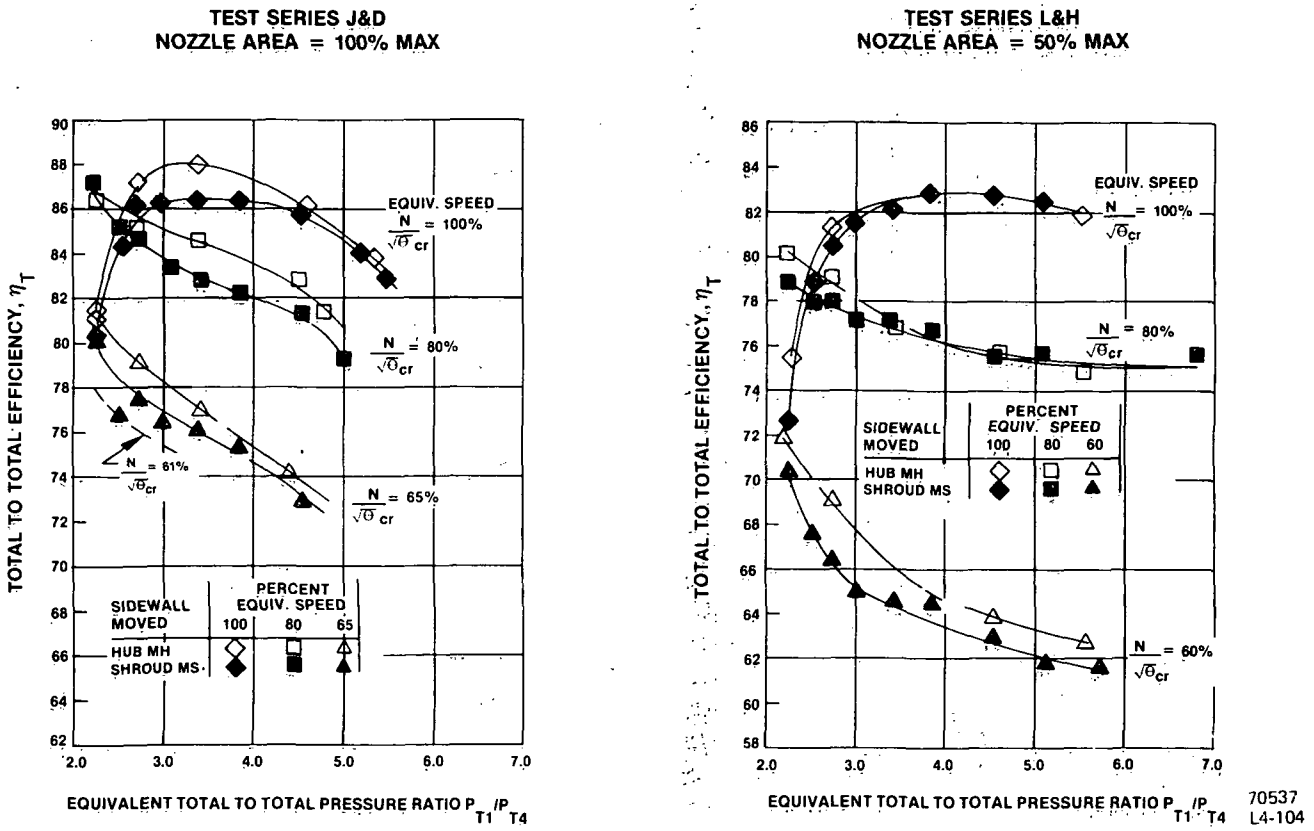

Figure 47. Moveable Hub and Moveable Shroud Performance Comparison

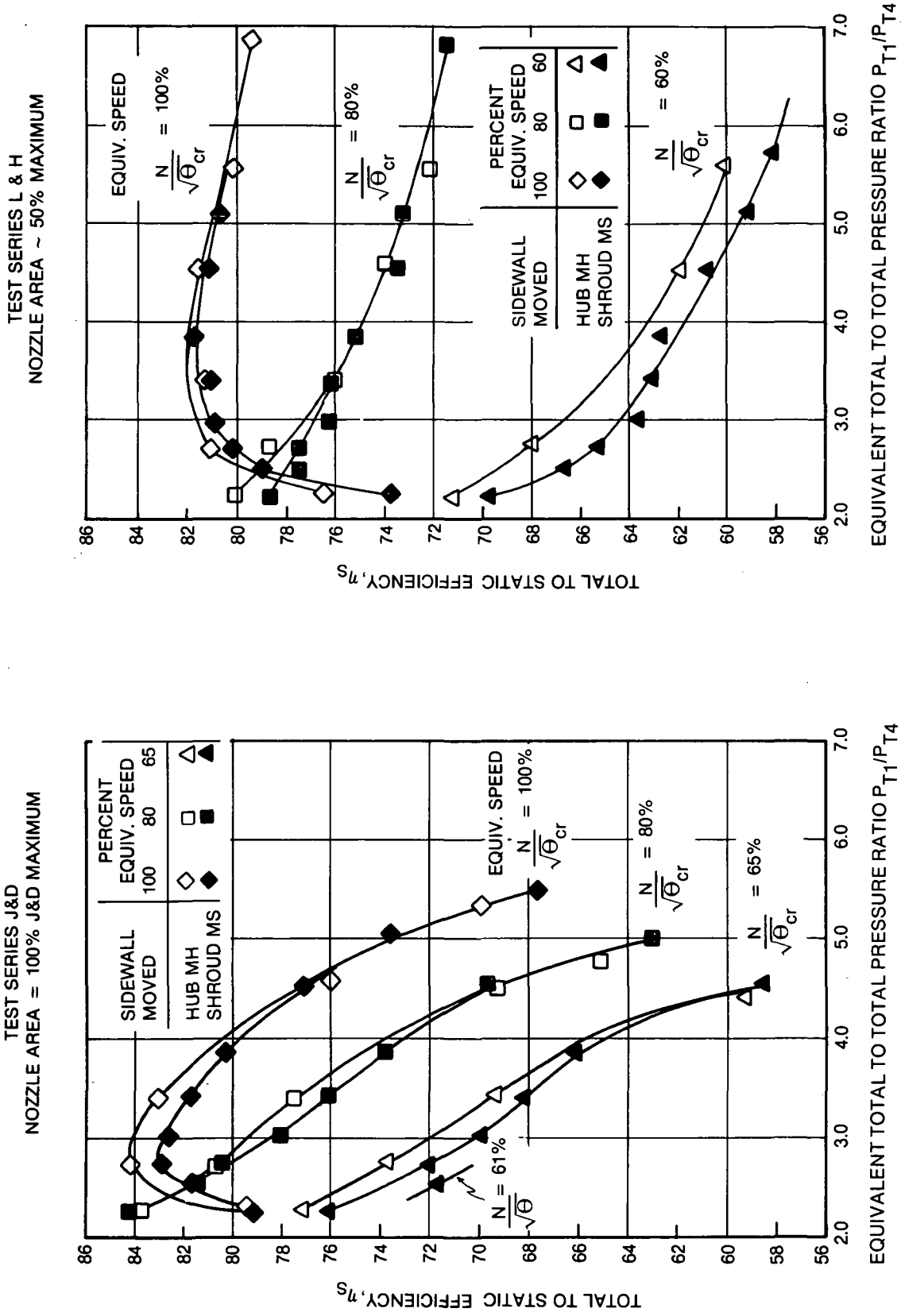

Figure 48. Moveable Hub and Moveable Shroud Total To Static Efficiency Comparisons.

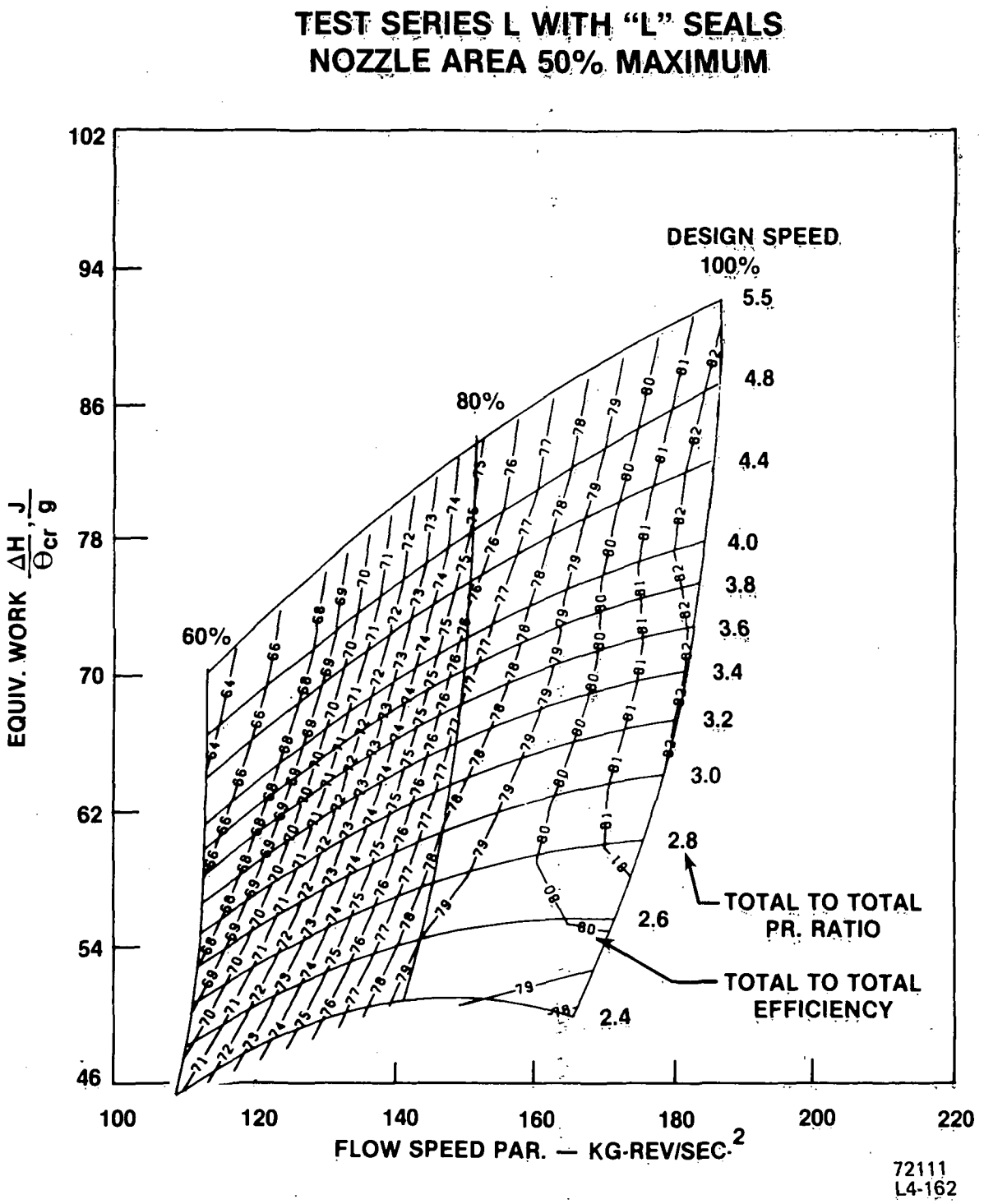

Figure 49. Overall Performance Map with "L" Seals - Moveable Hub Sidewall In Closed Position.

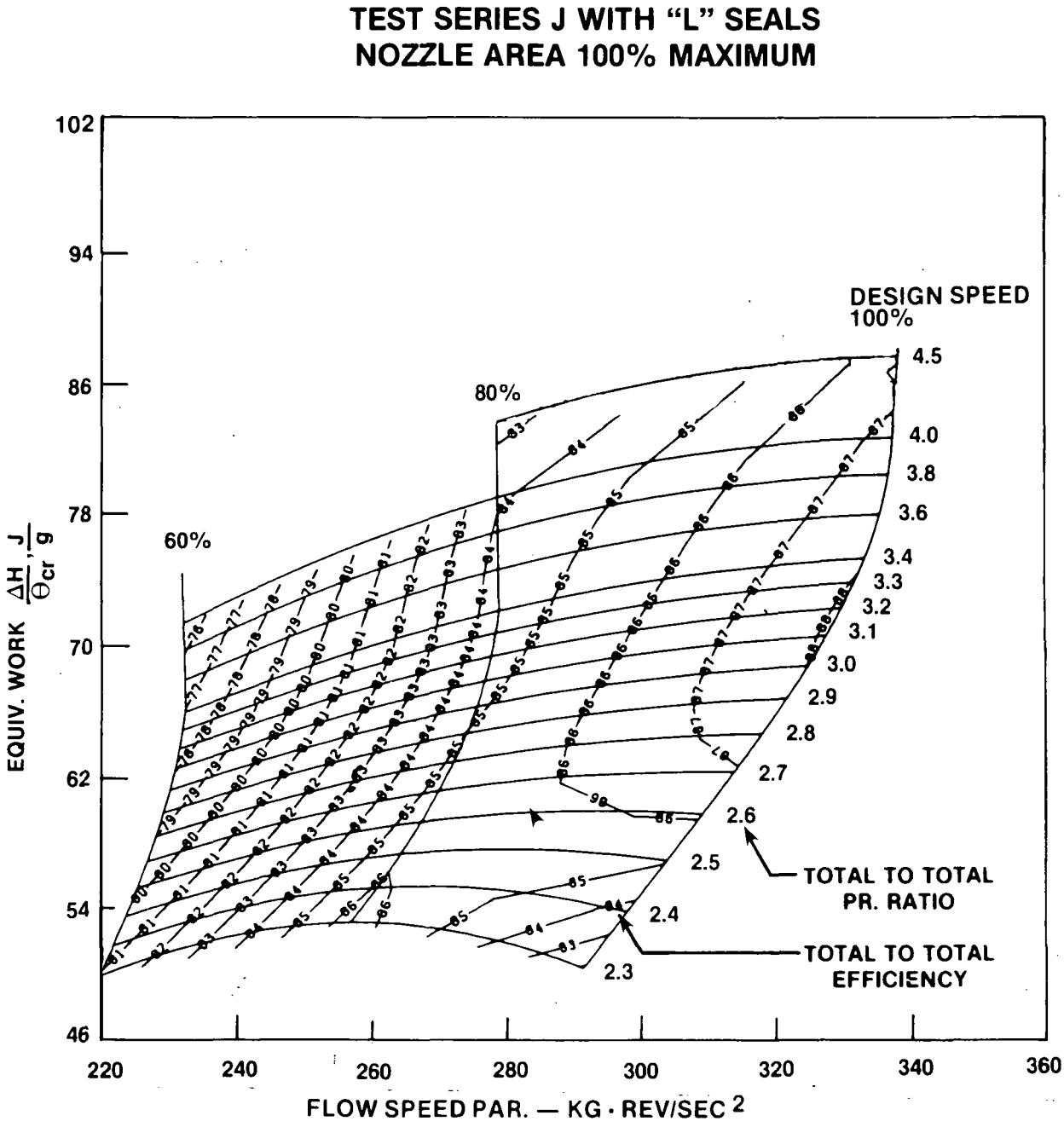

Figure 50. Overall Performance Map with "L" Seals - Moveable Hub Sidewall In Open Position.

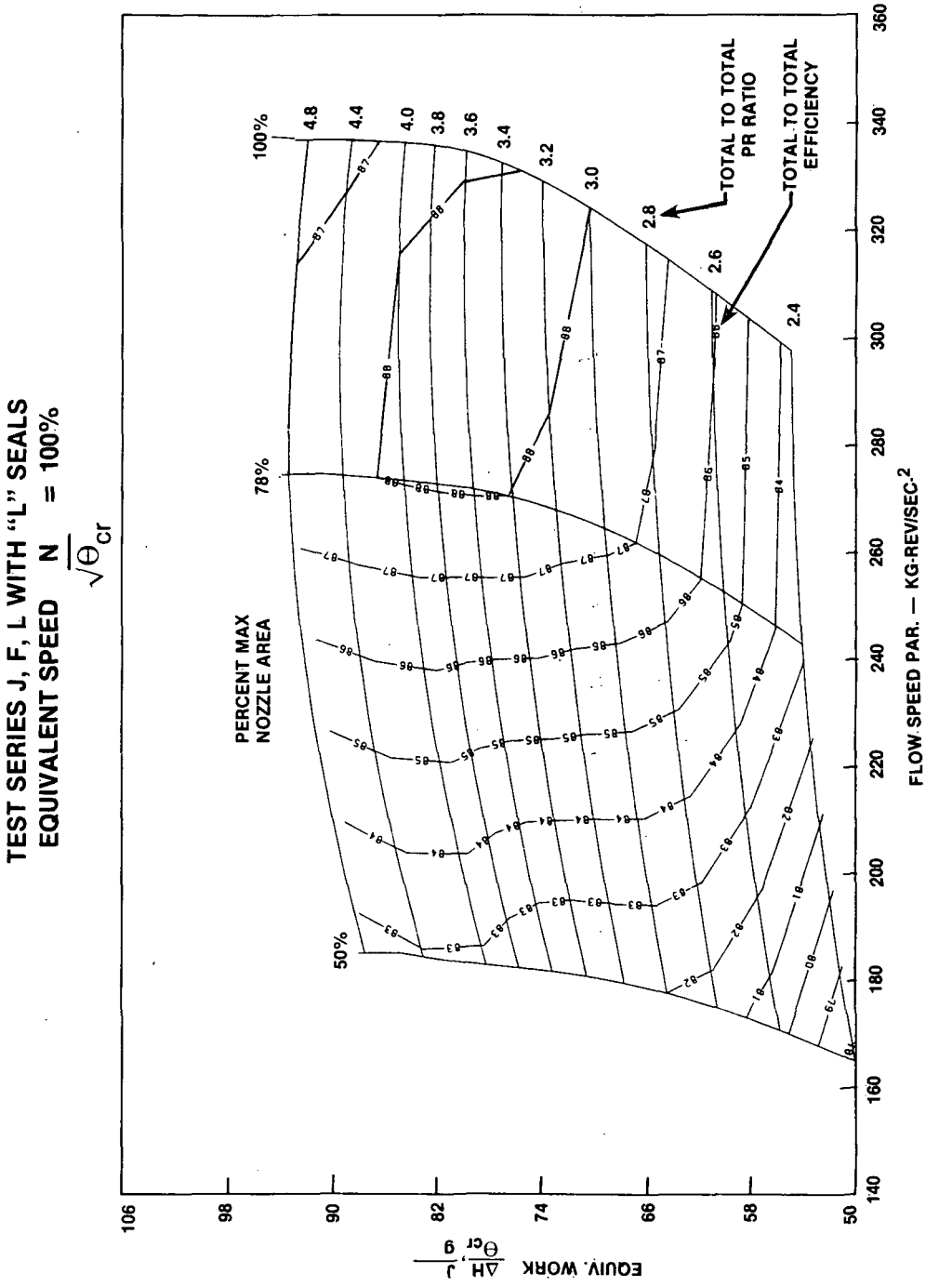

70546
L4-108

Figure 51. Overall Performance Variable Capacity Turbine Map - Moveable Hub Nozzle

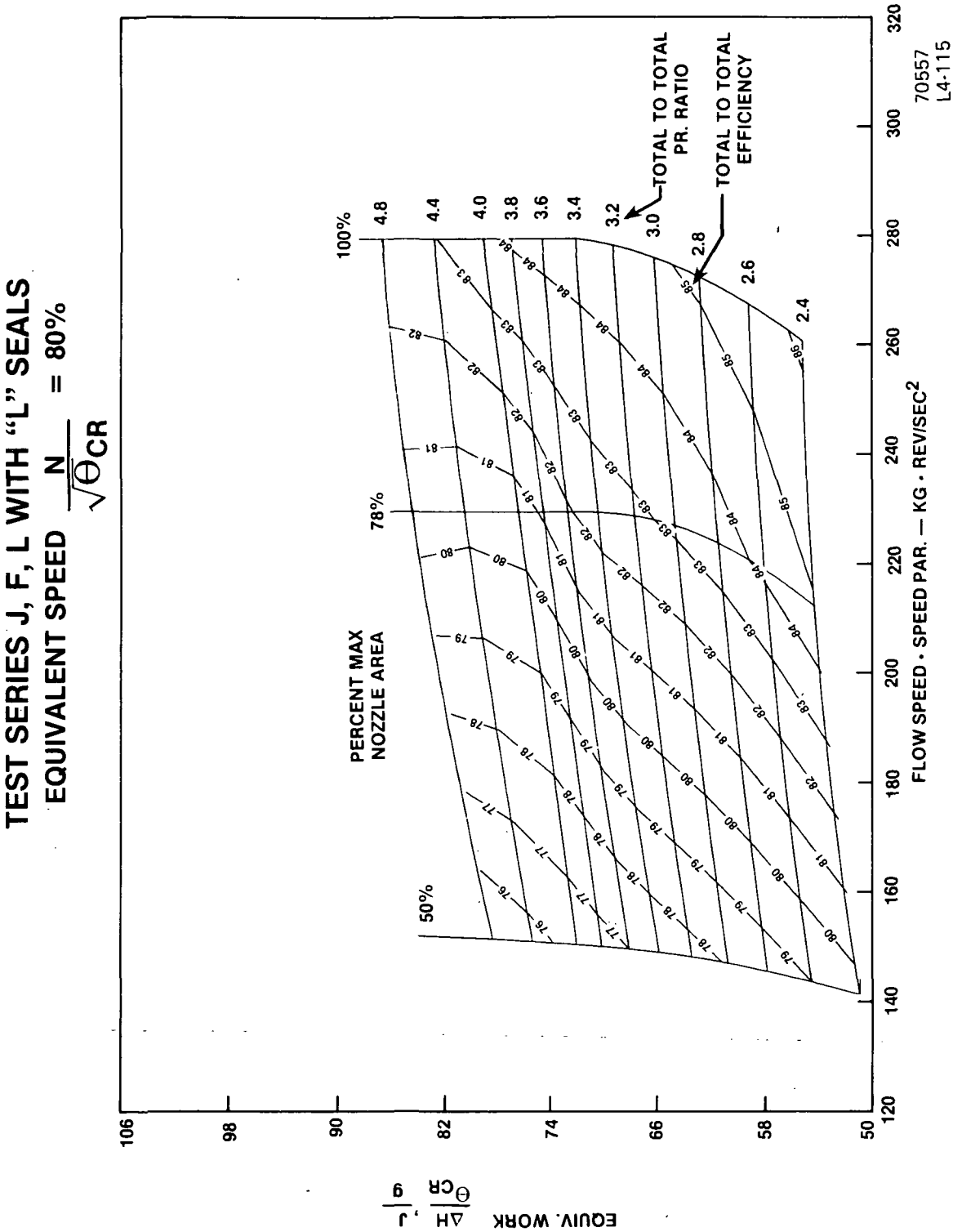

Figure 52. Reduced Speed Variable Capacity Turbine Map - Moveable Hub Nozzle

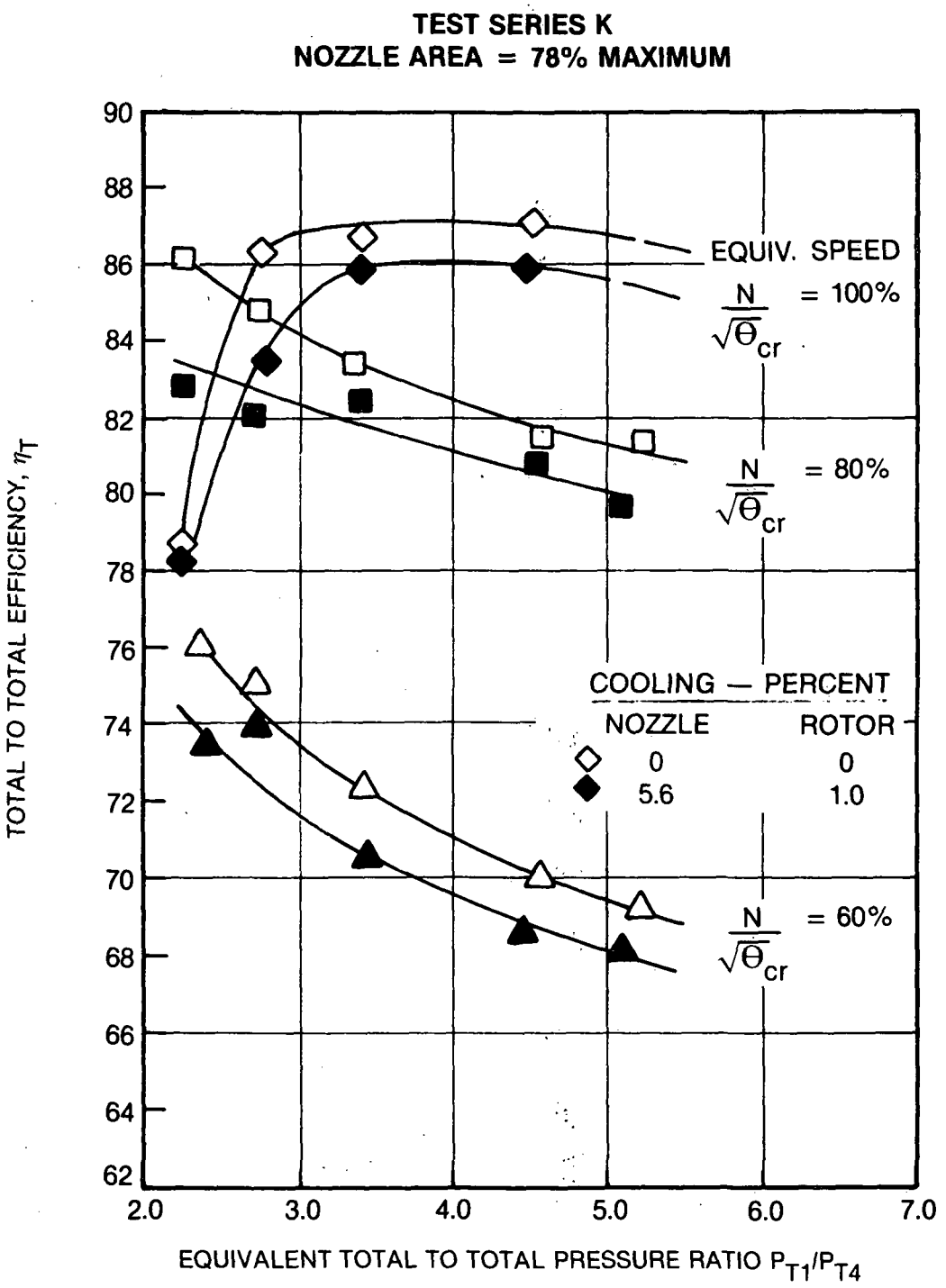

Figure 53. Cooling Injection Effects - Moveable Hub Wall In Flush Position

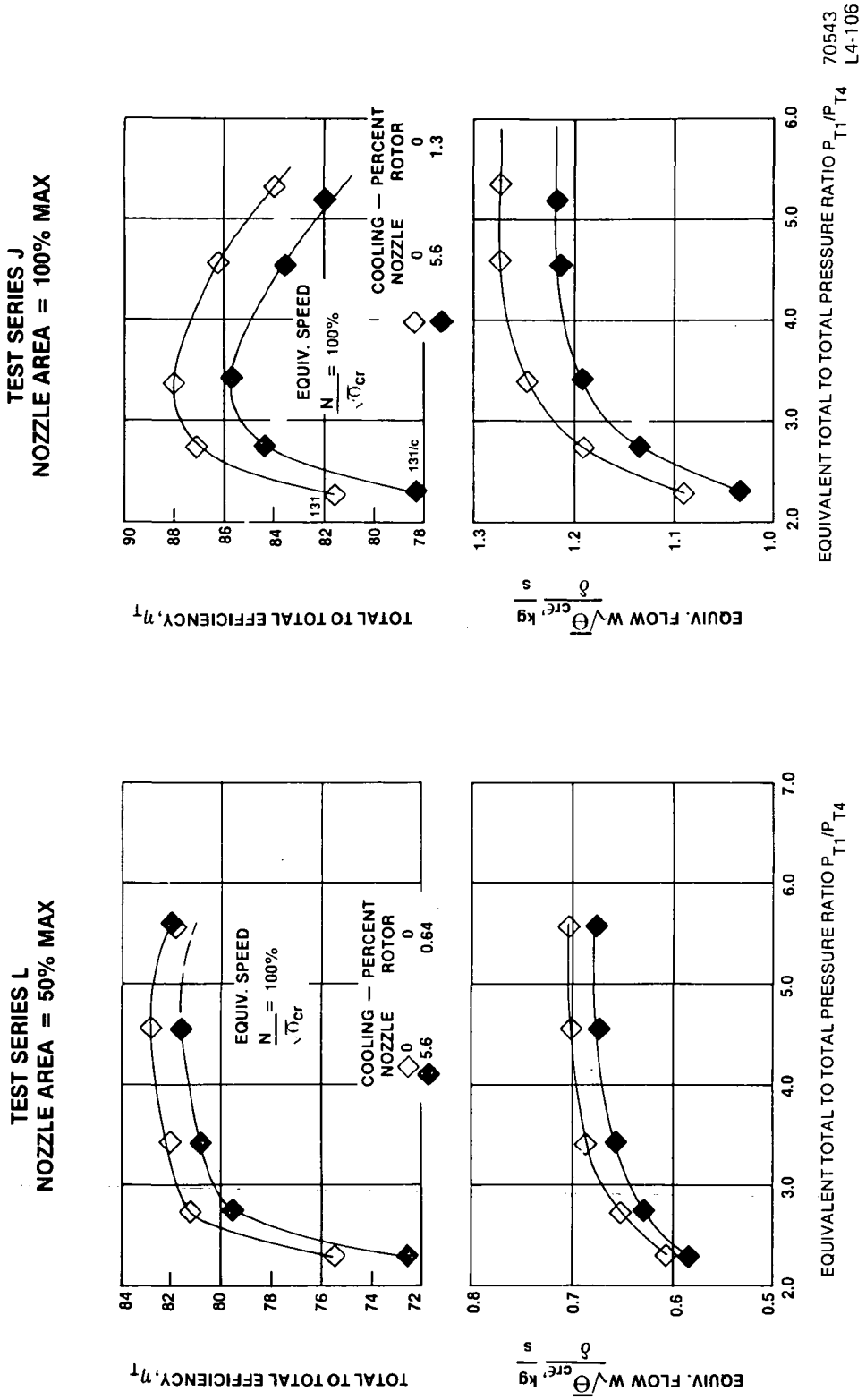

Figure 54. Cooling Injection Effects Moveable Hub Wall In Closed and Open Positions

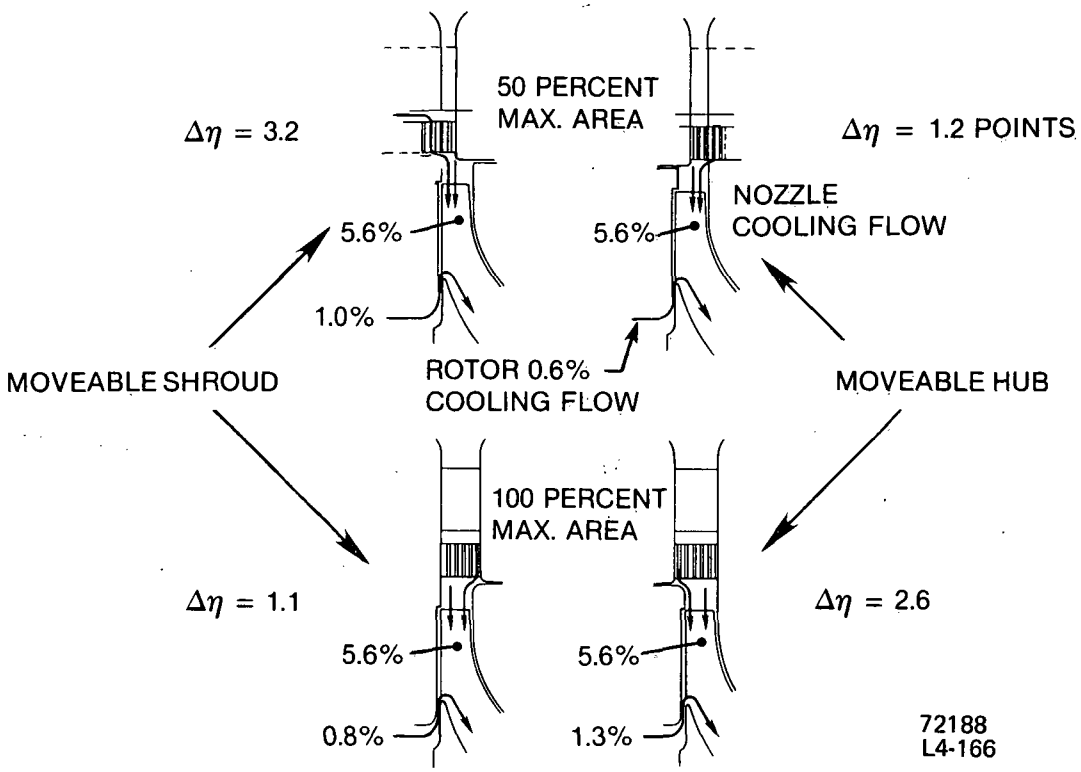

Figure 55: Moveable Hub and Moveable Shroud Cooling Injection Losses

5.3 COMPARISON TO PIVOTED VANE PERFORMANCE

Another common method for varing the flow capacity of a radial turbine is to hold the sidewalls fixed and vary the nozzle area by rotating the vanes or a portion of the trailing edge of the vanes about pivots supported by the sidewalls.

Figure 56 gives a qualitative performance comparison of two variable vane stagger angle turbines, a pivoted vane and two moveable sidewall turbines. A direct comparison was not possible because of differences of geometry, work level and design requirements. Therefore, efficiency data is shown normalized as the efficiency loss from maximum efficiency, vs percent change of flow from the flow at maximum efficiency. All comparisons are shown at fixed design pressure ratios of the respective turbines and with nozzle area as a main variable (operation typical of a VARICAP engine).

The two moveable sidewall turbines show comparable and in some flow ranges higher performance than the variable stagger angle turbines of references 10 and 11. The data for these reference turbines, is optimistic in the sense that the nozzle area was varied with different, zero leakage, integrated nozzle vane assemblies. The nozzles of reference 10 had an optimized vane solidity and airfoil shape for each respective area test (no. of vanes used noted on Figure 56). The turbine of reference 11 was tested in a similar manner except the same airfoil shape was used throughout. The design pressure ratios on the two turbines were very low and the nozzle operating Mach numbers were subsonic. The performance of these two turbines would be expected to be reduced when operated at higher Mach numbers, fixed geometry and number of vanes, and the penalties associated with vane sidewall clearance leakages.

The performance of an "in-house" pivoted vane turbine operating at a pressure ratio of 2.51 is also shown on Figure 56. This turbine was tested with the vanes moved to five different area positions. At each test position the sidewalls were clamped to the vanes to eliminate clearance leakage loss. Both of the moveable sidewall 4.50 and 4.54 pressure ratio turbines show substantially higher performance (leakage loss included) than the pivoted vane turbine for the entire flow range tested.

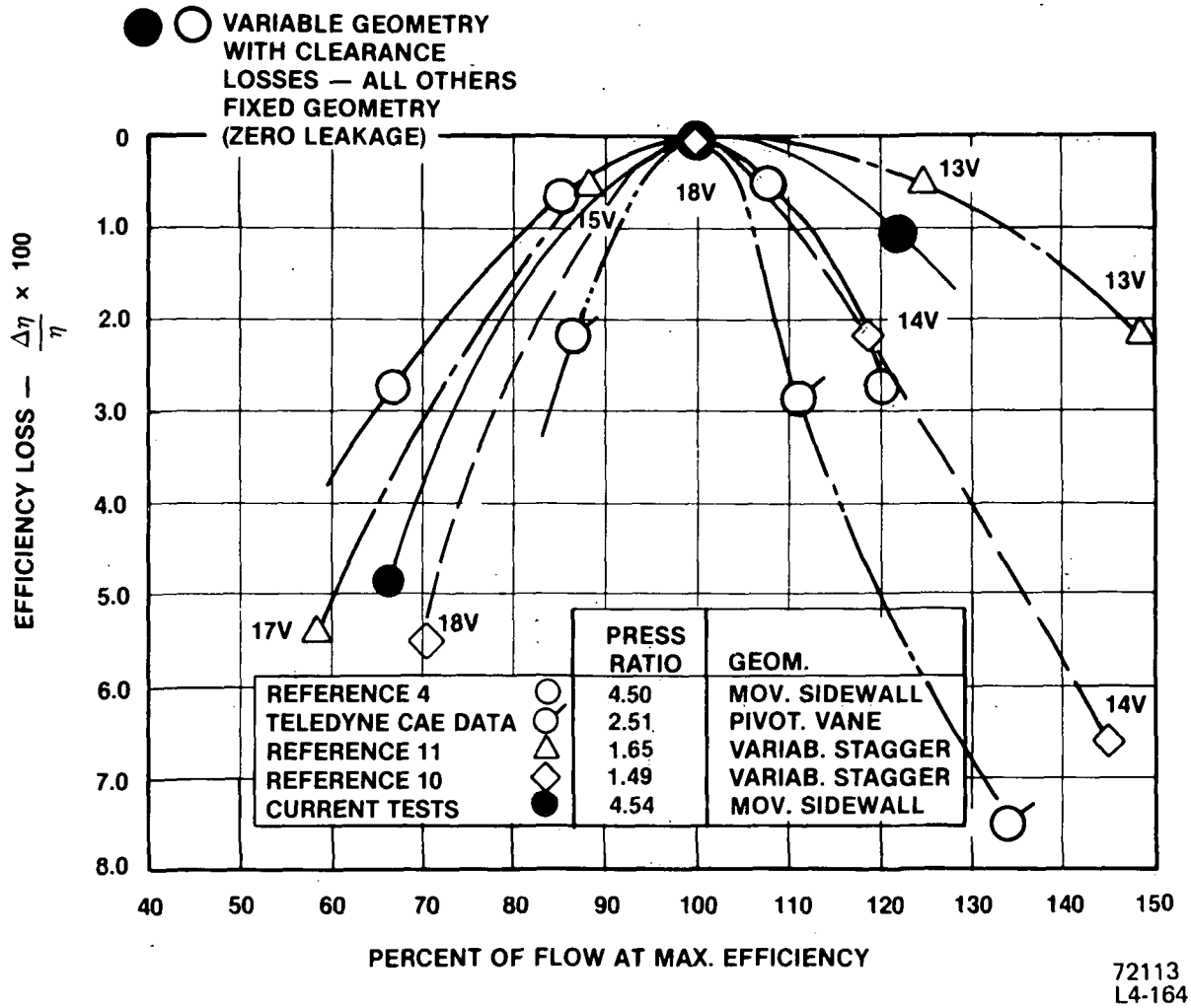

FIGURE 56. Moveable Sidewall and Pivoted Vane Nozzle Performance Comparison.

SECTION 6.0

CONCLUSIONS

The overall performance of a variable area radial turbine suitable for an advanced variable capacity turboshaft engine was evaluated in a turbine rig. A twice size actual turbine was used to duplicate engine Reynolds numbers and aerodynamics.

Tests were conducted with a moveable sidewall nozzle on both the hub and shroud sides, and with and without leakage and nozzle cooling flows. Baseline tests were conducted with the vane endwall clearance gaps sealed and also with metal "L" wiper seals simulating an engine configuration. With the wiper seals the efficiency loss was 1.0 point or less, compared to the completely sealed clearances, at all test conditions. This loss could be further reduced by locating the wiper seal closer to the main flow stream.

Figure 56 summarizes the turbine efficiency (with metal seals) as a function of nozzle area and sidewall geometry. The pressure ratio and equivalent speed were held constant at design values simulating a VARICAP engine operating mode. The test results showed:

1. The uncooled efficiency peaked at 87.9 for the flush wall nozzle which corresponds to cruise setting (78% maximum flow). The design flow of 1.044 kg/sec (2.296 lbs/sec) was achieved.

2. At the same setting but with 5.6 percent nozzle and 1.0 percent rotor backface coolant flows, the efficiency was reduced by 1.6 points to 86.3 percent.

3. Except at the 50 percent closed position; the same cooled performance was obtained with both moveable hub (MH) and moveable shoud (MS) sidewall geometries. In this position, the MH nozzle configuration showed 2.2 points higher cooled efficiency than the MS sidewall nozzle. The cooling losses can be reduced by closing off the inefficient flow of coolant in the nozzle sidewall clearance space. The need for cooling could also be eliminated by the use of a ceramic nozzle assembly.

Testing was also conducted with a MS sidewall splitline located closer to the rotor tip, where sudden contraction or expansion flow disturbances are confined closer to the low rotor relative Mach number plane. This configuration showed 1.0 point better efficiency over a perssure ratio range form 3.0 to 5.0.

The cooled turbine efficiency falls within a $\pm$ 2.2 point band over a 55 percent flow range at constant speed and pressure ratio. This is within the efficiency change assumed in earlier engine studies. The absolute level of performance of the turbine can be further increased by design refinements suggested above. The program demonstrated that the moveable sidewall concept can achieve the performance required to significantly reduce the part power SFC of the VARICAP engine.

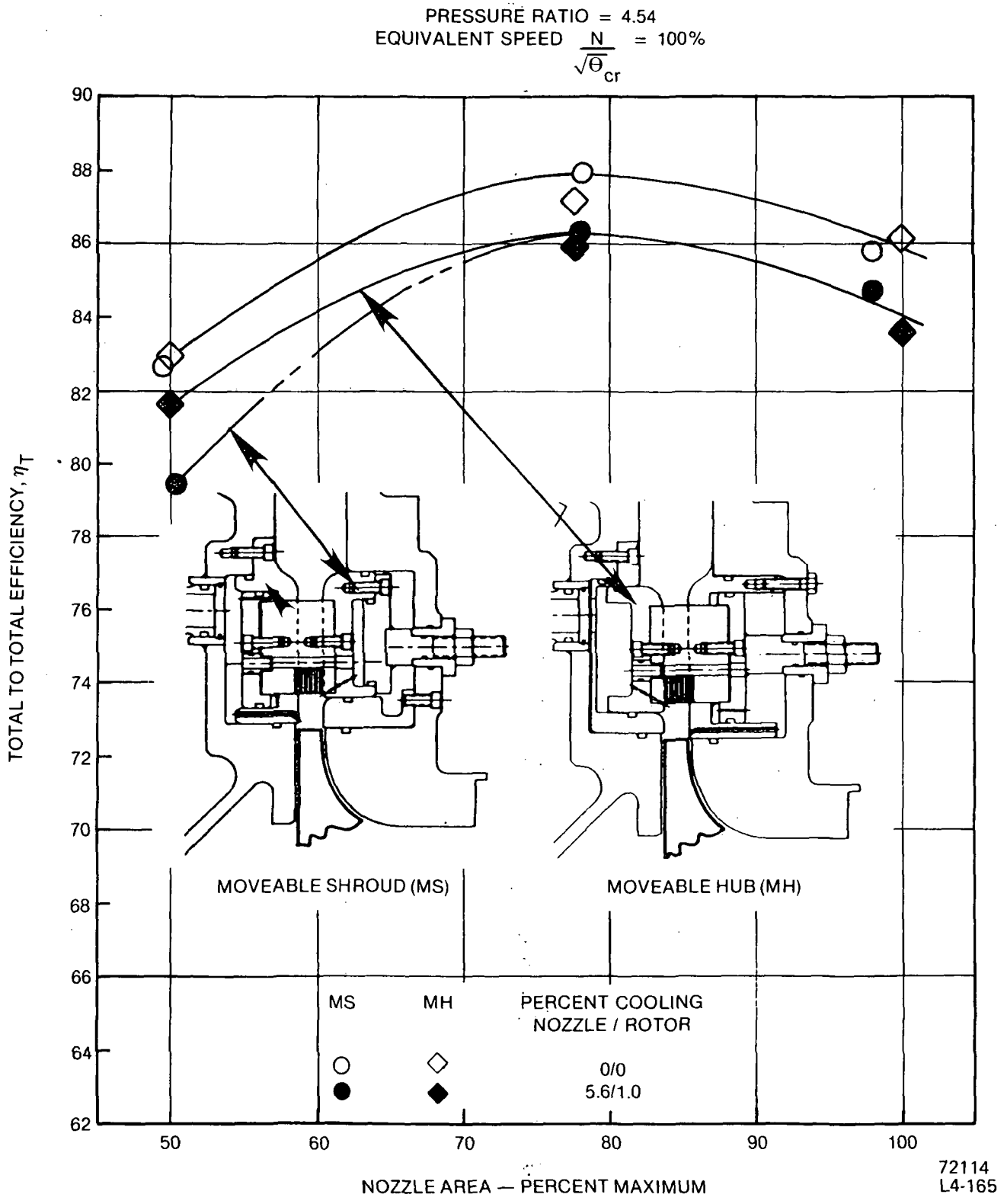

Figure 57. Constant Pressure Ratio Overall Stage Performance With Metal Wiper Seals Installed.

SECTION 7.0

RECOMMENDATIONS

The test data base on the moveable sidewall nozzle radial turbine concept has now been significantly broadened. A high level of design and off-design performance has been demonstrated. However, further improvements and expansion of the technology base can be made.

One approach would be to analyze, in detail, the new and current data on the variable capacity concepts for semi-empirical correlation and computer modeling. The models could then be applied to predict trends, improvements and pay-offs.

The radial turbine exit average swirl angles varied $\pm$ 25 degrees over the constant speed-pressure ratio, nozzle area range tested. Under some conditions severe hub-to-tip exit swirl gradients were exhibited. The exit transition duct performance could then be critical to the VARICAP concept. Overall performance testing with a transition duct diffuser typical of a duct leading to a power turbine is recommended.

In a qualitative comparison, the moveable sidewall nozzle was shown to have some performance advantage over a pivoted vane configuration. Since small performance differences are extremely important in the life cycle cost of an engine, the same turbine should be comparitively tested with a cooled pivoted vane assembly with a version of engine configuration wiper seals. Vane/rotor clearances could also be varied to provide a new data base.

In an actual hot environment the vane scaling arrangement could behave differently. Thermal distortions, vane coating, and durability are serious considerations. Further development should embody hot nozzle sidewall testing along with hot complete stage testing.

SECTION 8.0

NOMENCLATURE

SYMBOLS	DEFINITION
H	enthalpy, kJ/kg; Btu/lb
H'	enthalpy, kJ/kg; Btu/lb corresponding to isentropic expansion
N	rotational speed, rev/min
P	pressure, kPa; psia
R	radius, mm; in
T	temperature, K; °R
TORQ	measured torque corrected for bearing and windage, cm-kg; in-lb
U	blade velocity, m/sec; ft/sec
V	absolute gas velocity, m/sec; ft/sec
V_{cr}	critical velocity, m/sec; ft/sec
W	mass flow, kg/sec; lbs/sec or relative velocity, m/sec; ft/sec
γ	ratio of specific heats
Δ	difference or change
δ	ratio of inlet stagnation pressure to sea level standard
ϵ	function of γ defined as

$$\frac{\gamma_{st}}{\gamma}\left[\left(\frac{\gamma+1}{2}\right)^{\frac{\gamma-1}{\gamma}}\Big/\left(\frac{\gamma_{st}+1}{2}\right)^{\frac{\gamma_{st}}{\gamma_{st}-1}}\right]$$

η_T total-to-total adiabatic efficiency, based on pressure/temperature data

$$\frac{W_{AM}\,(H_{TI} - H_{T4}) + W_{AN}\,(H_{TN} - H_{T4}) + W_{AR}\,(H_{TR} - H_{T4})}{W_{AM}\,(H_{TI} - H'_{T4}) + W_{AN}\,(H_{TN} - H'_{T4}) + W_{AR}\,(H_{TR} - H'_{T4})}$$

η_S total-to-static adiabatic efficiency based on total pressure/temperature data and ideal work from total-to-static expansion

$$\frac{W_{AM}\,(H_{TI} - H_{T4}) + W_{AN}\,(H_{TN} - H_{T4}) + W_{AR}\,(H_{TR} - H_{T4})}{W_{AM}\,(H_{TI} - H'_{S4}) + W_{AN}\,(H_{TN} - H'_{S4}) + W_{AR}\,(H_{TR} - H'_{S4})}$$

η_D total-to-total adiabatic efficiency based on torque

$$\frac{\frac{2\pi}{60}\,(N)\,(TORQ)}{W_{AM}\,(H_{TI} - H'_{T4}) + W_{AN}\,(H_{TN} - H'_{T4}) + W_{AR}\,(H_{TR} - H'_{T4})}$$

θ_{cr} squared ratio of critical velocity at turbine inlet temperature to critical velocity at standard sea level temperature

viscosity, kg/sec-m; lbm/sec-ft

density, kg/m^3; $slugs/ft^3$

SUBSCRIPTS

AM	airflow, mainstream flow
AN	nozzle cooling flow
AR	rotor cooling flow
DES	design
S	static
ST	standard sea-level conditions
T	total or stagnation
1	nozzle inlet
2	rotor inlet
3	rotor exit
4	rotor exit mixed out plane

SECTION 9.0

REFERENCES

1. Rogo, C. and Holbrook, M.R.., "Cooled Variable Nozzle Radial Turbine for Rotor-Craft Applications," NASA Report No. CR-165397, March 1981.

2. Easterling, Albert E., "A Comparative Study of Simple, Regenerative and Variable Capacity Cycles for Gas Turbine Engines," USAAVRADCOM TR-81-D-1, October 1981.

3. Large, G.D., and Meyer, L.J., "Cooled Variable - Area Radial Turbine Program, NASA Report No. CR-165418, January, 1982.

4. Rogo, C., Hajek, T., and Chen, A.G., "Variable Stator Radial Turbine," NASA Report No. CR-174663, May 1984.

5. Rogo, C., Hajek, T., and Roelke, R., "Aerodynamic Effects of Moveable Sidewall Nozzle Geometry and Rotor Exit Restriction On The Performance of A Radial Turbine," SAE Paper No. 831517, Society of Automotive Transactions, Volume No. 92, 1984.

6. Abernethy, R. B, et. al. "Uncertainty in Gas Turbine Measurements Handbook," AD-755 356.

7. Penny, N., "Rover Case History of Small Gas Turbines," SAE Paper No. 634A, January 1, 1963.

8. Kidwell, J. R. and G. D. Large, "Advanced Technology Components for Model GTCP305-2 Aircraft Auxiliary Power System," AFAPL-TR-2106, February 1980.

9. Futral, Jr., W. M. and D. E. Holeski, "Experimental Results of Varying the Blade-Shroud Clearance in a 6.02-Inch Radial-Inflow Turbine," NASA TN D-5513, 1970.

10. Kofskey, M. S. and Wasserbauer, C. A., "Experimental Performance Evaluation of a Radial Inflow Turbine Over a Range of Specific Speeds", NASA Technical Note NASA TN D-3742, December, 1966

11. Kofskey, M. G., and Nusbaum, W. J., "Effects of Specific Speed on Experimental Performance of a Radial Inflow Turbine", NASA Technical Note *NASA TN D-6605, February 1972*